

Predicting the Behavior of a Lean-Burn, Hydrogen-Enhanced Engine Concept

by

Žiga Ivanic

B.S., Mechanical Engineering

Norwich University, 2002

Submitted to the Department of Mechanical Engineering
in Partial Fulfillment of the Requirements for the Degree of

Master of Science in Mechanical Engineering

at the

Massachusetts Institute of Technology

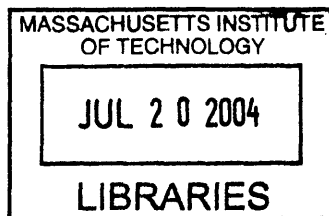
June 2004

© 2004 Massachusetts Institute of Technology
All Rights Reserved

Signature of the Author.....
Department of Mechanical Engineering
May 7, 2004

Certified by.....
John B. Heywood
Sun Jae Professor of Mechanical Engineering
Thesis Advisor

Accepted by:.....
Ain A. Sonin
Professor, Department of Mechanical Engineering
Chairman, Department of Graduate Committee



(This page was intentionally left blank.)

Predicting the Behavior of a Lean-Burn, Hydrogen-Enhanced Engine Concept

by

ŽIGA IVANIC

Submitted to the Department of Mechanical Engineering
on May 7, 2004 in partial fulfillment of the
requirements for the Degree of Master of Science in
Mechanical Engineering

ABSTRACT

Lean operation of a spark ignition (SI) internal combustion engine (ICE) offers attractive performance incentives. Lowered combustion temperatures inhibit formation of nitrogen oxides (NO_x), while reduced intake manifold throttling minimizes pumping losses leading to higher efficiency. These benefits are offset by the reduced combustion speed of lean mixtures, which can lead to high cycle-to-cycle variation and unacceptable engine behavior characteristics.

Hydrogen-enhancement can suppress the undesirable consequences of lean operation by accelerating the combustion process, thereby extending the “lean limit.” Hydrogen would be produced on-board the vehicle with a fuel reforming device. Since operating an engine in the lean regime requires a significant amount of air, boosting is required. Hydrogen is also an octane enhancer, enabling operation at higher compression ratios, which results in a further improvement in engine efficiency.

The focus of this thesis is on the modeling aspect of the lean boosted engine concept. Modeling provides a useful tool for investigating different lean boosted concepts and comparing them based on their emissions and fuel economy. An existing architectural concept has been tailored for boosted, hydrogen-enhanced, lean-burn SI engine. The simulation consists of a set of Matlab models, part physical and part empirical, that have been developed to simulate performance of a real ICE.

The model was calibrated with experimental data for combustion and emissions in regards to changes in air/fuel ratio, load and speed, and different reformate fractions. The outputs of the model are NO_x emissions and brake specific fuel consumption (BSFC) maps along with the cumulative NO_x emissions and fuel economy for the urban and highway drive cycles.

Thesis Advisor: John B. Heywood

Title: Sun Jae Professor of Mechanical Engineering

(This page was intentionally left blank.)

ACKNOWLEDGEMENTS

First, I would like to thank Professor Heywood for giving me the opportunity to be a research assistant under his supervision in the Sloan Automotive Laboratory (SAL). As my thesis advisor, he encouraged me every step of the way, providing guidance when needed, and at the same time giving me the freedom to contribute my own ideas to this research project. I have learned a great deal from him in terms of analyzing data, drawing conclusions from it, and presenting it in a formal way.

Joshua Goldwitz has worked side by side with me on this project from day one. He has been a very valuable colleague and also a great friend. He knew MIT inside out and that made my stay here a lot smoother. We shared many memories from our test cell in the SAL, Germany trip, to his visit of my home country, Slovenia, this past summer.

Jenny Topinka was the first person that I have met from the SAL and she was always willing to offer advice about everyday things that every graduate student runs into. She also helped me learn about the experimental setup and procedure used in this project.

My office-mate, Mike Gerty, has been a valuable resource when discussing modeling techniques and was always willing to listen and give advice on whatever issues I wanted to discuss.

Rudy Smaling built the modeling architecture that my model is based on. His visits to our laboratory always resulted in interesting discussion in regards to the big picture of the project that we were working on.

There were numerous other people that have made my stay at MIT a pleasant one. Professor Cheng was always willing to help with data acquisition issues, while Thane Dewitt provided me with solid technical guidance in the laboratory. Karla Stryker always found a way to fit me into Professor Heywood's busy schedule and cheered me up whenever I saw her. Brian Hallgren was the go to guy when I needed help with experimental setup and always provided advice when I needed it.

Tom Leone from Ford's advanced engine engineering group provided detailed engine performance data that are used in the model. Claus Hartmut, applications engineering manager at Borg Warner Turbosystems, provided the turbocharger performance maps.

I would like to thank my parents for believing in me and supporting me thorough out my life journey, because without their love and support I would not be where I am today. My wife, Natalie, has also been a great support throughout my days at MIT.

This research project was supported by funding from ArvinMeritor.

TABLE OF CONTENTS

ABSTRACT	3
ACKNOWLEDGEMENTS	5
TABLE OF CONTENTS	6
LIST OF TABLES.....	8
LIST OF FIGURES	9
NOMENCLATURE	11
CHAPTER 1 INTRODUCTION	13
1.1 Current Engine Technologies.....	13
1.2 Lean Burn Operation with Hydrogen Addition	14
1.3 The Plasmatron Engine System	16
1.3.1 Description	16
1.3.2 The Plasmatron.....	17
1.4 Previous Work.....	19
1.5 Objectives	20
1.6 Methodology	20
CHAPTER 2 EXPERIMENTAL METHOD	23
2.1 Overview.....	23
2.2 Operating Conditions.....	23
2.3 Experimental Procedure.....	24
2.4 Engine Setup	25
2.4.1 Engine Specifications.....	25
2.4.2 Air Intake System	25
2.4.3 Hydrocarbon Fuel	27
2.4.4 Exhaust Gas Recirculation System (EGR).....	27
2.5 Engine Control and Measurements	29
2.5.1 Intake Air (volume, pressure, temperature)	29
2.5.2 Engine Fluids Temperature	29
2.5.3 Gasoline Flow Rate.....	29
2.5.4 Gaseous Fuel Flow Rate	29
2.5.5 Lambda Measurement.....	30
2.5.6 In-Cylinder Pressure Measurement	30
2.5.7 Emissions Measurement	30
2.5.8 Exhaust Gas Recirculation Measurement	31
2.6 Experimental Results.....	31
2.6.1 In-Cylinder Combustion Data	32
2.6.1.1 Air Dilution	32
2.6.1.2 EGR Dilution.....	33

2.6.2	NOx Emissions.....	34
2.6.2.1	Air Dilution	34
2.6.2.2	EGR Dilution.....	35
2.6.3	Exhaust Temperature	35
CHAPTER 3	SIMULATION	47
3.1	Overview.....	47
3.2	Model Architecture.....	49
3.3	Model Subroutines	50
3.3.1	ADVISOR	50
3.3.2	Friction model	53
3.3.3	Indicated Fuel Conversion Efficiency	56
3.3.4	Brake Specific Fuel Consumption Model.....	58
3.3.4.1	Volumetric Efficiency Correction	60
3.3.4.2	Manifold Air Pressure.....	61
3.3.4.3	Empirical Relationships from Experimental Data.....	62
3.3.5	Boost.....	63
3.3.5.1	Turbocharging	63
3.3.5.2	Mechanical Supercharging.....	68
3.3.6	NOx model	69
3.3.6.1	Engine data.....	69
3.3.6.2	Dilution correction.....	70
3.4	Concepts of Interest.....	71
CHAPTER 4	DISCUSSION OF RESULTS	73
4.1	Introduction of Concepts	73
4.2	Comparison of Concepts.....	86
4.3	Downsizing Effect on Fuel Economy.....	87
CHAPTER 5	CONCLUSIONS	89
REFERENCES	90
APPENDIX A:	Experimental data for 350 kPa NIMEP @ 1500 rpm	92
APPENDIX B:	Experimental data for 750 kPa NIMEP @ 1500 rpm	96
APPENDIX C:	Experimental data for 750 kPa NIMEP @ 2500 rpm	101
APPENDIX D:	EGR data for 520 kPa NIMEP @ 1500 rpm	106
APPENDIX E:	EGR data for 350 kPa NIMEP @ 1500 rpm.....	111

LIST OF TABLES

Table 1-1	Combustion characteristics for hydrocarbon fuels, H ₂ , and CO [1]	15
Table 1-2	Plasmatron product composition and efficiency	18
Table 2-1	Engine Specifications for Volvo-Ricardo Research Engine	25
Table 2-2	Fuel Properties of UTG-96	27
Table 3-1	Engine Specifications Used in the Model	48

LIST OF FIGURES

Figure 1-1	Set-up of plasmatron engine system	17
Figure 1-2	Plasmatron Schematic (Courtesy of PSFC)	19
Figure 2-1	Typical engine operating regime	24
Figure 2-2	Engine instrumentation and air intake system.....	26
Figure 2-3	Picture of the Engine Setup.....	26
Figure 2-4	EGR System Schematic	28
Figure 2-5	Picture of EGR System	28
Figure 2-6	Air Dilution - Net Indicated Efficiency at 350 kPa @ 1500 rpm.....	36
Figure 2-7	Air Dilution - Net Indicated Efficiency at 750 kPa @ 1500 rpm.....	36
Figure 2-8	Air Dilution - Net Indicated Efficiency at 750 kPa @ 2500 rpm.....	37
Figure 2-9	Lean Limit at 350 kPa @ 1500 rpm	37
Figure 2-10	Lean Limit at 750 kPa @ 1500 rpm	38
Figure 2-11	Lean Limit at 750 kPa @ 2500 rpm	38
Figure 2-12	EGR Dilution - Net Indicated Efficiency at 350 kPa @ 1500 rpm	39
Figure 2-13	EGR Dilution - Net Indicated Efficiency at 520 kPa @ 1500 rpm	39
Figure 2-14	EGR Limit at 350 kPa @ 1500 rpm	40
Figure 2-15	EGR Limit at 520 kPa @ 1500 rpm	40
Figure 2-16	NOx emissions vs. Lambda at 350 kPa @ 1500 rpm	41
Figure 2-17	Air Dilution - NOx emissions vs. TDP at 350 kPa @ 1500 rpm	41
Figure 2-18	Air Dilution – NOx Emissions at 750 kPa @ 1500 rpm.....	42
Figure 2-19	Air Dilution – NOx Emissions at 750 kPa @ 2500 rpm.....	42
Figure 2-20	EGR Dilution – NOx Emissions at 350 kPa @ 1500 rpm	43
Figure 2-21	EGR Dilution – NOx Emissions at 520 kPa @ 1500 rpm	43
Figure 2-22	Normalized exhaust temperature as a function of air dilution	44
Figure 2-23	Normalized exhaust temperature as a function of EGR dilution.....	44
Figure 2-24	Correlation of TDP with lambda for air dilution data	45
Figure 2-25	EGR and air dilution correlation	45
Figure 3-1	Schematic of the engine system encompassed by the model.....	49
Figure 3-2	Conventional vehicle drivetrain in ADVISOR	50
Figure 3-3	HWFET drive cycle	51
Figure 3-4	FTP drive cycle.....	52
Figure 3-5	Friction model validation: fmep versus engine speed	55
Figure 3-6	Breakdown of friction components in the model	56
Figure 3-7	Fuel-air cycle efficiency correction for equivalence ratio	58
Figure 3-8	Fuel-air cycle efficiency correction for changes in compression ratio.....	59
Figure 3-9	Data derived TDP - plasmatron fraction correlation	63
Figure 3-10	Performance map for a Borg Warner compressor K06	64
Figure 3-11	Performance map for a Borg Warner Variable Geometry Turbine.....	64
Figure 3-12	Supercharger performance map from Wave	68
Figure 3-13	NOx emissions index model as a function of load and speed.....	69
Figure 3-14	NOx emissions index map for baseline engine	70
Figure 3-15	Dilution correction factors for NOx emissions	71
Figure 4-1	Baseline: Mechanical Efficiency	74

Figure 4-2	Baseline: Gross Indicated Efficiency.....	74
Figure 4-3	Baseline: Brake Fuel Efficiency.....	75
Figure 4-4	Baseline: BSFC	75
Figure 4-5	Baseline: MAP.....	76
Figure 4-6	Baseline: BSNO _x	76
Figure 4-7	Baseline: Volumetric Efficiency	77
Figure 4-8	Baseline: Exhaust Pressure.....	77
Figure 4-9	Baseline: Exhaust Temperature	78
Figure 4-10	Baseline: Stoichiometric Gross Indicated Efficiency	78
Figure 4-11	10% EGR: Mechanical Efficiency.....	79
Figure 4-12	10% EGR: BSFC	79
Figure 4-13	10% EGR: BSNO _x	80
Figure 4-14	10% EGR: Exhaust Temperature	80
Figure 4-15	10% EGR: MAP	81
Figure 4-16	Lean Boost: Mechanical Efficiency.....	81
Figure 4-17	Lean Boost: Gross Indicated Efficiency	82
Figure 4-18	Lean Boost: Brake Fuel Efficiency.....	82
Figure 4-19	Lean Boost: BSFC	83
Figure 4-20	Lean Boost: MAP	83
Figure 4-21	Lean Boost: Exhaust Temperature.....	84
Figure 4-22	Lean Boost: Exhaust Pressure	84
Figure 4-23	Lean Boost: BSNO _x	85
Figure 4-24	Fuel economy comparison of all three concepts	86
Figure 4-25	NO _x emissions comparison of all three concepts.....	86
Figure 4-26	Benefits of Lean Boost vs 10% EGR.....	87
Figure 4-27	Impact of downsizing on fuel economy.....	87

NOMENCLATURE

<u>Symbol</u>	<u>Units</u>	<u>Description</u>
\dot{m}	g/s	mass flow rate
\dot{W}_c	kW	compressor work
\dot{W}_t	kW	turbine work
γ		ratio of specific heats
γ_a		ratio of specific heats for air
γ_e		ratio of specific heats for exhaust gas
μ	kg/(m*s)	kinematic viscosity
η_c		compressor efficiency
η_C		combustion efficiency
η_e		mechanical to electrical conversion efficiency
$\eta_{f,b}$		brake fuel conversion efficiency
$\eta_{f,ig}$		gross indicated fuel conversion efficiency
$\eta_{f,s}$		fuel system efficiency
η_{loss}		heat loss fraction
η_m		mechanical efficiency
Δp	kPa	pressure drop in the exhaust system after the turbine
$\Delta P_{turbine}$	kPa	pressure drop across the turbine in the exhaust manifold
η_{vol}		volumetric efficiency
$\eta_{vol,ideal}$		ideal volumetric efficiency
$\rho_{a,i}$	kg/m ³	manifold charge mixture density
ρ_e	kg/m ³	exhaust gas density
A/F		air-fuel ratio
amep	kPa	auxiliary component mean effective pressure
B	mm	bore
bmep	kPa	brake mean effective pressure
bsfc	g/kWh	brake specific fuel consumption
BSNOx	g/kWh	brake specific NOx emissions
cfmep	kPa	crankshaft rubbing friction mean effective pressure
c_p	kJ/kgK	constant pressure specific heat
C_r		piston roughness constant
D_b	mm	bearing diameter
EGR		percent of recycled exhaust gas
emep	kPa	plasmatron electric consumption mean effective pressure
F		piston ring tension ratio
fn(N)		speed correction for volumetric efficiency
imep _g	kPa	gross indicated mean effective pressure
L	m	characteristic length
L_b	mm	bearing length
L_v	mm	maximum valve lift

M		lean or EGR multiplier for NOx emissions
M_T		temperature multiplier for NOx emissions
N	rpm	engine speed
n_b		number of bearings
n_c		number of cylinders
$NO_{x\text{index}}$		NOx emissions index (% mass flow of fuel mass flow)
n_e		number of exhaust valves
n_i		number of intake valves
n_r		number of crank revolutions per power stroke per cylinder
n_v		number of valves
O/C		oxygen to carbon ratio in plasmatron gas
p_a	kPa	atmospheric pressure
P_b	kW	brake power
p_e	kPa	exhaust back pressure
p_i	kPa	intake manifold pressure
p_{mep}	kPa	pumping friction mean effective pressure
p_{mep_v}	kPa	pumping friction mean effective pressure across the valves
Pr		Prandtl number
R	kJ/kgK	universal gas constant
r_c		compression ratio
Q	kW	heat loss to coolant and oil
q_{E,H_2}	MJ/kg H_2	plasmatron power consumption
$q_{E,H_2,C}$	kW	plasmatron constant power consumption
Q_{LHV}	MJ/kg	lower heating value of the fuel
r_{cfmep}	kPa	reciprocating rubbing friction mean effective pressure
r_e		exhaust valve diameter / bore
Re		Reynolds number
r_{fmep}	kPa	rubbing friction mean effective pressure
r_i		intake valve diameter / bore
R_P		percent plasmatron fraction
S	mm	stroke
s_{cmep}	kPa	mean effective pressure required to drive the supercharger
S_p	m/s	mean piston speed
T_1	K	temperature at compressor inlet
T_2	K	temperature at compressor exit
T_3	K	same as T_{exhaust}
T_4	K	temperature after turbine
T_{charge}	K	cylinder charge temperature
TDP		thermal dilution parameter
T_{exhaust}	K	exhaust gas temperature at exit port before turbine
t_{fmep}	kPa	total friction mean effective pressure
T_{manifold}	K	charge temperature after compressor and intercooler
$T_{\text{plasmatron}}$	K	plasmatron gas temperature
Tq	Nm	torque output of the engine
V_d	dm^3	cylinder displacement
v_{fmep}	kPa	valvetrain rubbing friction mean effective pressure

CHAPTER 1 INTRODUCTION

1.1 Current Engine Technologies

Internal combustion engine (ICE) combines high power density, with low relative cost, and widely available fuel that has a high energy density. These attributes have helped the ICE remain the best source for automotive propulsion for over a century. The increasing concern about its impact on the environment has resulted in automobile emission regulations. Another set of regulations, Corporate Average Fuel Economy (CAFE), has been introduced to curb the petroleum consumption of the light duty vehicles in US. With emission regulations becoming tighter and CAFE regulations becoming more aggressive, automobile manufacturers must produce automobiles that deliver both good fuel economy and low toxic emission levels.

Current gasoline engines operate with low hydrocarbon (HC) and NO_x emissions at the expense of fuel efficiency and carbon dioxide (CO₂) emissions. A three-way catalyst is used to reduce the exhaust emissions (NO_x, CO, and HC) to meet the current emission regulations. It works most efficiently when the exhaust gas composition alternates between slightly rich and slightly lean, restricting the gasoline engines to an average stoichiometric mixture. A stoichiometric mixture, as a working fluid, does not have optimal properties due to a relatively low ratio of specific heats. Combusting a stoichiometric mixture causes very high burned gas temperatures resulting in high heat losses that lower engine efficiency.

Another downside of gasoline engines is that at part load the incoming mixture of air and fuel is throttled resulting in lowered density of the mixture in the cylinder. The pressure drop in the intake, caused by throttling, results in pumping losses over the exhaust and intake strokes, decreasing part load efficiency.

Diesel engines perform favorably over gasoline engines in the areas mentioned above but face different problems. In diesel engines, regulating the amount of fuel that is injected in the cylinder, while the cylinder is always filled with air, controls the power without the need for throttling. Burning lean mixtures results in higher ratio of specific heats and lower burned gas temperatures, both increasing efficiency. Diesel engines are not limited by knock because burning involves a diffusion flame instead of flame propagation. This allows for use of higher compression ratios thereby increasing efficiency.

Injecting the fuel directly in the cylinder causes inhomogeneous mixtures resulting in high levels of NO_x and particulates in the exhaust. Good diesel engine aftertreatment is not yet available and because of that, diesel engines represent an insignificant part in the U.S. light duty vehicle market.

The lean burn engine concept combines the attractive features of gasoline and diesel engine technologies. This concept involves lean operation along with stoichiometric air-fuel mixture for high efficiency and low NO_x emissions. The advantages of a lean burn concept increase as more air is used. To achieve comparable emission levels to current gasoline engines with a three-way catalyst, very lean mixtures, close to air/fuel ratio of two, must be used.

Lean burn engines are not widely used due to poor combustion that occurs with increasingly leaner mixtures. Poor combustion is a result of loss of flame speed and can be observed in combustion variation from one cycle to the next. Non-optimal combustion phasing, partial burns and misfires cause cycle-to-cycle variation. Combustion phasing means that the spark timing is not properly adjusted to achieve maximum brake torque; partial burns occur when the flame speed is quenched before the whole mixture is ignited; misfires occur when the mixture is too diluted to be ignited by a spark plug. As the combustion stability becomes worse, engine output and efficiency decrease. The lean limit occurs where the mixture's burning properties are unacceptable. The lean-burn gasoline engines encounter the lean limit of operation before significant benefits of lean operation can be reached.

Adding a small amount of hydrogen can extend the lean limit and greater benefits of lean operation can be achieved. This project examines the possible emission and fuel economy benefits of different gasoline engine concepts that are highly diluted with air or recycled exhaust and enhanced with hydrogen.

1.2 Lean Burn Operation with Hydrogen Addition

Hydrogen enhanced lean operation is an attractive alternative to stoichiometric operation. The benefits are higher engine efficiency and lower engine out NO_x emissions. There is a possibility of an additional efficiency improvement when a small amount of hydrogen is added to the mixture. Since hydrogen is known to suppress engine knock, higher compression ratios could be utilized.

Higher efficiencies of lean operation, compared to stoichiometric, are a result of increased ratio of specific heats, which increases because more air is present in the air/fuel mixture in the cylinder. Another factor contributing to the efficiency increase is reduced throttling, since higher intake pressures are required to allow more air to flow into the cylinder.

NOx emissions are significantly reduced in a homogeneous lean charge mixture because the peak combustion temperatures are lower than in diesel or SI engines. Lower peak temperatures are a result of the air/fuel mixture in the cylinder being more diluted. Since the NOx emission levels of lean operation with no hydrogen are higher than the levels of stoichiometric operation with a three-way catalyst, most engines operate with stoichiometric mixtures. As hydrogen rich gas is added to the mixture, the lean limit of combustion is extended and the engine can operate even leaner where the NOx emissions may be low enough to eliminate the need for aftertreatment.

Hydrogen has a very high flame speed when compared to other conventional fuels (Table 1-1). When added to the mixture, mixture's overall flame speed increases, due to diffusion properties of hydrogen, and flame stability is maintained beyond the lean limit of operation without hydrogen addition. Hydrogen's high spontaneous ignition temperature suggests that it is a knock-resistant fuel. Due to these properties, hydrogen is an optimal additive to extend the lean limit of a SI engine.

Table 1-1 Combustion characteristics for hydrocarbon fuels, H₂, and CO [1]

Fuel	Flame Speed at 100 °C and 1 atm. [cm/s]		Spontaneous Ignition Temperature in Air [°C]
	Stoichiometric	Maximum	
Isooctane	57.8	58.2	447
Normal-heptane	63.8	63.8	247
Hydrogen	170.0	325.0	572
Carbon monoxide	28.5	52.0	609

Ongoing research at MIT confirmed that hydrogen is very effective in extending the lean limit of gasoline SI engine. The results show that by adding small amounts of hydrogen rich gas, the lean limit can be extended close to air/fuel ratio of two where engine out NO_x emissions are reduced up to 99% and net engine fuel conversion efficiency is increased by 12% [2].

Data from the literature seemed to suggest that when the engine operates lean of stoichiometric the compression ratio could be increased due to the lean mixtures being more resistant to knock [3]. Recent results from research at MIT have shown that this is true for constant intake pressures, but for constant load the octane number requirement (ONR), tendency to knock, does not decrease with lean operation but slightly increases. However, the same research has shown that by adding small amounts of hydrogen rich gas the ONR decreases at constant load [4]. A linear trend was observed with a decrease of around 10 octane numbers (ON) with 15 percent plasmatron addition and close to 20 ON with 30 percent plasmatron addition. SI engine operation is constrained by the knock limit at low speeds. A decrease in the ONR would allow for use of higher compression ratios. Typical compression ratio of a conventional SI engine operating at stoichiometry is around 10. Based on previous research relating a change in compression ratio to octane requirements (e.g. Kalghatgi [5] and Russ [6]), the ONR increases by around 5 numbers per compression ratio increase in the 10-15 compression ratio range.

1.3 The Plasmatron Engine System

1.3.1 Description

Figure 1-1 illustrates the generalized engine concept. A fraction of the fuel goes to the plasmatron and the rest of the fuel mixes with air in the intake port like in a normal port fuel injected engine. In this concept, gasoline and air enter the reformer and the mixture is partially oxidized to H₂, N₂, and CO mixture, with small amounts of water and carbon dioxide. This hydrogen rich gas is cooled if needed and combined with air/fuel mixture just before it enters the cylinder to form a homogenous mixture prior to combustion.

The main advantage of the reformer engine concept is that current engine technology can be used. The disadvantages are: electrical power requirement of the reformer, fuel conversion efficiency of the reformer, and added complexity.

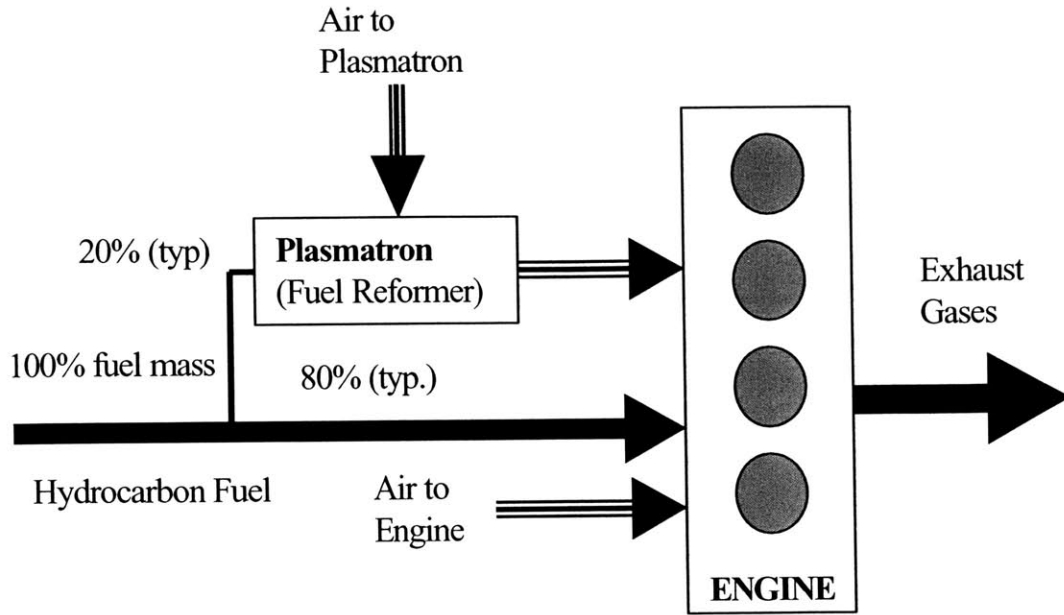
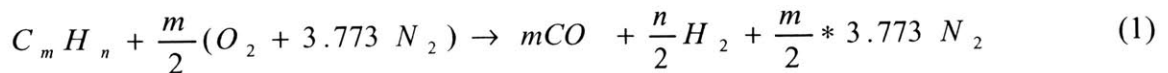


Figure 1-1 Set-up of plasmatron engine system

1.3.2 The Plasmatron

While hydrogen for this application could come from numerous sources, the particular technology used in this concept is an on board Plasmatron fuel reformer (Figure 1-2). Invented at the MIT Plasma Science and Fusion Center, the Plasmatron is a partial oxidation fuel reformer. Several studies have shown that the use of an on board fuel reformer can significantly reduce NOx emissions and increase efficiency [7,8]. Ignition of the rich mixture is provided by a high-energy, non-thermal plasma discharge. After ignition, the mixture completes a partial oxidation reaction within the reactor volume downstream of the electrodes. The ideal chemical reaction is shown in equation (1).



The majority of the reactants participate in the ideal reaction but a small portion undergoes complete oxidation, producing carbon dioxide and water. The ideal and typical product compositions are shown in Table 1-2.

Table 1-2 Plasmatron product composition and efficiency

Plasmatron Products	Ideal Plasmatron	Typical Plasmatron
H ₂	25%	20%
CO	26%	22%
N ₂	49%	51%
CO ₂	0	2%
H ₂ O	0	4%
Small hydrocarbons	0	Less than 1%
Fuel conversion efficiency	84%	76.5%

The power requirement of the Plasmatron is around 4-5 MJ/kg H₂. In addition to this, the partial oxidation reaction is exothermic, indicating that some energy is lost as waste heat. The fuel conversion efficiency of the Plasmatron is defined as the chemical energy of the products divided by the chemical energy of the reactants (equation (2)).

$$\eta_{Plasmatron} = \frac{\dot{m}_{H_2} \cdot Q_{LHV_H_2} + \dot{m}_{CO} \cdot Q_{LHV_CO}}{\dot{m}_{Gasoline} \cdot Q_{LHV_Gasoline}} \quad (2)$$

where \dot{m} is the mass flow rate [kg/s] and LHV is the lower heating value [MJ/kg].

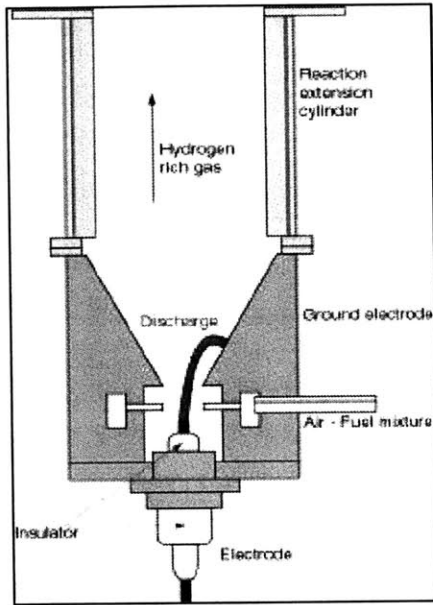


Figure 1-2 Plasmatron Schematic (Courtesy of PSFC)

Air fuel ratio or lambda does not represent true dilution when plasmatron is added to the charge mixture. Other diluents (CO , CO_2 , N_2) besides air are present and their heat capacities must be accounted for when comparing data with and without plasmatron gas in the charge mixture. A thermal dilution parameter (TDP) was proposed by Professor Heywood to normalize data with different diluents and compare them on a common basis. TDP is also useful when comparing dilutions of recycled exhaust gas and air. Most of experimental data are plotted versus TDP and it is also used in the model for emissions and efficiency calculations.

1.4 Previous Work

A model for evaluation of system-level vehicle architectural concepts was recently developed by Smaling at MIT [9]. This model encompasses the entire vehicle. The main focus is placed on the modeling of the fuel supply system, the engine, and the electrical system that supplies the power to the fuel reformer. An existing vehicle simulation called ADVISOR is used to model all other powertrain and vehicle systems. The objective of Smaling's work was to identify the most promising architecture of hydrogen enhanced, high efficiency, low emissions, homogeneous charge, highly diluted SI engine. After identifying high level architecture

attributes, Smaling focused on the three most attractive concepts. The methodology used in his analysis was derived from multi-variable, multi-objective optimization, known as multi-disciplinary system design optimization.

The most attractive concept, according to the analysis, is a boosted high compression ratio downsized lean SI engine. This model proved very valuable when assessing a wide range of possible concepts. However, to better assess the fuel economy and emissions benefits of this particular concept, the model needed improvement.

1.5 Objectives

The intent of this work is to improve the existing Smaling model to allow for more accurate evaluation of fuel economy and emissions of a lean-burn hydrogen-enhanced boosted SI engine concept. The existing model requires improvements in the following areas:

- engine friction
- boosting
- knock limitation on compression ratio
- brake specific fuel consumption (BSFC)
- SI engine emissions and performance maps
- integration of experimental combustion and emissions data

1.6 Methodology

Engine data from a modern 2.0 liter engine is used in this project. Given the engine geometry, net indicated engine efficiency can be extracted from the BSFC map using a friction model. Net indicated efficiency is then adjusted for lean operation and compression ratio changes due to presence of reformat gas. Empirical correlation is used to determine the air/fuel ratio at which the engine has the highest efficiency and stable combustion, based on the amount of reformat. Once this air/fuel ratio is calculated, it is used to determine the efficiency according to a correlation from the literature. Mechanical efficiency, obtained from the friction model using boosted intake pressures if required, together with the new indicated efficiency give the brake fuel efficiency.

Similarly, a correlation obtained from the experimental data is used to adjust the baseline engine brake specific NO_x (BSNO_x) emissions for a given engine concept. Experimental NO_x emissions as a function of air/fuel ratio and EGR are used to correct stoichiometric NO_x emissions for lean or EGR operation.

A 12 by 12 matrix, with load on one axis and speed on the other, is used to construct BSFC and BSNO_x emissions maps. Each load and speed point is run through the model separately to calculate the fuel consumption and NO_x emissions for a particular concept. These maps serve as an input to ADVISOR where the vehicle is configured and run through a specified drive cycle. Fuel economy and emissions are calculated and serve as a basis for comparison among the concepts of interest.

The first step in the process of improving the existing model was to obtain more combustion and emissions data. Data were collected for experiments run at three different load and speed points. After analysis, correlations were developed to incorporate experimental results into the BSFC and NO_x emissions models.

The next step was to evaluate each sub-model and try to improve it by incorporating experimental data and theoretical correlations from the literature. By doing so, the architecture of the model itself needed reevaluation and large parts of Smaling's model needed rewriting. Detailed descriptions of sub-models are included in chapter three. Once the model was completed, a conventional, naturally aspirated stoichiometric SI engine concept was evaluated as a baseline for comparison.

(This page was intentionally left blank.)

CHAPTER 2 EXPERIMENTAL METHOD

2.1 Overview

A large portion of the model is based on well-established physical models for given engine parameters. NO_x emissions and engine efficiency are the two most important parameters in this study, therefore, experimental data is used to calibrate the physical efficiency model and develop an empirical model for engine out NO_x emissions. Data were collected from experiments conducted at operating conditions that were representative of the engine operation during the chosen drive cycles.

This chapter describes the experimental apparatus and procedure. The results for efficiency, NO_x emissions and exhaust temperature are presented at the end of this chapter. All other experimental data are in the appendix. The efficiency, NO_x emissions, and exhaust temperature models, based on this experimental data, are presented in Chapter 3.

2.2 Operating Conditions

Shaded region in Figure 2-1 represents most common area of engine operation during highway and urban drive cycles, which are introduced in more detail in Chapter 3. Three operating points were chosen to represent this whole region. Two different loads and two different speeds were chosen to allow for straightforward interpolation between these points, if the data were a lot different. For EGR dilution, two test points were taken in the same region.

Air dilution experimental operating conditions:

- 350 kPa NIMEP at 1500 rpm
- 750 kPa NIMEP at 1500 rpm
- 750 kPa NIMEP at 2500 rpm

EGR dilution experimental operating conditions:

- 350 kPa NIMEP at 1500 rpm
- 520 kPa NIMEP at 1500 rpm

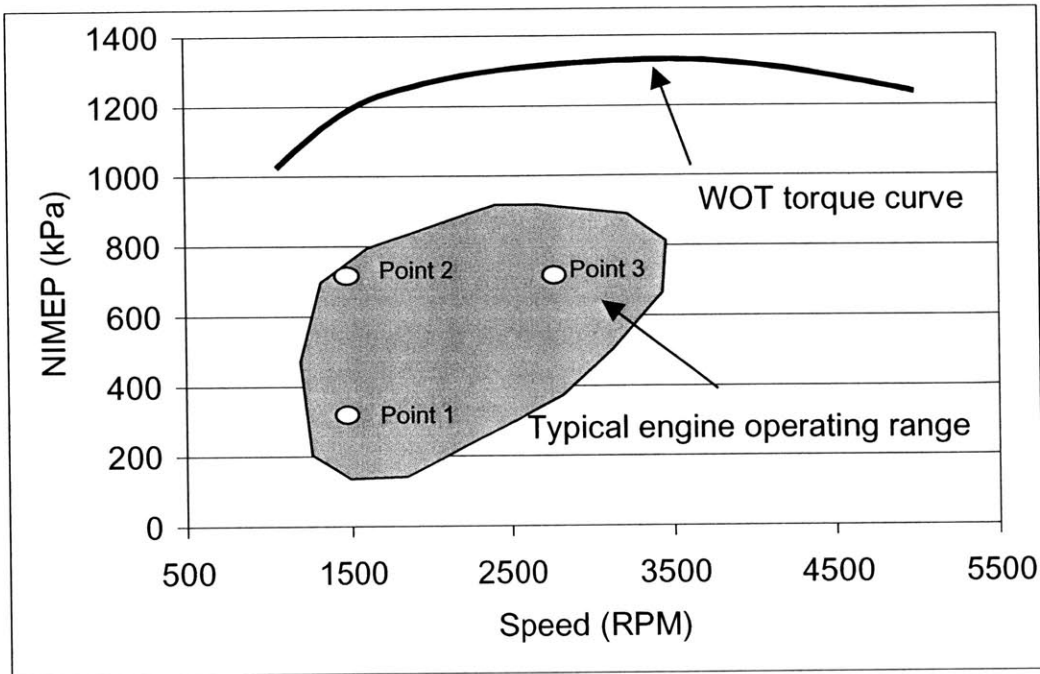


Figure 2-1 Typical engine operating regime

2.3 Experimental Procedure

At each of the three operating conditions, experiments were performed with three different fuel combinations: indolene only, indolene and 15 percent plasmatron gas addition, and indolene and 30 percent plasmatron addition. For each of the three different fuel supplies, data was recorded at constant load and speed for a number of points, starting from stoichiometric and adding diluent until the misfire limit was reached.

The source of plasmatron gas for the experiments was bottled gas mixed to represent ideal plasmatron gas with composition as defined in Table 1-2. The actual Plasmatron reformer is still being developed at the Plasma Science and Fusion Center and for the purpose of this study, it was much simpler to use bottled gas that simulates the ideal output gas of the reformer instead of dealing with added complexity of controlling the Plasmatron.

2.4 Engine Setup

2.4.1 Engine Specifications

The engine used in this study is a single-cylinder Ricardo Hydra MK III. The original engine head was replaced with a B5254 Volvo head that has a modern combustion chamber. The spark plug is located in the center of the pentroof combustion chamber with two intake and two exhaust valves on opposite sides. The valves are actuated with belt-driven dual overhead camshafts. Turbulence, mainly tumble, is increased with a charge motion control plate that was added in the intake manifold as described by Tully [2]. Table 2-1 shows detailed engine specifications.

Table 2-1 Engine Specifications for Volvo-Ricardo Research Engine

Displaced Volume (cm ³)	487
Clearance Volume (cm ³)	54
Bore (mm)	83
Stroke (mm)	90
Connecting Rod Length (mm)	158
Compression Ratio	10.1
Valve Timing	IVC 60° ABDC; IVO 0° ATDC
	EVO 8° ATDC; EVO 68° BBDC
EGR Pipe Diameter (mm)	19.1
Exhaust Manifold Diameter (mm)	28.6

The operator controls the engine by adjusting the fuel injector pulse width (IPW) and spark timing with a MoTeC M4 engine controller. Other important parameters specified by the engine controller are injection timing (end of injection set to 385 CA degrees BTDC) and coil dwell time (4 ms).

2.4.2 Air Intake System

A stationary Atlas Copco air compressor was added to the intake air system to allow for intake pressures higher than one atmosphere. The compressor supplies air at 60 psi that is regulated to a desired maximum boost in the damping tank upstream the throttle. The air supplied to the engine is controlled in a conventional way by the throttle. There is a valve that can switch between boosted and atmospheric air supply and is shown in Figure 2-2.

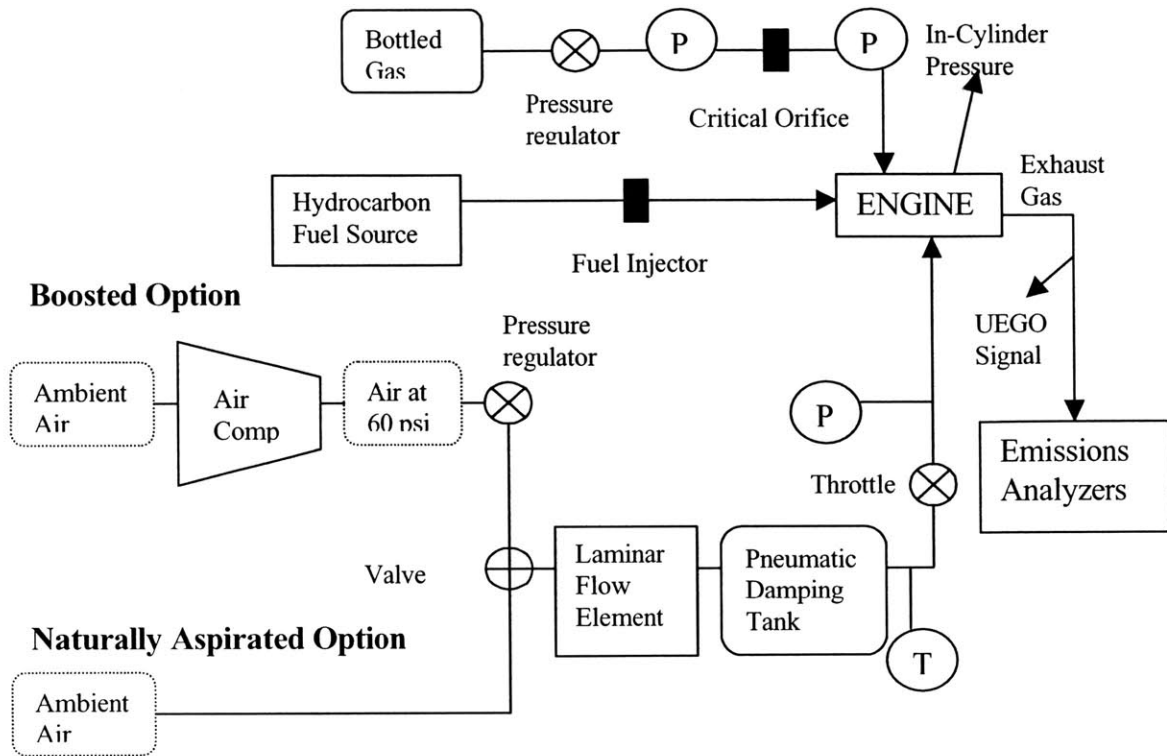


Figure 2-2 Engine instrumentation and air intake system

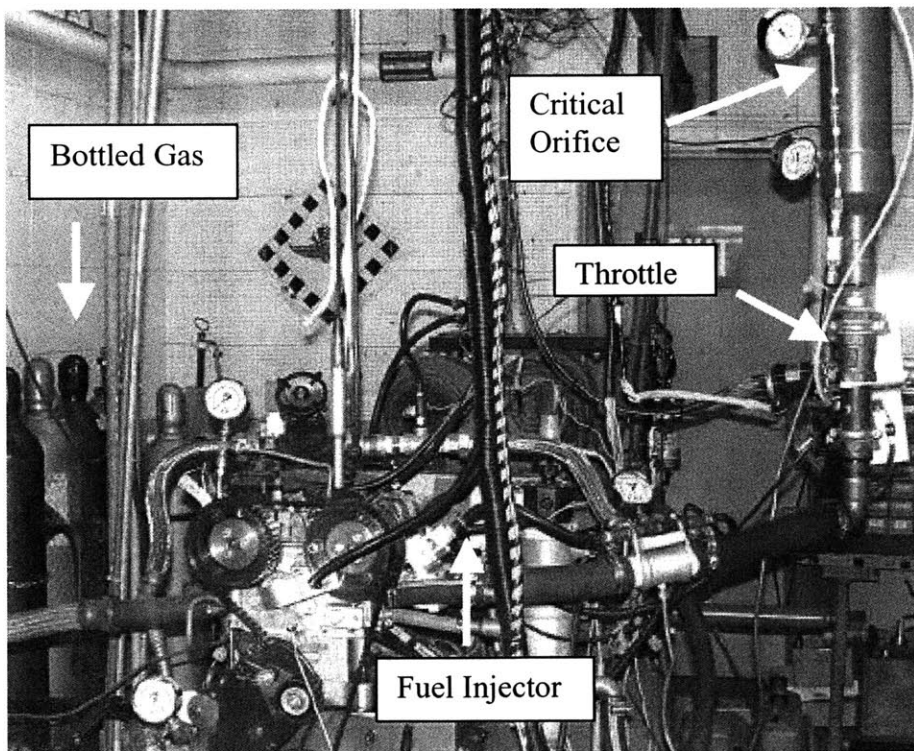


Figure 2-3 Picture of the Engine Setup

2.4.3 Hydrocarbon Fuel

Indolene, Phillips Chevron UTG-96 [10], was used as a reference fuel in the experiments. Table 2-2 lists important fuel properties of UTG-96.

Table 2-2 Fuel Properties of UTG-96

PROPERTY	
Research Octane Number	96.1
Motoring Octane Number	87.0
Lower Heating Value (MJ/kg)	43.1
Carbon Content (%)	86.5
Hydrogen Content (%)	13.5
Antiknock index	92
H/C molar ratio	1.93

2.4.4 Exhaust Gas Recirculation System (EGR)

An external EGR system was added to the experimental engine setup (Figure 2-4) to investigate the effect of very high levels of dilution with exhaust gas and compare this data to air dilution data. A pipe, with a diameter larger than fifty percent of the exhaust pipe diameter (Table 2-2), was attached to the exhaust manifold about three inches away from the exhaust port. On the intake side, the EGR pipe was connected through a tee into the intake manifold in the same location, where the reformat gas was added, downstream of the throttle and before the fuel injector.

A high temperature gate valve was connected to the EGR pipe along with an orifice. The valve and the orifice were used to adequately control the EGR flow. Based on the EGR flow and operating conditions, a range of orifices was used with diameters ranging from 4 to 18 mm. The EGR line was not heated since the EGR temperature remained sufficiently high to prevent condensation. The recycled exhaust gas was not cooled either and temperatures depended on the operating conditions and flow rate.

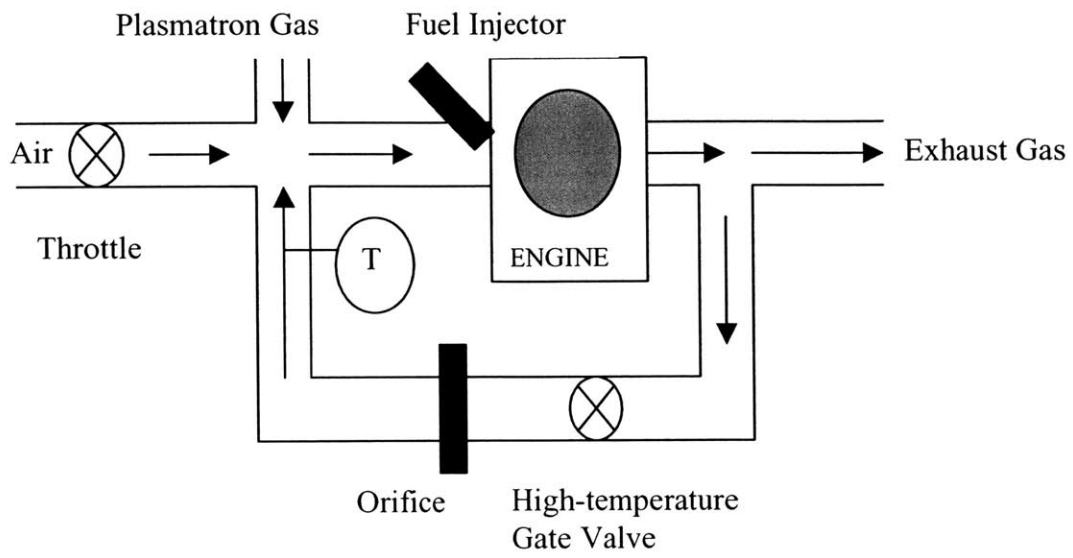


Figure 2-4 EGR System Schematic

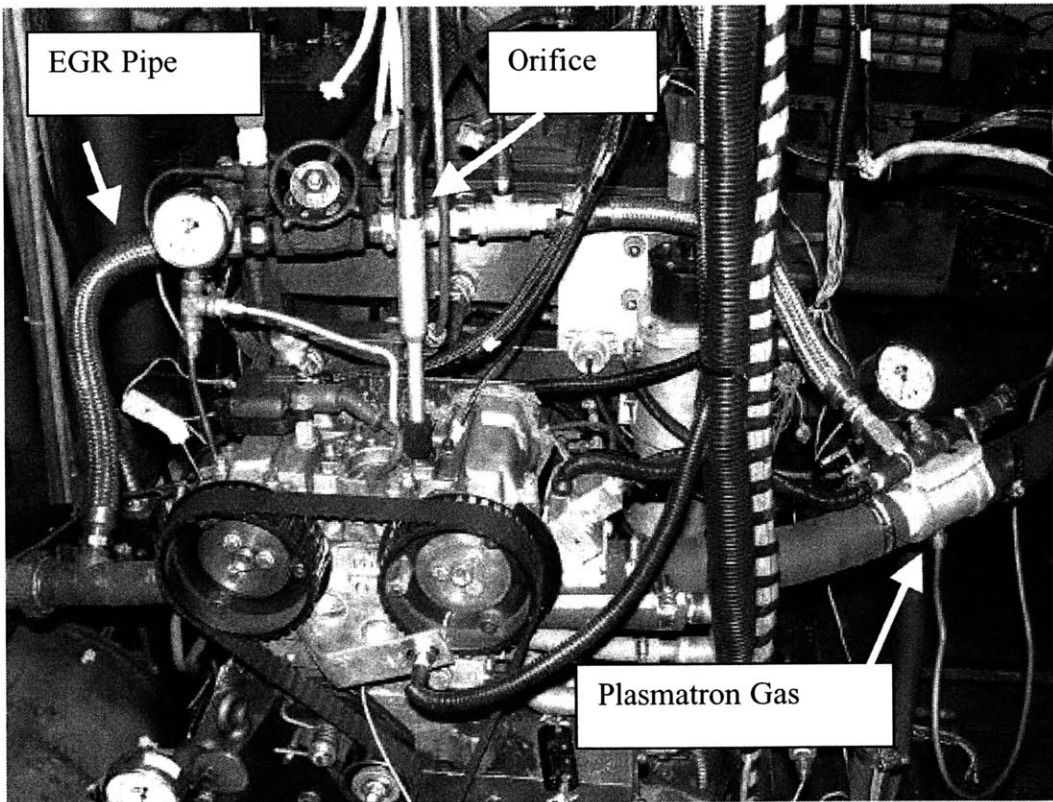


Figure 2-5 Picture of EGR System

2.5 Engine Control and Measurements

2.5.1 Intake Air (volume, pressure, temperature)

A butterfly valve controlled by a stepper motor regulates the flow of air. Omega pressure sensor (PX 176, 0-50 psi range) is used to measure the manifold air pressure. The volume of air entering into the engine is measured by a Ricardo Viscous Flow Meter (laminar flow element). Omega differential pressure sensor (PX 140, 0-20 psi gage) measures the differential pressure across the meter. The mass flow rate of air is calculated from the volume flow rate using the temperature (after the damping tank) and the pressure (after the throttle) of air, to calculate its density.

2.5.2 Engine Fluids Temperature

For all experiments, the coolant temperature was held constant at warmed-up conditions (85-90°C). An inline heater is used to raise the coolant temperature and cold water is used to cool the coolant through a heat exchanger when the temperature of the coolant exceeds 90 degrees Celsius. The oil temperature is not controlled, but it was around 60 degrees Celsius throughout the tests.

2.5.3 Gasoline Flow Rate

A production Volvo fuel injector is used in the engine. This is a single hole injector whose fuel flow rate is determined by the injector pulse width since the pressure drop across the injector is held constant. The pulse width is characterized by the duration of injector orifice being open. The injector was calibrated by measuring the mass of fuel injected into a chilled graduated cylinder for a specified number of cycles at a specified injection pulse width. Engine controller provides an injector calibration option where the pulse width and number of injection cycles are controlled. The mass flow was linearly related to the IPW. The constant of linearity was used along with the IPW to measure the fuel flow rate in the experiments.

2.5.4 Gaseous Fuel Flow Rate

A calibrated critical orifice was used to measure the flow of plasmatron gas into the engine. High-pressure bottled gas was used to simulate the plasmatron gas from the reformer.

The mass flow rate of the gas is proportional to the upstream pressure only, when the flow is choked. A regulator on the high-pressure gas bottle was used to control the upstream pressure. The range of pressures was kept well above twice the downstream pressure of the orifice (intake manifold pressure) to ensure choked flow. The manufacturer of the orifices provided calibration tables from which the mass flow of plasmatron gas was determined as a function of upstream pressure.

2.5.5 Lambda Measurement

A wideband Horiba MEXA-110 λ Universal Exhaust Gas Oxygen (UEGO) meter was used to measure the relative air/fuel equivalence ratio in the exhaust. This measurement was checked with the mass ratio of fuel to air entering the engine and agreement within three percent was reached for all experiments.

2.5.6 In-Cylinder Pressure Measurement

In-cylinder pressure was measured with a side-mounted Kistler Model 6125B piezoelectric pressure transducer. The transducer was calibrated with a dead weight test to verify the linearity and establish the scaling factor. Since the piezoelectric transducers do not measure absolute pressure but only the changes in pressures, the pressure signal was pegged by processing data with an MIT Cycle Analysis program [11] [12]. The voltage at bottom dead center (start of compression) was set equal to the intake manifold pressure (absolute pressure). A flame arrestor was used on the pressure transducer to prevent thermal shock. The output of the pressure transducer was converted from current to voltage by a Kistler charge amplifier using calibration and sensitivity constants of the transducer. This signal was then sampled once per crank angle by a PC based data acquisition system running LabVIEW and processed to calculate indicated engine performance, such as: engine load, combustion characteristics and pressure statistics.

2.5.7 Emissions Measurement

Both NO_x and HC emissions were sampled by analyzers from California Analytical Instruments. Chemiluminescent NO/NO_x analyzer, model number 400 HCLD, utilizes the chemiluminescence principle for analyzing the NO or NO_x concentration in a gaseous sample.

Heated total hydrocarbon gas analyzer, model 300 HFID, uses the Flame Ionization Detection method to determine the total hydrocarbon concentration within a gaseous sample. Horiba Automotive Emission Analyzer, MEXA-554JU was used to measure the CO₂ concentration in the intake and exhaust. A vacuum pump, Varian 949-9451, was used to provide sufficient suction when measuring the CO₂ concentration in the intake.

2.5.8 Exhaust Gas Recirculation Measurement

To determine the concentration of recycled exhaust gas, the mixture of air, plasmatron gas and EGR in the inlet manifold was sampled and CO₂ emissions were measured. This reading was divided by the measured engine-out CO₂ reading, equation (3), to give the fraction of exhaust gas that is recycled from the exhaust manifold back into the intake manifold. This is a commonly used procedure in the automotive industry.

$$\%EGR = \frac{CO_{2_inlet}}{CO_{2_exhaust}} \cdot 100 \quad (3)$$

Knowing the fraction of the recycled exhaust gas, the mass flow rate of EGR was calculated according to equation (4).

$$\dot{m}_{EGR} = \frac{\%EGR \cdot (\dot{m}_{air} + \dot{m}_{Plasmatron} + \dot{m}_{fuel})}{1 - \%EGR} \quad (4)$$

2.6 Experimental Results

This section presents experimental results that are of importance for calibration of the model. All other supporting data such as burn angles, spark timings and peak pressures are included in the appendix. As mentioned in the description of plasmatron-engine concept, TDP is the main independent variable for presentation of experimental data. It is used instead of lambda or EGR to compare data for experiments with various fractions of plasmatron gas. TDP also allows for correlation of an equivalent dilution with air and EGR.

$$TDP = \frac{\Delta T_{stoichiometric}}{\Delta T} \quad (5)$$

where ΔT is defined as the chemical energy released during combustion per constant volume heat capacity of the unburned cylinder charge and thus represents thermal dilution of the mixture:

$$\Delta T = \frac{\sum_{i=1}^9 m_{X_i} \cdot Q_{LHV, X_i}}{\sum_{j=1}^5 m_{X_j} \cdot C_{V, X_j}} \quad (6)$$

with

$$\begin{cases} \chi_i \in (C_7H_{14}, H_2, CO, CH_4, C_2H_2) \\ \chi_j \in (H_2O, H_2, CO, CO_2, N_2, C_7H_{14}, C_2H_2, O_2, CH_4) \end{cases}$$

Since the change in specific heat of gases was ignored, ΔT only approximates adiabatic constant volume temperature difference between the burned and unburned gas. In the analysis of experimental data and in the model, specific heats of all species were evaluated at a temperature of 600 degrees Kelvin, approximately the temperature at the time of spark. $\Delta T_{\text{stoichiometric}}$ was determined, experimentally and by the model, to be around 3040 degrees Kelvin for a baseline configuration with no plasmatron operating at stoichiometric air-fuel ratio. Many of the combustion related parameters scale well with TDP since the flame speed is largely determined by the temperature rise across the flame [2].

2.6.1 In-Cylinder Combustion Data

2.6.1.1 Air Dilution

Net indicated fuel conversion efficiency data are presented in Figures 2-6 through 2-8 for three different operating points. All three graphs show a similar trend: as stoichiometric charge mixture is diluted with increasing amount of air, efficiency increases rapidly at first, reaches a peak and starts decreasing until it significantly drops off at the onset of partial burns and misfires. Efficiency increases due to higher ratio of specific heats, smaller heat losses, and less pumping work. As expected, efficiency increases with load and does not change with speed when comparing data for the three operating points. This trend is also seen on efficiency maps in Chapter 4. Peak efficiency in the experiments is around 12-14 % higher than at stoichiometry. For low load-low speed point, plasmatron addition seems to have a positive effect on efficiency

whereas for the other two points there does not seem to be a clear trend. Regardless of the amount of plasmatron used, data differs by less than 3% absolute, which is within the experimental error. However, 15% plasmatron data for all three operating points has a higher efficiency than indolene only and 30% plasmatron. It is important to keep in mind that this data is net indicated engine efficiency and not the system efficiency that includes plasmatron losses. The later is presented in appendix.

TDP at which peak efficiency occurs does not vary much for the three operating points. The same is true for the lean limit that is defined here as 3% COV of NIMEP presented in Figures 2-9 through 2-11. Peak efficiency and lean limit TDP move together and TDP of lean limit is about 7% higher than TDP of peak efficiency regardless of operating conditions. COV of NIMEP, which represents stability of combustion, remains relatively low for all experiments until first partial burns occur causing stability to rapidly deteriorate. Increasing the load extends the lean limit as can be observed when comparing Figures 2-9 and 2-10. On the other hand, increasing engine speed decreases TDP where lean limit occurs (Figures 2-9 and 2-11). As expected, a linear trend is observed between the amount of plasmatron addition and extension of lean limit. 15 % plasmatron addition extends the limit by about 7% while 30% plasmatron addition extends it by around 15%.

2.6.1.2 *EGR Dilution*

Efficiency does not increase as much with exhaust gas dilution as it does with air. Smaller pumping work due to higher intake pressures and lower heat losses contribute to efficiency gain, which is initially large but it levels off relatively quickly. However, up to 9% efficiency improvement was observed with plasmatron addition at high dilution levels when compared to zero dilution point. Peak efficiency is reached just before combustion becomes unstable and when compared to air dilution the efficiency curves in Figures 2-12 and 2-13 have much flatter peaks. Same trend is observed here as in air dilution plots, which is that at low load-low speed plasmatron addition has increasingly positive effect on net engine efficiency, whereas at higher load plasmatron addition does improve efficiency but as plasmatron fraction is increased from 15 to 30 percent there is not an evident gain. Again, the differences in efficiencies for a given TDP are very small and within experimental error.

At low load-low speed point, EGR dilution does not extend the limit as far as air dilution does (Figures 2-9 and 2-14). The lean limit is extended by 10% with 15% plasmatron and 20% with 30% plasmatron addition (Figure 2-14). Plasmatron addition seems to have a more significant effect on extending the EGR dilution levels when compared to air dilution. However, higher absolute levels of dilution are reached with air as a diluent.

Figure 2-24 shows all air dilution data from three different operating points for 0, 15, and 30 percent plasmatron addition on the same graph and a linear relation between lambda and TDP is evident. EGR dilution levels are not linearly related to TDP but when equivalence ratio is plotted versus TDP, the straight line from Figure 2-24 shown as parabola in Figure 2-25, a good match is established with EGR dilution data plotted versus TDP. Figure 2-25, with EGR data for both operating points, represents the correlation between amounts of EGR and air required for equivalent dilution levels. Plasmatron addition results in higher TDPs but this difference is relatively small when all air dilution data is plotted together in Figure 2-24. The same is true for dilution with exhaust gas.

2.6.2 NO_x Emissions

Regardless of the fact whether air or exhaust gas is used as a diluent, NO_x emissions decrease substantially with high dilution levels. NO_x emissions are very closely related to the peak in-cylinder temperature. EGR dilution at part load is a common strategy that automotive manufacturers use in their production engines to meet emission regulations. This section also graphically portrays the value of thermal dilution parameter.

2.6.2.1 *Air Dilution*

Figure 2-16 shows NO_x engine out emissions in grams per kilowatt-hour versus lambda. It is clear that all three curves have the same shape but they are horizontally offset, with larger plasmatron addition curve being the furthest to the left, showing the lowest dilution levels. Accounting for the contribution of additional diluents present in plasmatron gas, same data is plotted versus TDP in Figure 2-17. In this case all the data collapses into a single curve and TDP is clearly a better choice than lambda for presenting data with plasmatron addition. All three Figures, 2-16, 2-17, and 2-18 show the expected peak in NO_x emissions slightly lean of stoichiometric point and then emissions linearly decrease with almost identical slopes on the

semi-logarithmic graph as more air is added to the charge mixture. Reductions of up to 99% are observed at the lean limit when compared to stoichiometric levels. Actual levels of NO_x emissions vary with operating conditions, with higher NO_x at higher load due to higher in-cylinder temperatures, but the shapes of the curves past TDP of 1.2 are almost identical.

2.6.2.2 *EGR Dilution*

Figures 2-20 and 2-21 show similar trends as air dilution data with a linear decrease in emissions from TDP of 1.2 onwards on a semi-logarithmic graph. Comparable levels of NO_x emissions are achieved with EGR when compared to air dilution data except that with EGR, equivalent NO_x emissions are reached with lower dilution.

2.6.3 Exhaust Temperature

Exhaust temperature is another parameter that is used in this modeling study. It is used in the NO_x model and also when the concept involves a turbocharger. Figure 2-22 displays all air dilution data normalized to stoichiometric values for the three operating points plotted as a function of lambda. Lambda is used here instead of TDP since there is a linear relationship between the two parameters. Exhaust temperature is plotted in the same way for EGR dilution in Figure 2-23. The relationship is not quite linear but a cubic formula correlates the two parameters well.

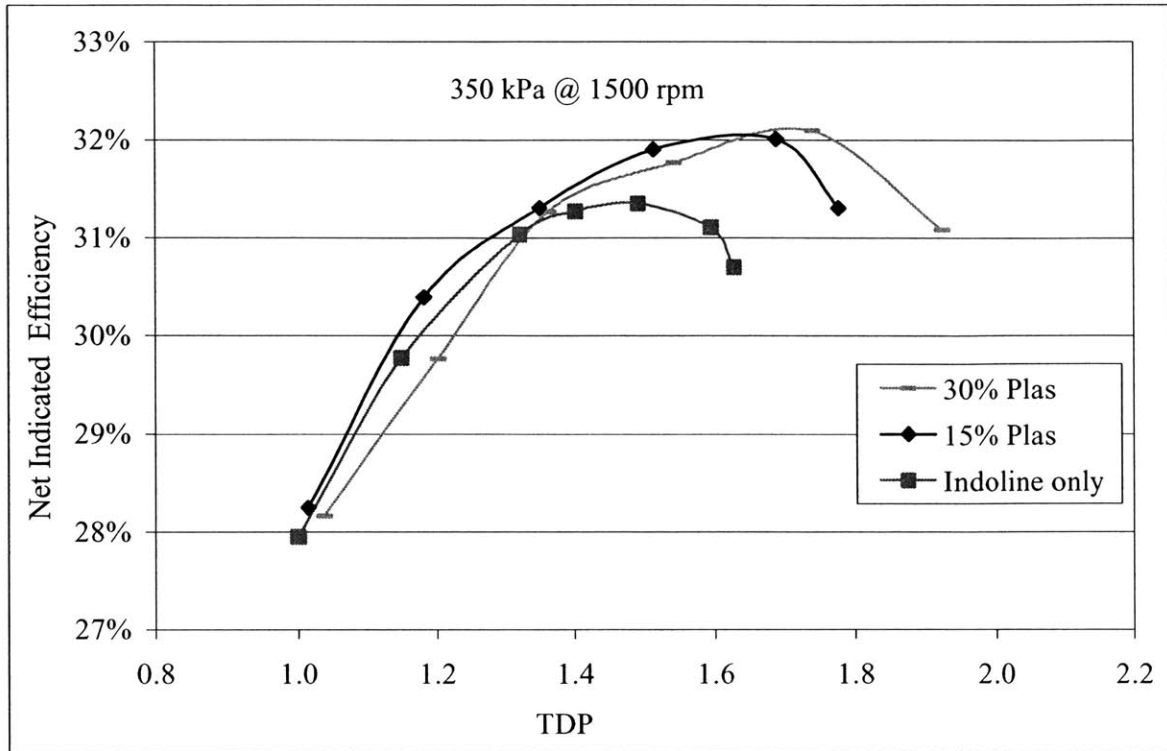


Figure 2-6 Air Dilution - Net Indicated Efficiency at 350 kPa @ 1500 rpm

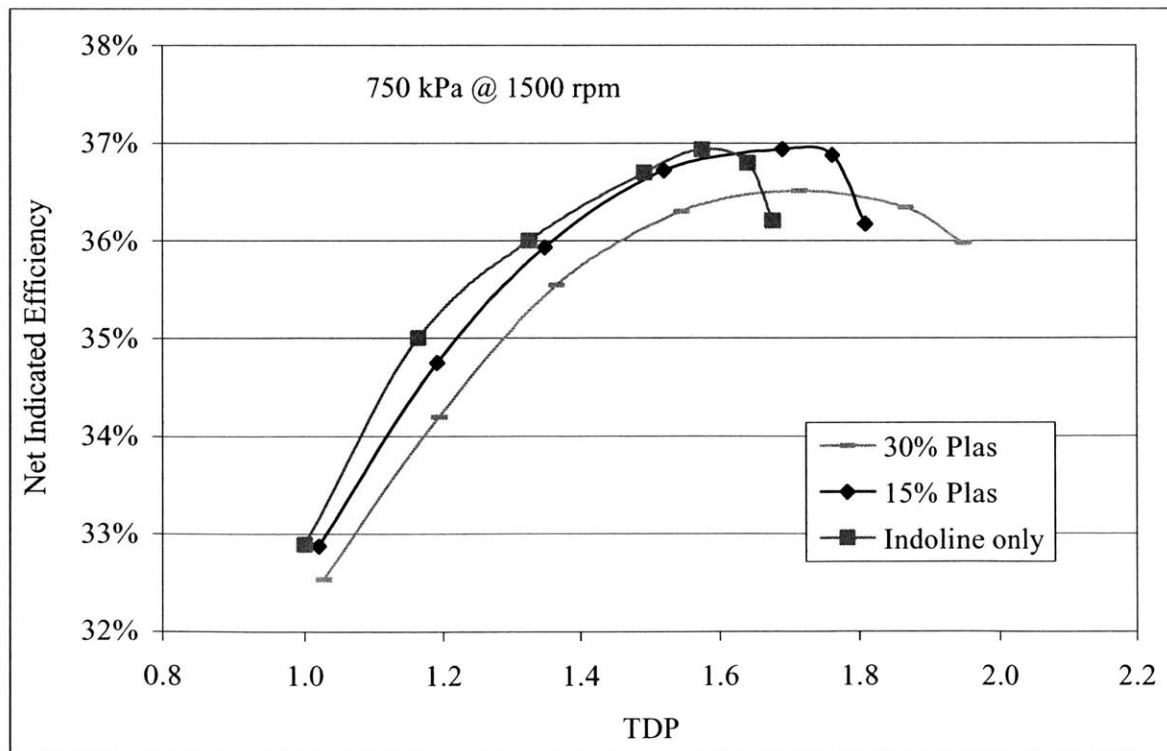


Figure 2-7 Air Dilution - Net Indicated Efficiency at 750 kPa @ 1500 rpm

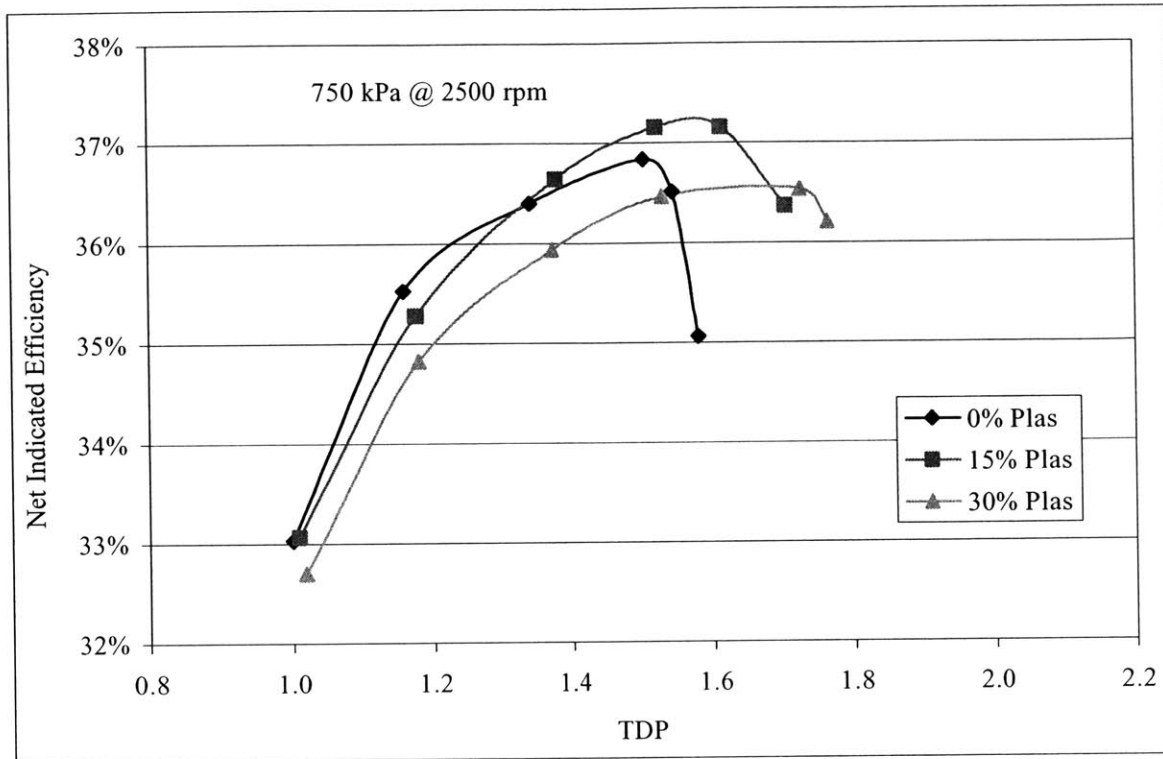


Figure 2-8 Air Dilution - Net Indicated Efficiency at 750 kPa @ 2500 rpm

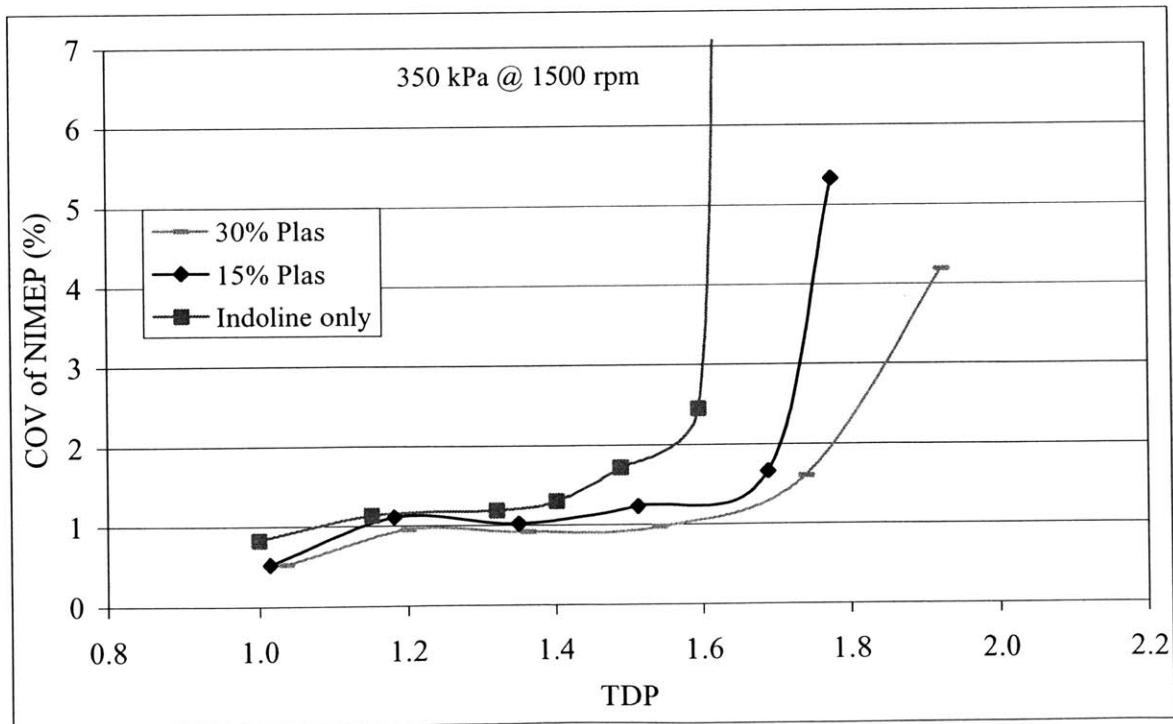


Figure 2-9 Lean Limit at 350 kPa @ 1500 rpm

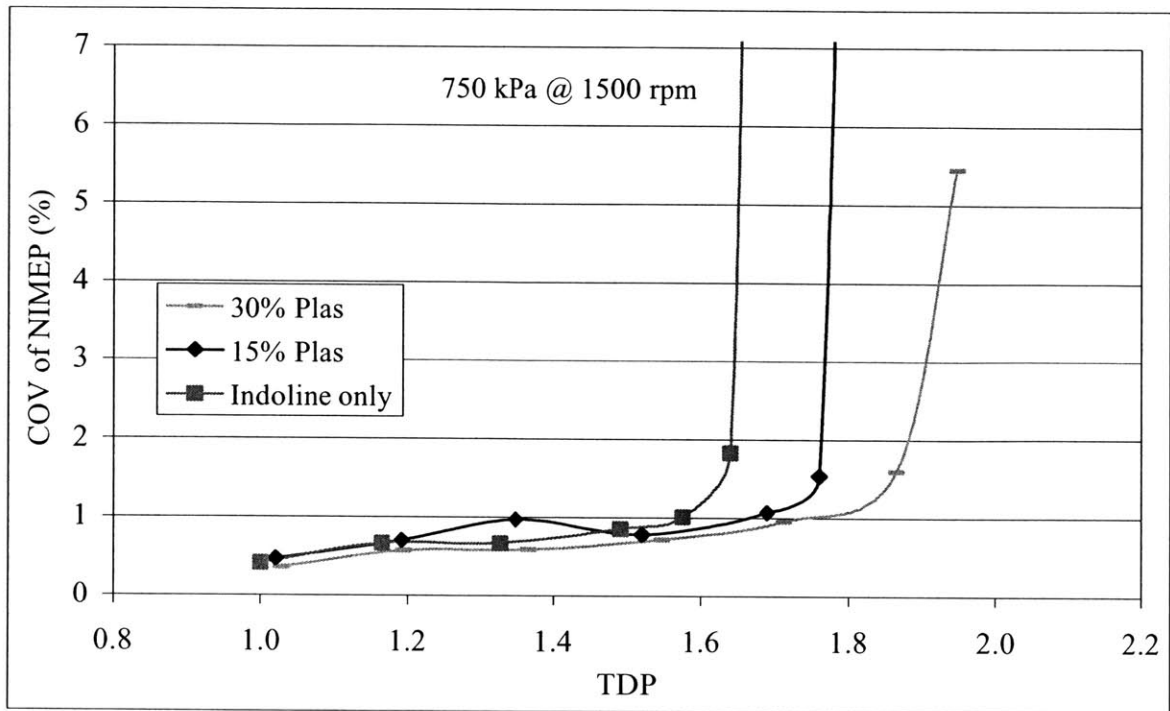


Figure 2-10 Lean Limit at 750 kPa @ 1500 rpm

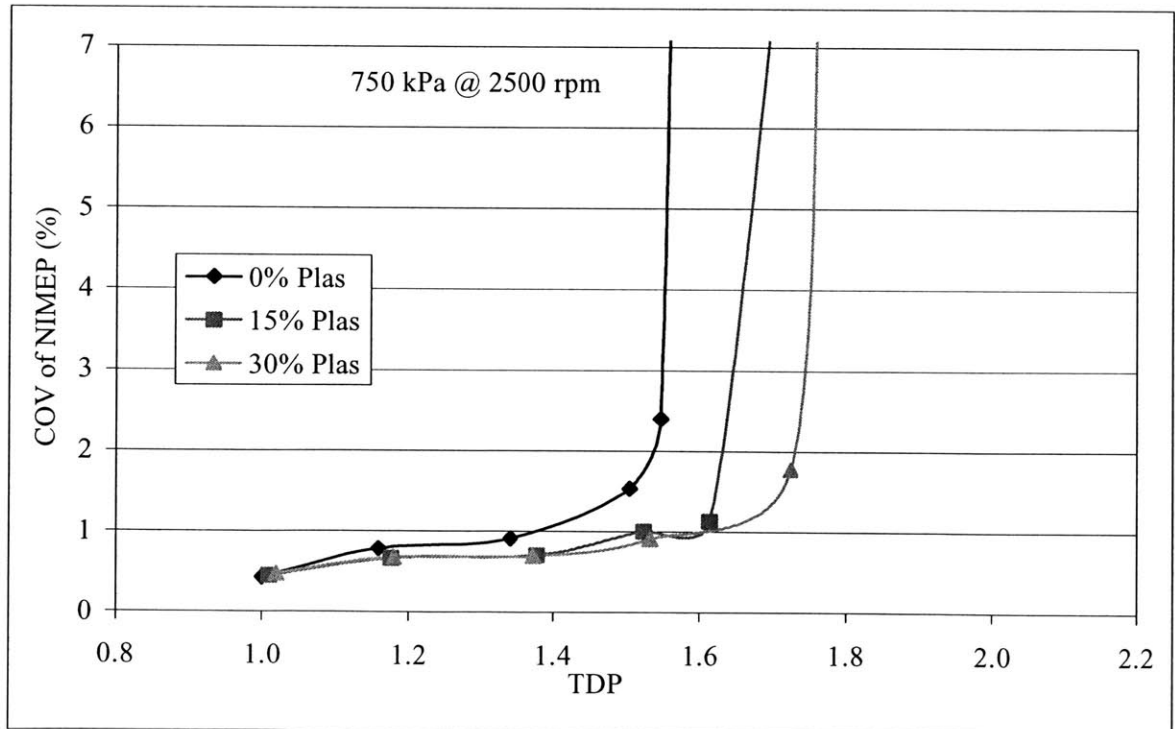


Figure 2-11 Lean Limit at 750 kPa @ 2500 rpm

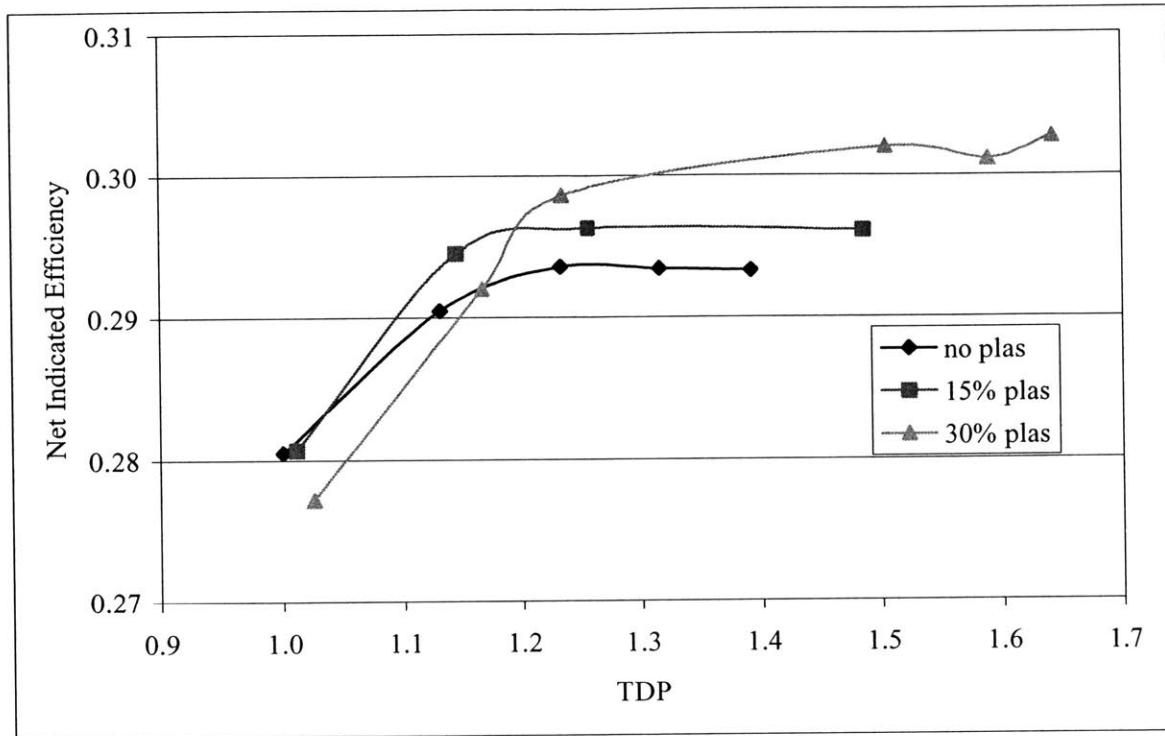


Figure 2-12 EGR Dilution - Net Indicated Efficiency at 350 kPa @ 1500 rpm

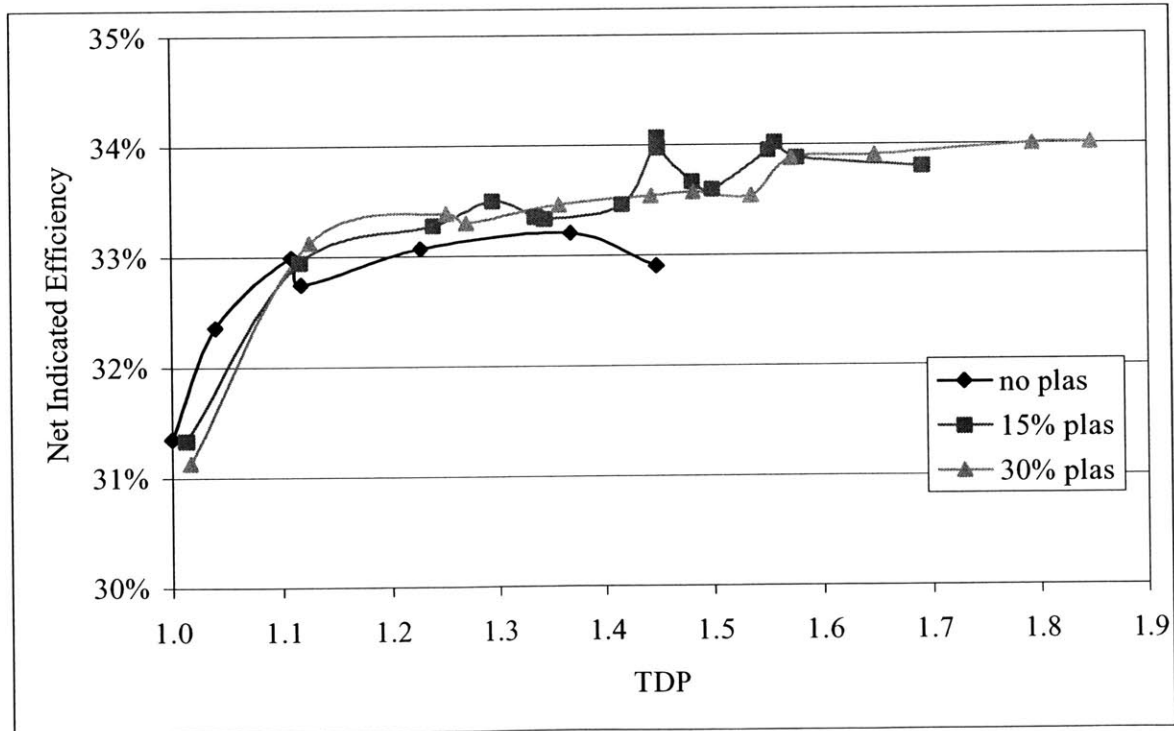


Figure 2-13 EGR Dilution - Net Indicated Efficiency at 520 kPa @ 1500 rpm

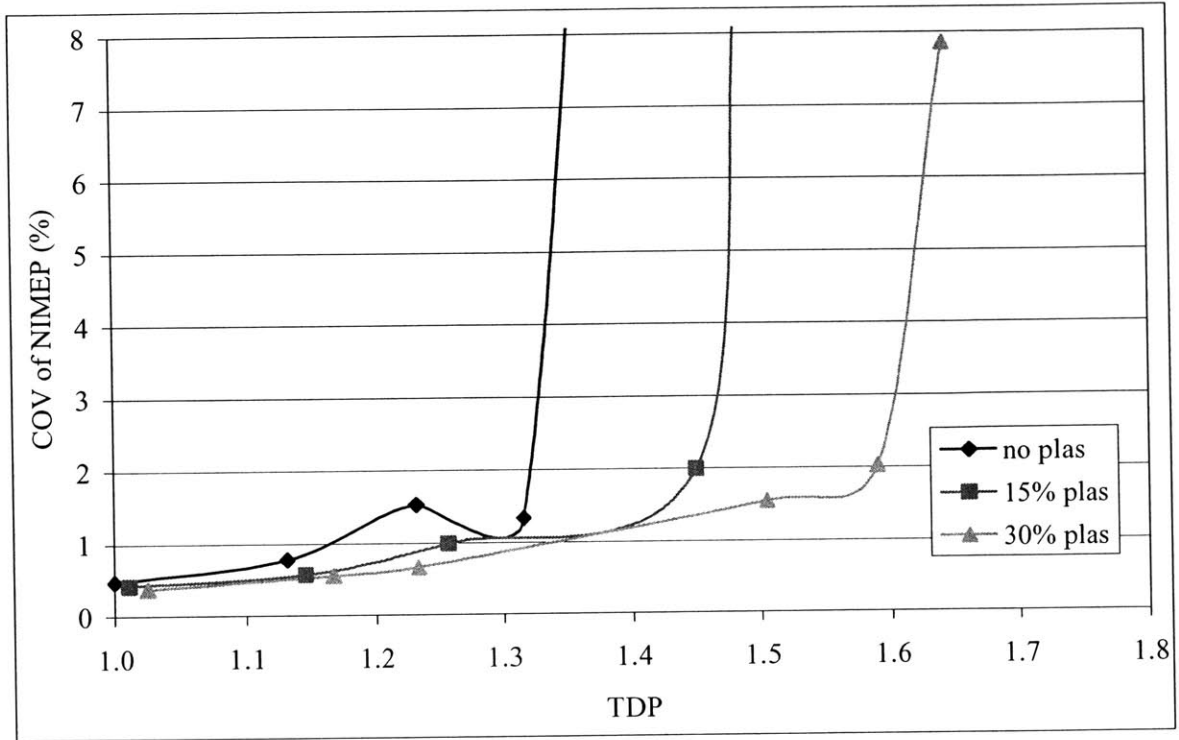


Figure 2-14 EGR Limit at 350 kPa @ 1500 rpm

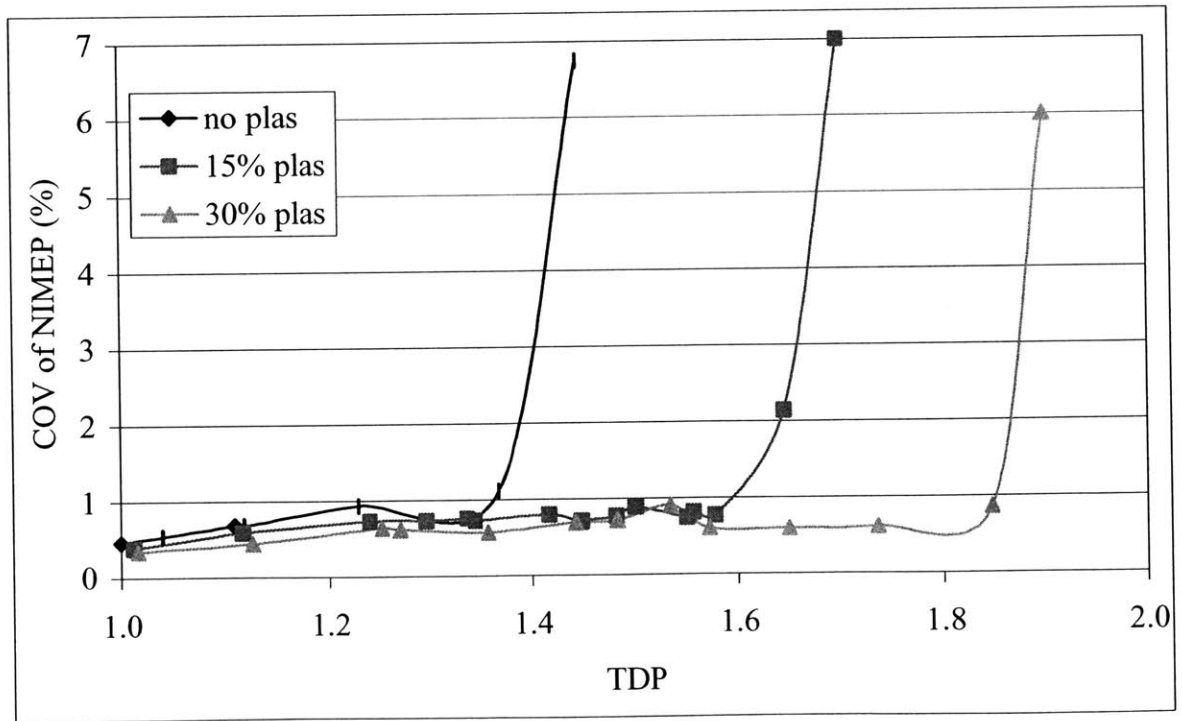


Figure 2-15 EGR Limit at 520 kPa @ 1500 rpm

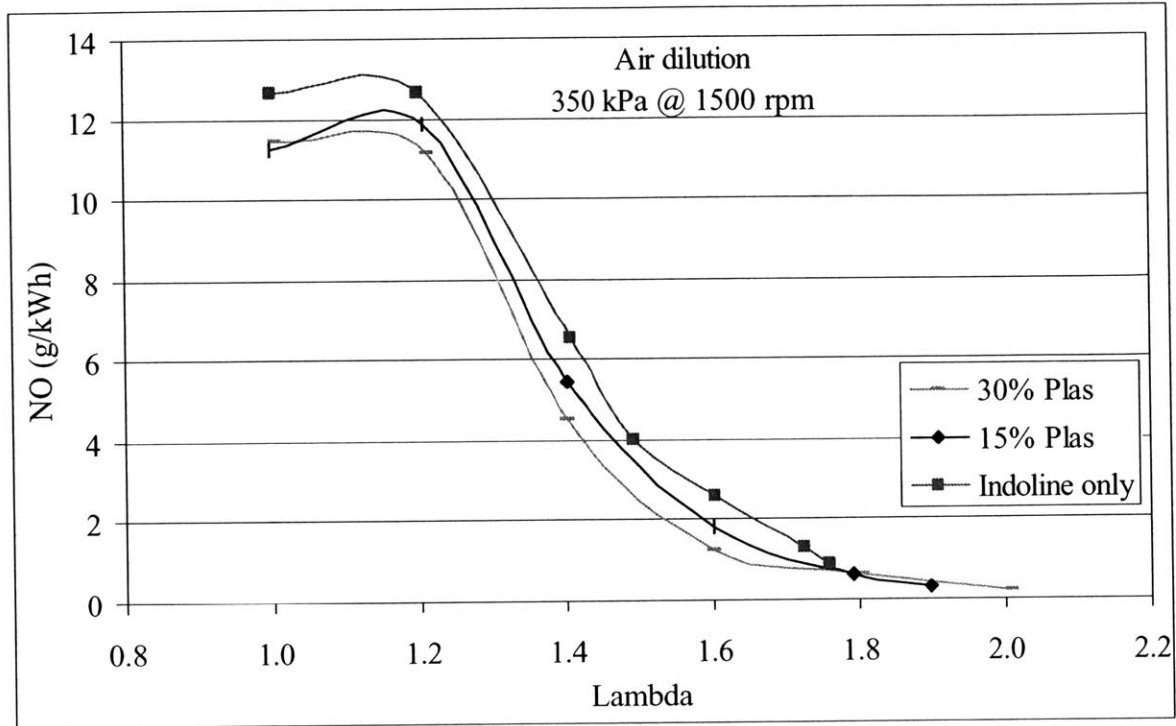


Figure 2-16 NOx emissions vs. Lambda at 350 kPa @ 1500 rpm

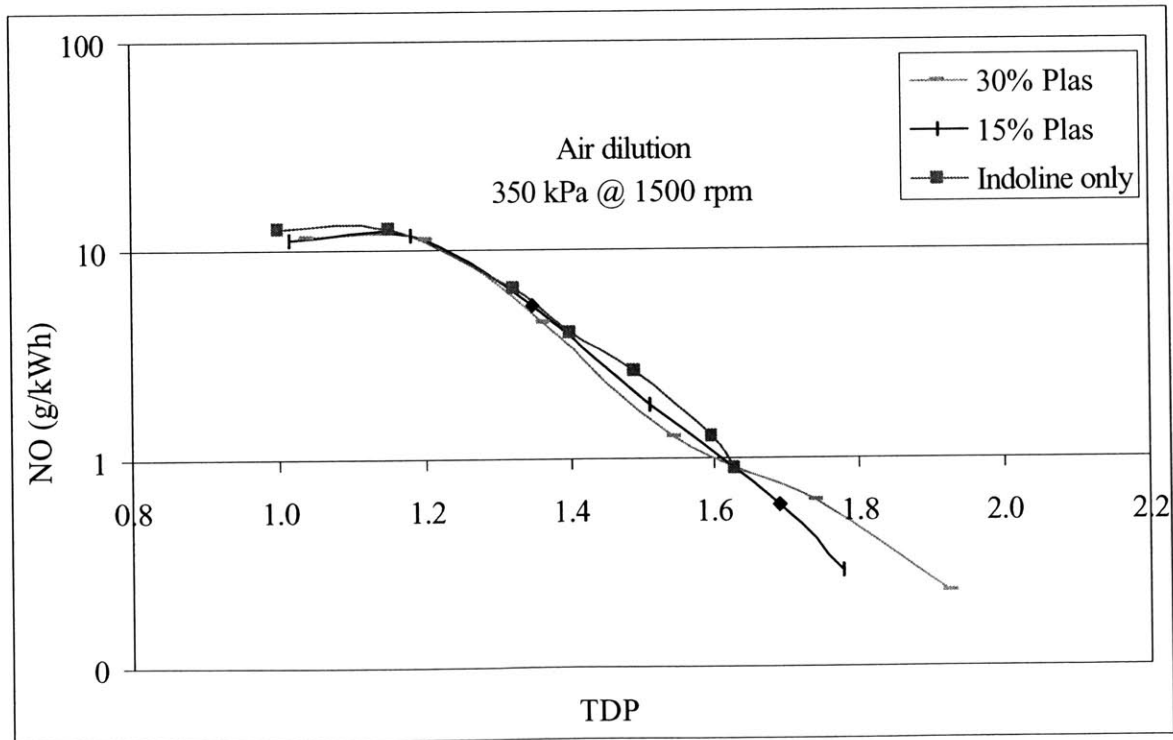


Figure 2-17 Air Dilution - NOx emissions vs. TDP at 350 kPa @ 1500 rpm

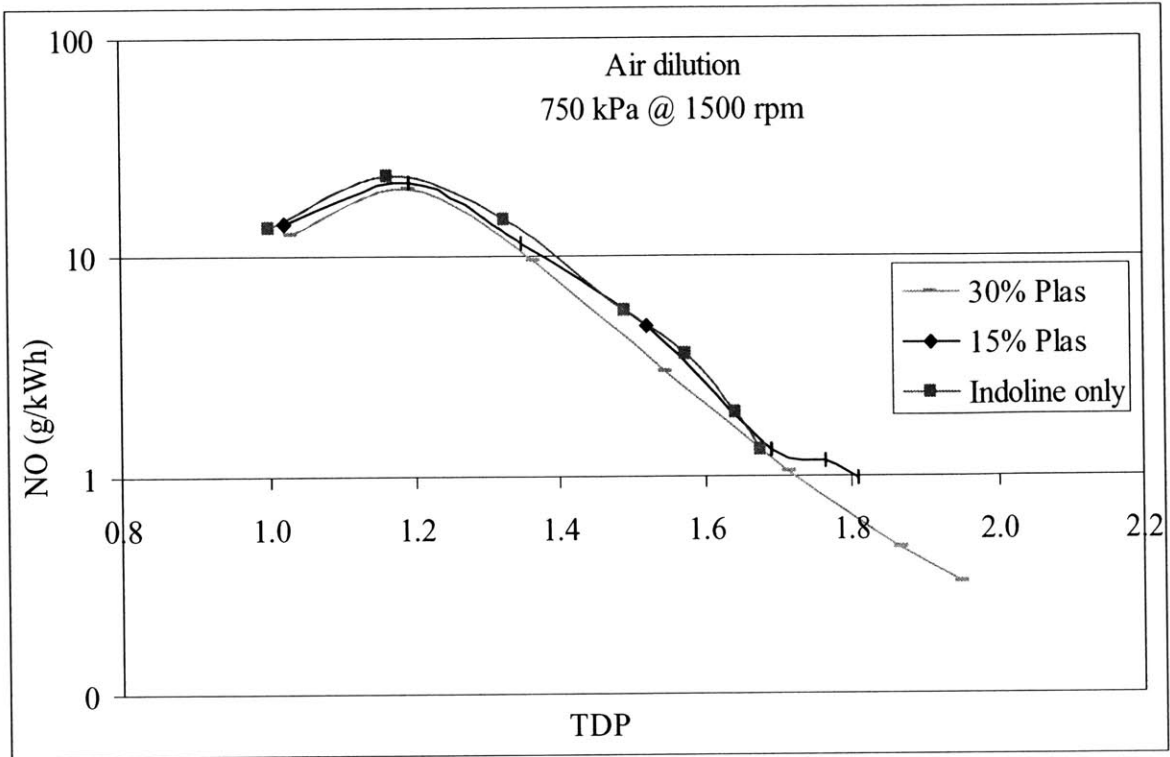


Figure 2-18 Air Dilution – NOx Emissions at 750 kPa @ 1500 rpm

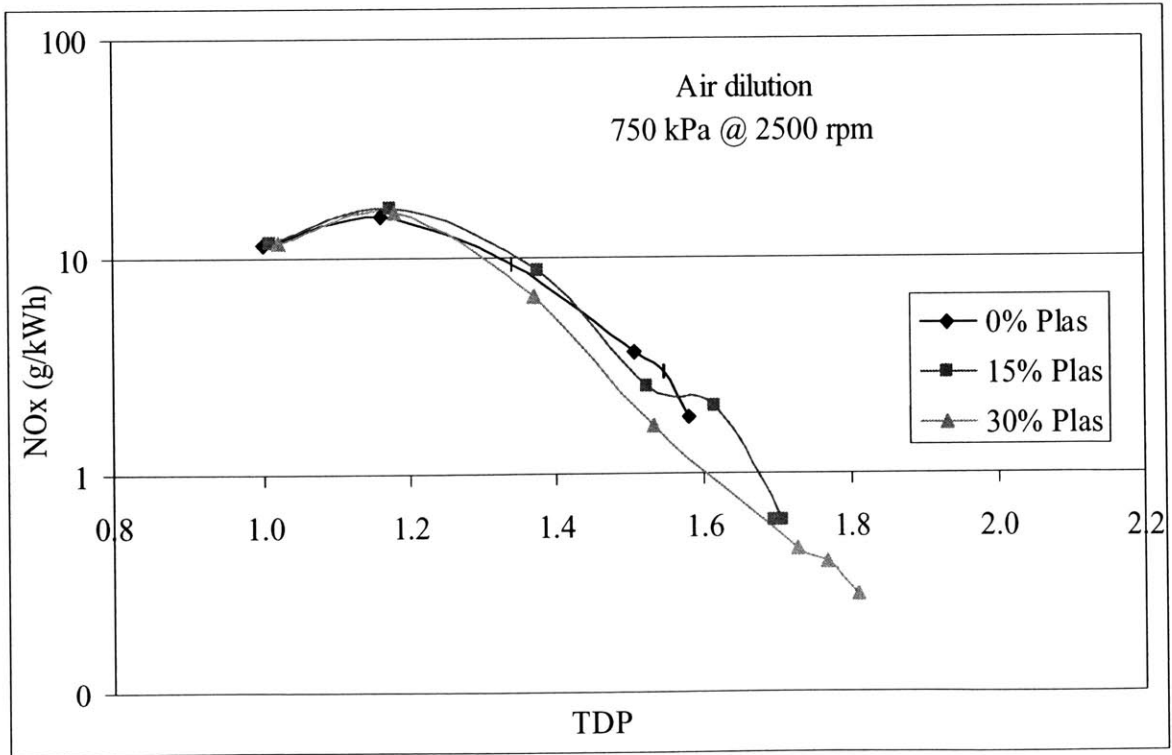


Figure 2-19 Air Dilution – NOx Emissions at 750 kPa @ 2500 rpm

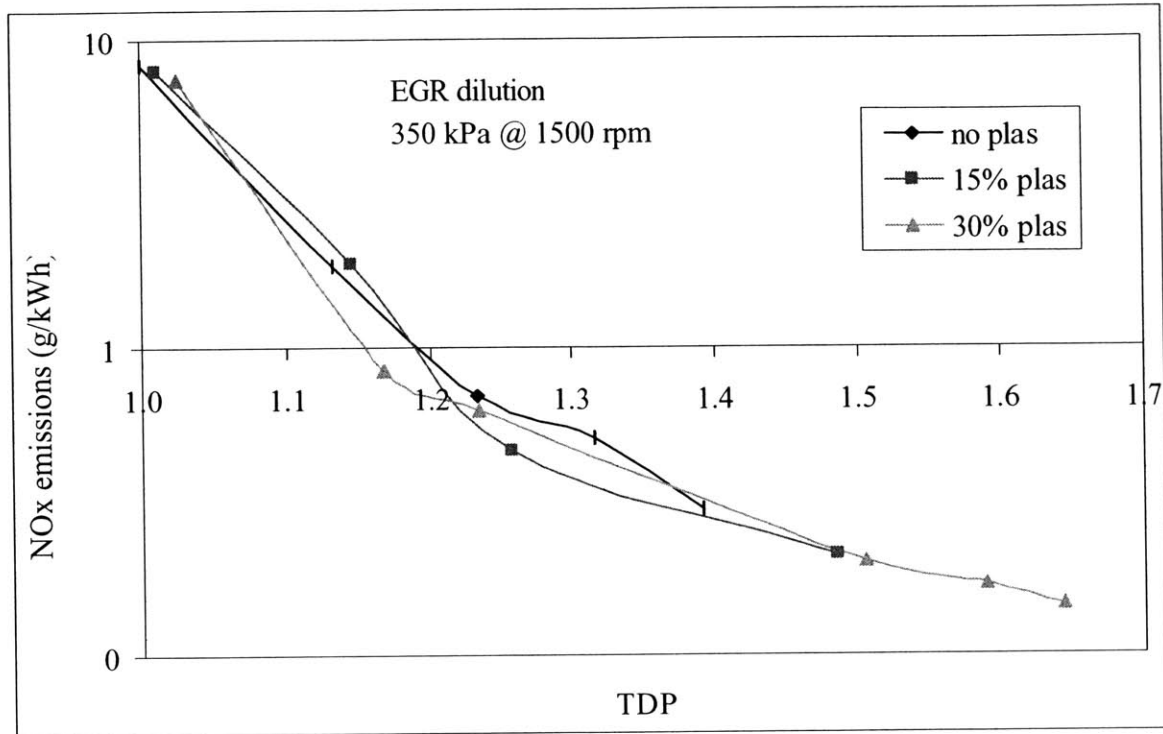


Figure 2-20 EGR Dilution – NOx Emissions at 350 kPa @ 1500 rpm

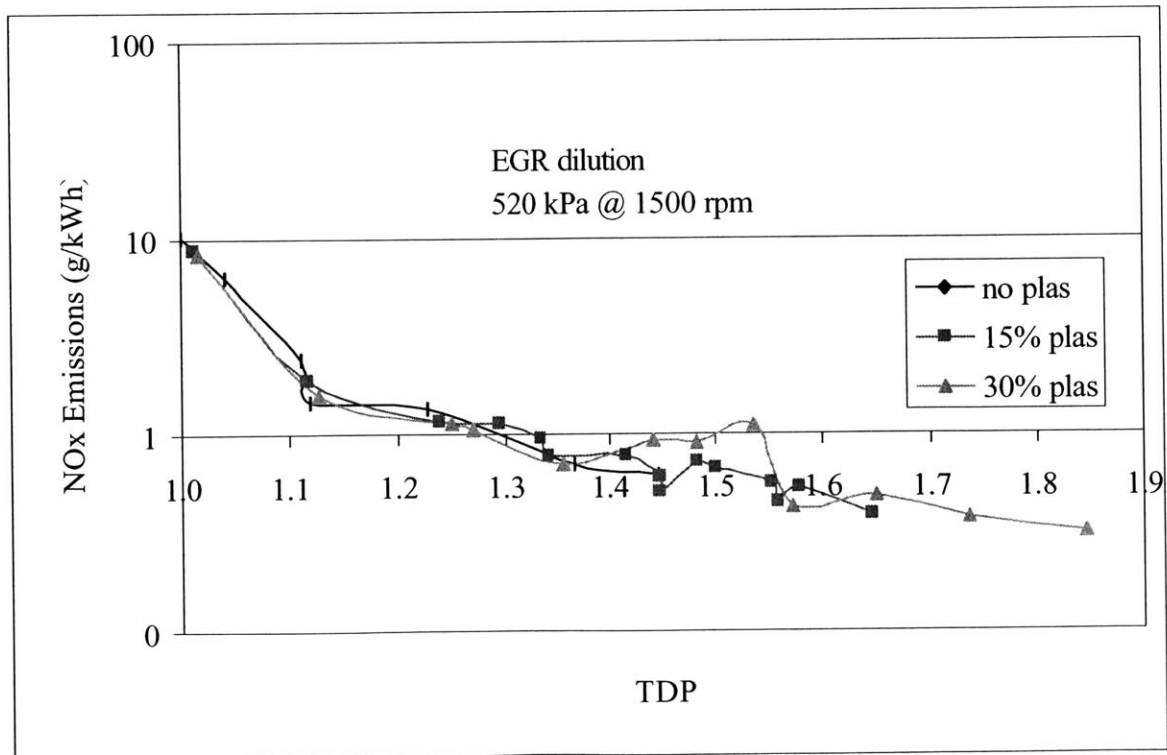


Figure 2-21 EGR Dilution – NOx Emissions at 520 kPa @ 1500 rpm

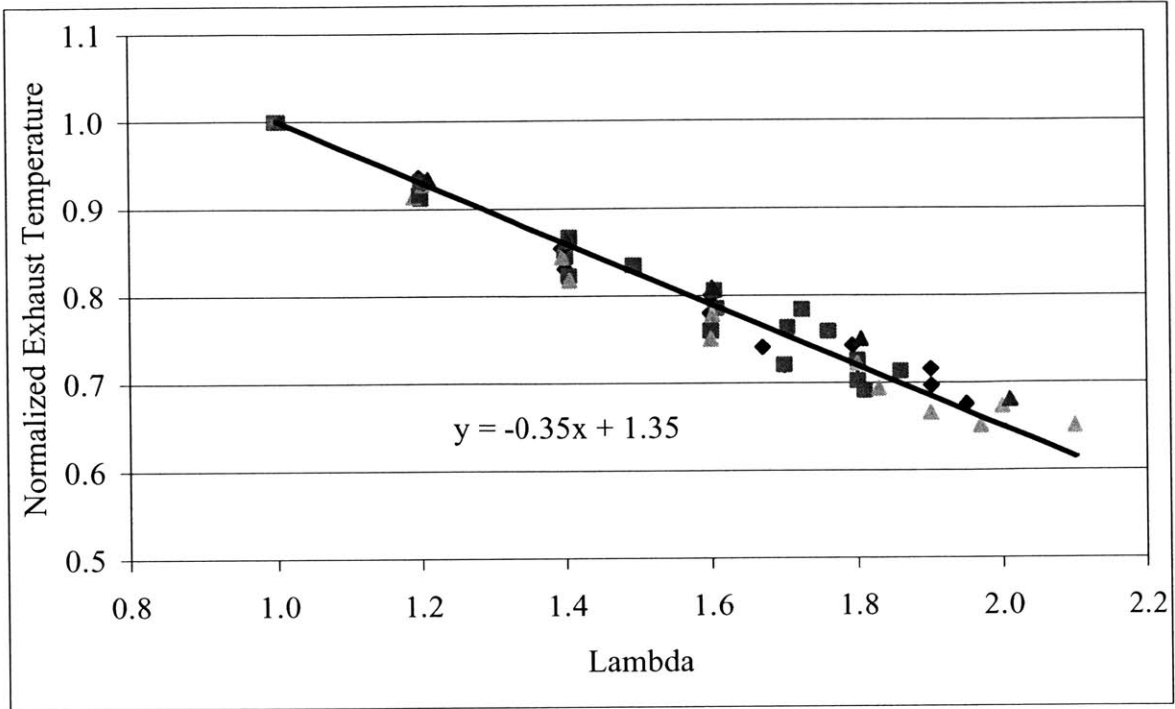


Figure 2-22 Normalized exhaust temperature as a function of air dilution

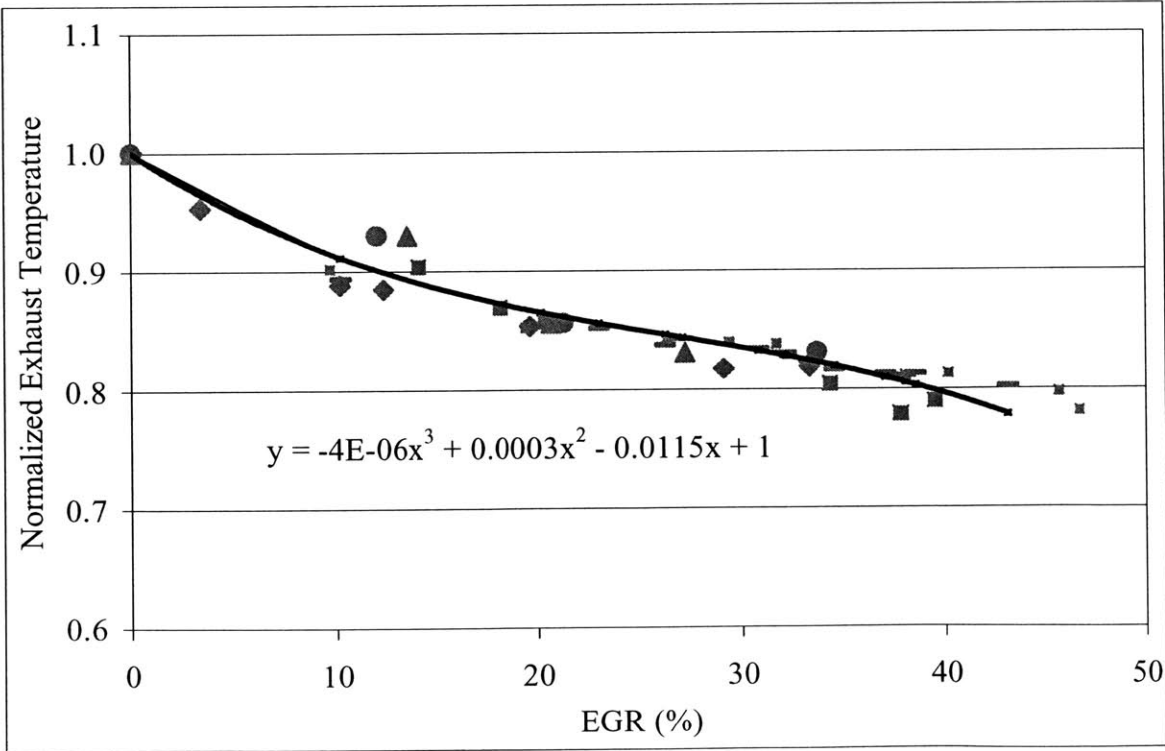


Figure 2-23 Normalized exhaust temperature as a function of EGR dilution

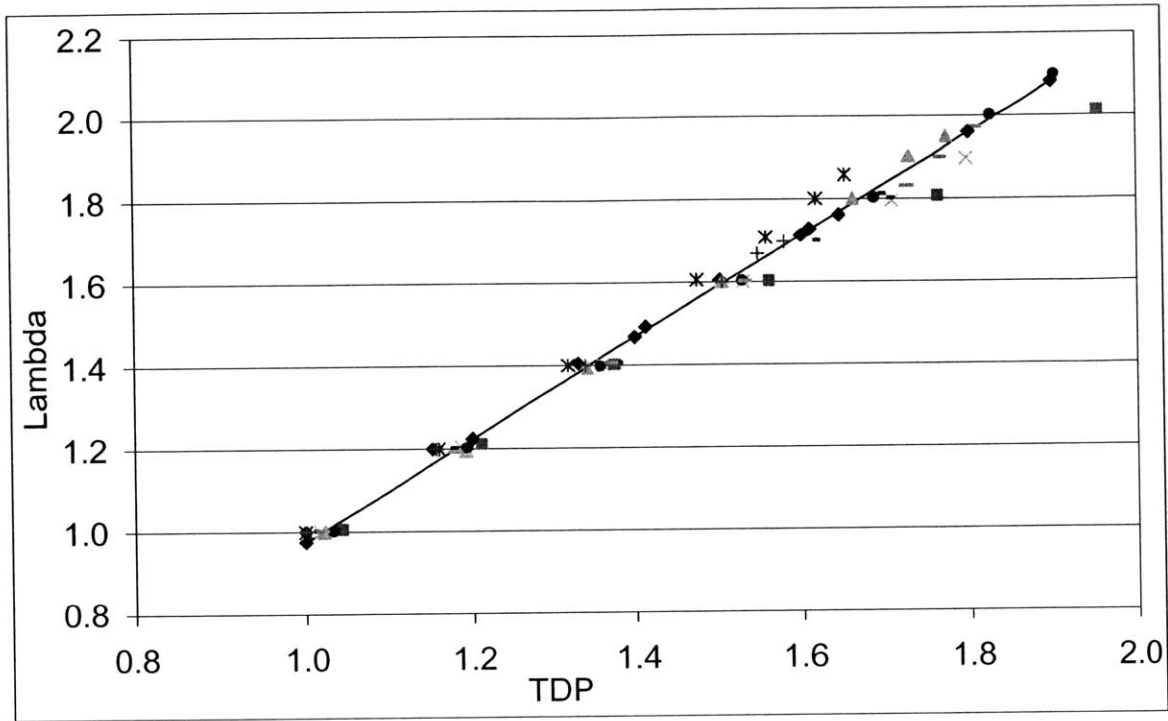


Figure 2-24 Correlation of TDP with lambda for air dilution data

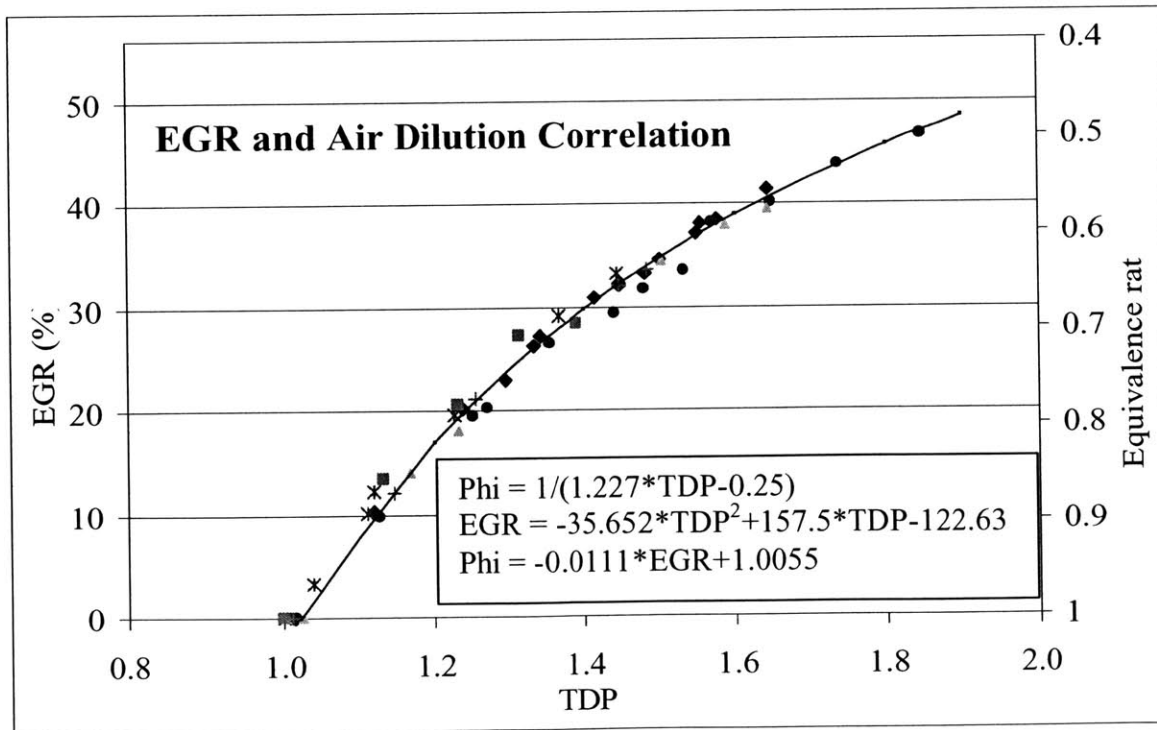


Figure 2-25 EGR and air dilution correlation

(This page was intentionally left blank.)

CHAPTER 3 SIMULATION

3.1 Overview

This simulation is a tool for investigating different alternatives to reduce engine emissions and fuel consumption. The performance of the vehicle is constant to allow for a fair comparison of different concepts. When using this model for evaluation of a particular engine concept, the user defines the concept by specifying a few key parameters that provide sufficient input to run the model. The driving parameters for evaluation of different concepts are:

- **Cylinder Charging;** naturally aspirated, turbocharged or supercharged. Boosting is necessary in lean operation to maintain the baseline torque of naturally aspirated engine with stoichiometric mixture. Whenever an engine is boosted, turbocharged or supercharged, the power output of the engine increases if displaced volume remains constant. Due to higher density of air, larger mass of air can be inducted into the cylinder. For a stoichiometric mixture this allows for extra fuel, resulting in more useful work per cycle. For equal performance, boosting provides an opportunity to downsize the engine. Boosted engine has higher fuel efficiency due to reduced pumping work.
- **Exhaust Gas Recirculation;** percentage of recycled exhaust gas with stoichiometric charge mixture. Presence of recycled exhaust gas in the charge mixture significantly reduces engine out NO_x emissions and slightly increases engine fuel conversion efficiency. Efficiency increases due to slightly higher combustion efficiency and reduced pumping work since higher intake pressures are required.
- **Engine Operation;** three options are given: specified fuel/air equivalence ratio, stoichiometric operation with EGR, and operating lean for maximum efficiency based on the amount of plasmatron gas.
- **Cylinder Displacement Downsizing;** total engine displacement is reduced by a user specified percentage. Bore and stroke ratio remains the same as new values for both are calculated. Smaller bore and stroke reduce rubbing friction.
- **Plasmatron Fraction;** the fraction of the total fuel that passes through the Plasmatron and is reformed into hydrogen rich gas. It determines how lean the engine can operate and how much can the compression ratio be raised.

The following two primary objectives have been selected as outputs from this model:

- **Fuel Economy**; this objective is expressed as miles per gallon over the two combined drive cycles used in this modeling study.
- **NOx Emissions**; this is expressed as engine out NOx emissions in grams per mile driven over a drive cycle. The model does not include any emission aftertreatment, although the use of a three-way catalyst for stoichiometric operation reduces the NOx emissions by close to two orders of magnitude. On the other hand, there are very few aftertreatment solutions for NOx under lean conditions and are quite costly.

Ford Motor Company provided engine data from one of their recent production engines, 2.0 liter Zetec, used in Ford Contour for the purpose of this modeling study. Main parameters are listed in table 3-1. Beside the engine geometry, motoring friction data and emissions were made available to the author and are used in this study. All emissions data were taken with no EGR. These data are used along with a number of models to construct engine maps of various parameters that are of interest in this study. The engine maps are presented in Chapter 4.

Table 3-1 Engine Specifications Used in the Model

Number of cylinders	4 inline
Valves per cylinder	4
Compression ratio	9.5
Combustion chamber	Pentroof
Cylinder displaced volume	1.99 L
Maximum rated torque	176 Nm @ 4750 rpm
Maximum rated power	93 kW @ 5000 rpm

Two different drive cycles are used for evaluation of a given concept. Federal test procedure (FTP) represents urban driving conditions while highway fuel economy test (HWFET) is representative of highway driving. NOx emissions are based on FTP only, while the fuel economy number is a combination of FTP and HWFET. Drive cycles are explained in more detail in section 3.3.1.

3.2 Model Architecture

Figure 3-1 shows the schematic of the plasmatron engine concept. A turbocharger is added to provide above atmospheric intake pressures that are required when an engine operates with lean mixtures. One intercooler is used to cool the compressed air after the compressor and another intercooler is used to cool the plasmatron gas at the exit of the reformer. Plasmatron gas is combined with air in the intake manifold while the fuel is injected in the intake port. All of the components in Figure 3-1 are modeled in this study. Important components are modeled in greater detail while simple relationships are developed for less important ones. The model maintains the performance characteristics of the engine, torque and power, while all other parameters are adjusted based on the user input. The model follows the required mass flow of air to produce a given output from the atmosphere through the intake system (compressor, throttle, plasmatron addition and intake port) to the cylinder. Simultaneously the fuel flow is followed to the intake port where it is combined with plasmatron and air mixture. As the burned mixture exits from the cylinder, it is followed through the exhaust system (turbine, catalytic converter, muffler) out to the atmosphere. The simulation does not include an in-cylinder combustion model, which could prove to be valuable for a more detailed study.

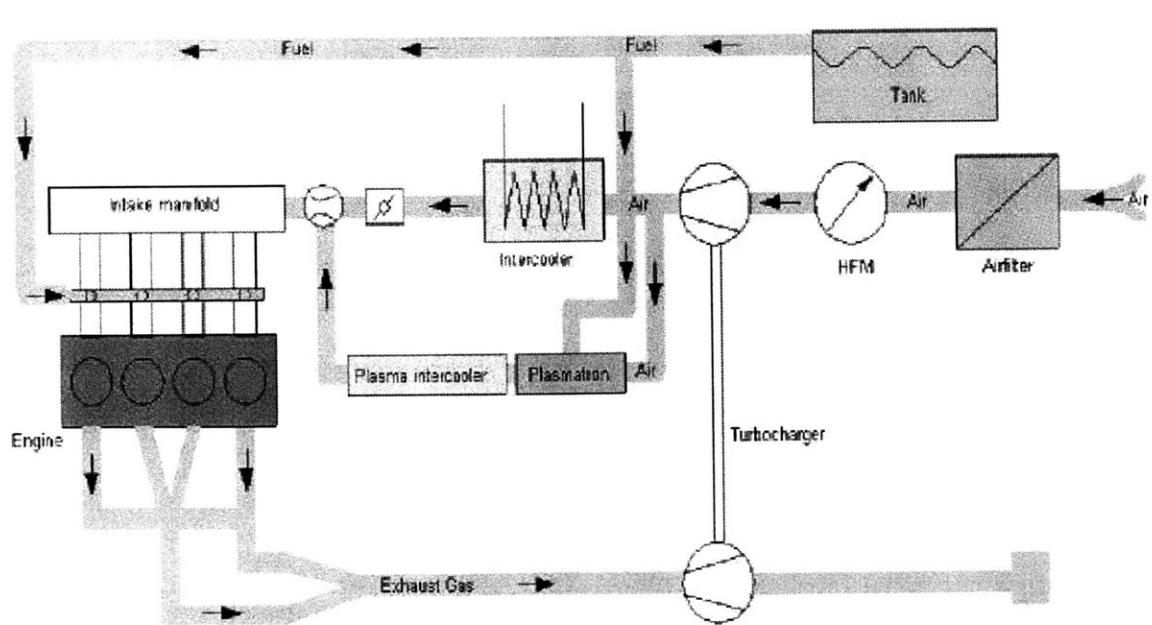


Figure 3-1 Schematic of the engine system encompassed by the model

3.3 Model Subroutines

3.3.1 ADVISOR

ADVISOR, Advanced VehIcle SimulatOR [13] is a freely available program developed by the National Renewable Energy Laboratory (NREL). It is a set of model, data, and script text files for use with Matlab and Simulink. It is designed for rapid analysis of the performance and fuel economy of conventional, electric, and hybrid vehicles. ADVISOR also provides a backbone for detailed simulation and analysis of user defined drivetrain components, a starting point of verified vehicle data and algorithms from which to take full advantage of the modeling flexibility of Simulink and analytic power of MATLAB. As an analysis tool, ADVISOR takes the required speed as an input, and determines what drivetrain torques, speeds, and powers would be required to meet that vehicle speed. Because of this flow of information back through the drivetrain, from tire to axle to gearbox and so on, ADVISOR is what is called a backward-facing vehicle simulation. ADVISOR makes extensive use of maps based on empirical data to define various components of a vehicle drivetrain. Examples are BSFC or engine out emissions as a function of engine torque and speed.

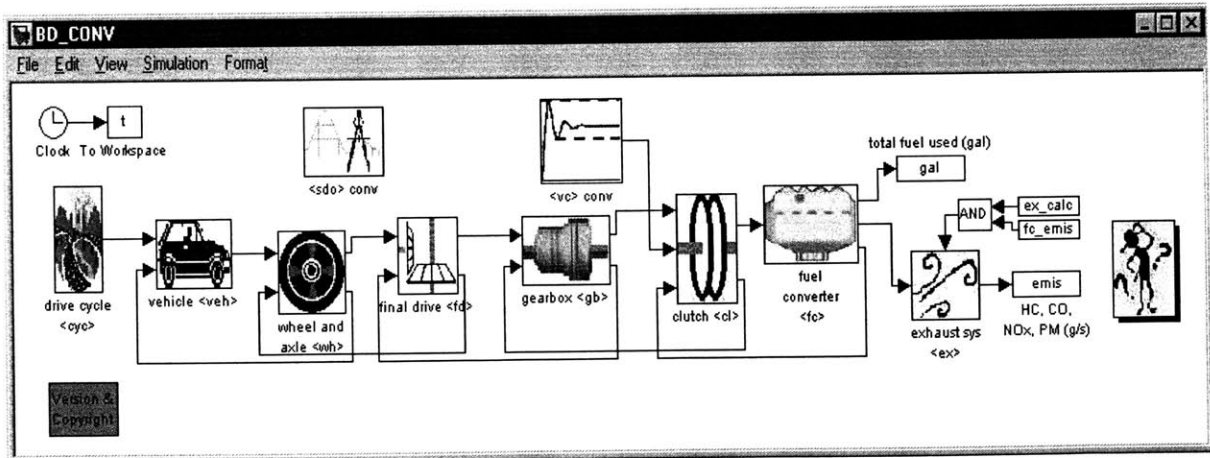


Figure 3-2 Conventional vehicle drivetrain in ADVISOR

The above figure represents a conventional vehicle's drivetrain using components from ADVISOR. The drive cycle requests or requires a given speed. Each block between the driving cycle and the torque provider, in this case the ICE, then computes its required input given its required output. It does this by applying losses, speed reductions or multiplications, and its performance limits.

For the purpose of this project, Highway Fuel Economy Test (HWFET) and Federal Test Procedure (FTP) driving cycles are used. US EPA uses the HWFET driving cycle for Corporate Average Fuel Economy (CAFE) certification and the FTP driving cycle for emissions certification of passenger vehicles in the US.

Figure 3-3 shows the operating points of the HWFET driving cycle, which is used to simulate highway driving and estimate typical highway fuel economy. The official test consists of a warm-up phase followed by a test phase. The driver follows the same driving trace in both the warm-up and the test phase. In ADVISOR the warm up phase is replaced by starting the vehicle with hot initial conditions. A top speed of 59.9 mph is reached with an average speed of 47.6 mph.

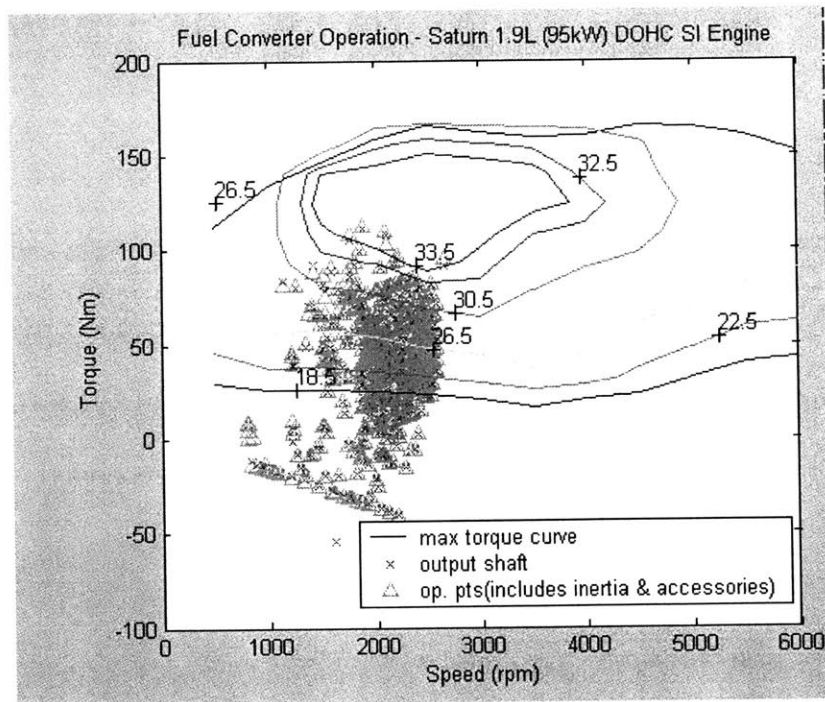


Figure 3-3 HWFET drive cycle

Figure 3-4 shows the operating points of FTP-75, the standard federal exhaust emissions driving cycle, on a torque and speed engine map. This cycle has three separate phases: a cold-start (505-second) phase, a hot-transient (870-second) phase, and a hot-start (505 second) phase. During a 10-minute cool-down between the second and third phase, the engine is turned off. The 505-second driving trace for the first and third phase are identical. The total test time is 2457

seconds with the top speed of 56.7 mph and the average speed of 21.4 mph. The distance driven is approximately 11 miles.

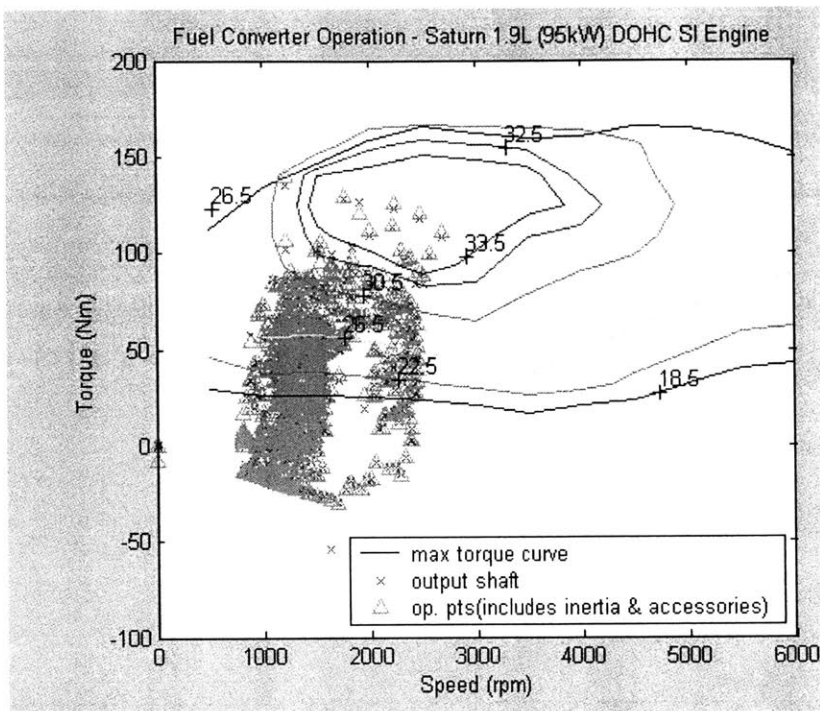


Figure 3-4 FTP drive cycle

The fuel economy number that is used from here on is a combined fuel economy of the two drive cycles according to equation (7). This equation is used by the EPA for fuel economy certification¹ of passenger vehicles in the U.S.

$$FE_{combined} = \frac{1}{(0.55 / FE_{FTP-75} + 0.45 / FE_{HWFET})} \quad (7)$$

A compact vehicle representative of a Ford Contour 4-door sedan is assembled in ADVISOR. It is modeled with a 5-speed manual transmission and a curb weight of 2800 lbs. EPA fuel economy for this vehicle is reported to be 24 miles per gallon (mpg) for city driving and 34 mpg for highway driving. Very similar fuel economy numbers resulted when a baseline concept was simulated. However, the numbers presented in Chapter 4 are a combined fuel economy of the two drive cycles as shown in (7).

¹ FE_{FTP-75} and FE_{HWFET} do not include 0.9 and 0.78 correction factors respectively which are often used.

3.3.2 Friction model

Engine friction losses are divided into three main categories [14]: mechanical or rubbing losses, pumping losses and auxiliary component losses. These are all expressed as mean effective pressures: ie., the mechanical friction, auxiliary drive and pumping work per cycle, per unit of displaced volume. Mechanical losses result from the relative motion between solid surfaces in the engine. Pumping losses are the work done by the piston as gases are pulled into or pushed out of the cylinder during intake and exhaust strokes. Auxiliary component losses are the work required to drive the essential engine accessories. Rubbing friction, auxiliary component and pumping work models were taken from Sandoval [15]. All the symbols are defined in the nomenclature section. Sandoval breaks down the rubbing friction into three component groups:

- Crankshaft

$$cfmep = 1.22 \times 10^5 \left(\frac{D_b}{B^2 S n_c} \right) + 3.03 \times 10^{-4} \left(\frac{N D_b^3 L_b n_b}{B^2 S n_c} \right) + 1.35 \times 10^{-10} \left(\frac{D_b^2 N^2 n_b}{n_c} \right) \quad (8)$$

- Reciprocating

$$rcfmep = 1294 \frac{S_p}{B} + 40600 \cdot \frac{F \cdot C_r}{B^2} \left(1 + \frac{500}{N} \right) + 3.03 \times 10^{-4} \left(\frac{N D_b^3 L_b n_b}{B^2 S n_c} \right) + 1.35 \times 10^{-10} \left(\frac{D_b^2 N^2 n_b}{n_c} \right) + 6.89 \frac{P_i}{P_a} \left[0.088 r_c + 0.182 F \cdot r^{(1.33 - 0.056 S_p)} \right] \quad (9)$$

- Valvetrain

$$vfmep = 244 \frac{N n_b}{B^2 S n_c} + C_{ff} \left(1 + \frac{500}{N} \right) \frac{n_v}{S n_c} + C_{rf} \frac{N n_v}{S n_c} + C_{oh} \frac{L_v^{1.5} N^{0.5} n_v}{B S n_c} + C_{om} \left(1 + \frac{500}{N} \right) \frac{L_v n_v}{S n_c} + 4.12 \quad (10)$$

The constants for the valvetrain terms (C_{ff} , C_{rf} , C_{oh} , C_{om}) depend on the valvetrain configuration being modeled and can be found in reference 15. Since the engine modeled has a double overhead cam valvetrain, coefficients for this configuration were used. Total rubbing friction is then equal to:

$$rfmep = cfmep + rcfmep + vfmep \quad (11)$$

Pumping work depends on intake manifold and exhaust back pressure, and losses across intake and exhaust valves. The exhaust pressure depends upon the pressure drop through exhaust system to ambient conditions. According to Shyler [16], this is given to a good approximation by:

$$\Delta p = c \cdot \frac{\dot{m}_e^2}{\rho_e} \quad (12)$$

and

$$p_e = p_a + \Delta p \quad (13)$$

in which c is the resistance coefficient and ρ_e is the density of the exhaust gas at inlet to the system. In case a turbocharger is used, $\Delta P_{\text{turbine}}$, pressure drop across the turbine, is added to the exhaust pressure in (13). The resistance coefficient for a 2.0 liter engine with an underbody catalyst was determined to be $1.49 \times 10^6 \text{ m}^{-4}$ [16]. Assuming ideal gas behavior and substituting for density in (12), (13) can be rearranged to give exhaust gas pressure:

$$p_e = \frac{p_a}{2} \left(1 + \sqrt{1 + 4 \cdot c \cdot R \cdot T_e \cdot \frac{\dot{m}_e^2}{p_e^2}} \right) \quad (14)$$

The valve pumping work for intake and exhaust in Sandoval's model is equal to:

$$pmep_v = 0.003 \cdot S_p^2 \cdot \left(\frac{p_i}{p_a} \right)^2 \cdot \left(\frac{1}{n_i^2 r_i^4} + \frac{1}{n_e^2 r_e^4} \right) \quad (15)$$

The pumping mean effective pressure is:

$$pmep = (p_e - p_i) + pmep_v \quad (16)$$

where p_i is the intake manifold pressure in kPa. The auxiliary friction component is modeled as:

$$afmep^1 = 6.23 + 5.22 \times 10^{-3} N - 1.79 \times 10^{-1} N^2 \quad (17)$$

Since the plasmatron fuel reformer requires some electrical energy for its operation, Smaling [9] developed the following model that is added to the auxiliary friction component:

$$emep = \frac{\left(q_{e,H2} \cdot \dot{m}_{H2} + q_{e,H2,c} \right) \cdot 2000 \cdot 60}{V_d \cdot n_c \cdot N \cdot \eta_e} \quad (18)$$

In case a supercharger is used, an additional component is added to the auxiliary friction and it comes from the Boost model described later in this chapter. It is the mean effective pressure that is required to provide mechanical work to drive the supercharger. The total auxiliary friction is then:

$$afmep = afmep' + emep + scmep \quad (19)$$

Heywood [14] defines the total friction mean effective pressure as:

$$tfmep = pmep + rfmep + amep \quad (20)$$

All the quantities in equation (20) are positive, except for pmep when $p_i > p_e$ at lower engine speeds. While this model requires numerous inputs, the output of this model is the total friction mean effective pressure. Figure 3-5 shows the real motoring friction of the Ford engine compared to the total friction mean effective pressure predicted by the friction model. The breakdown of the total friction from the model is shown in Figure 3-6.

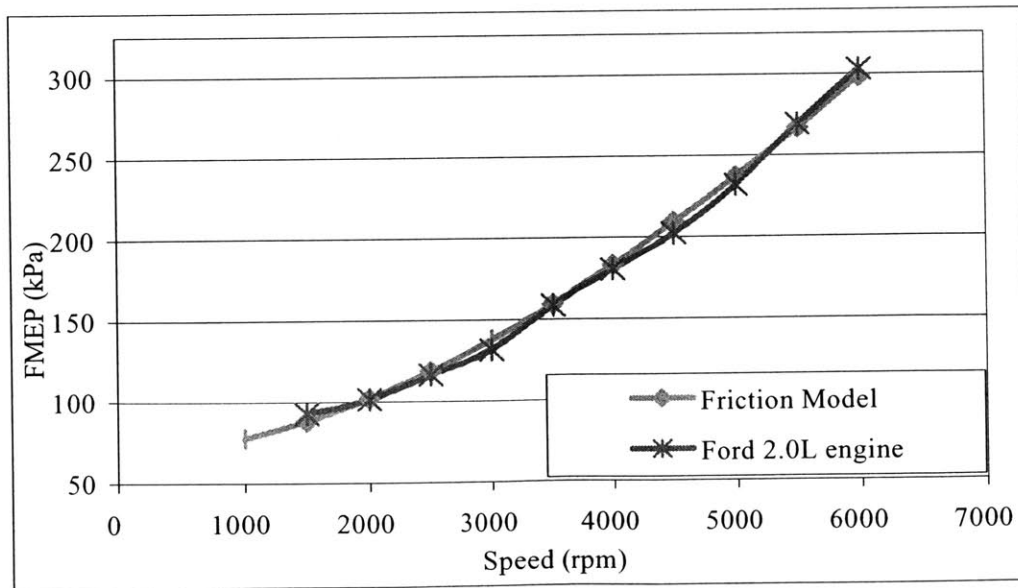


Figure 3-5 Friction model validation: fmep versus engine speed

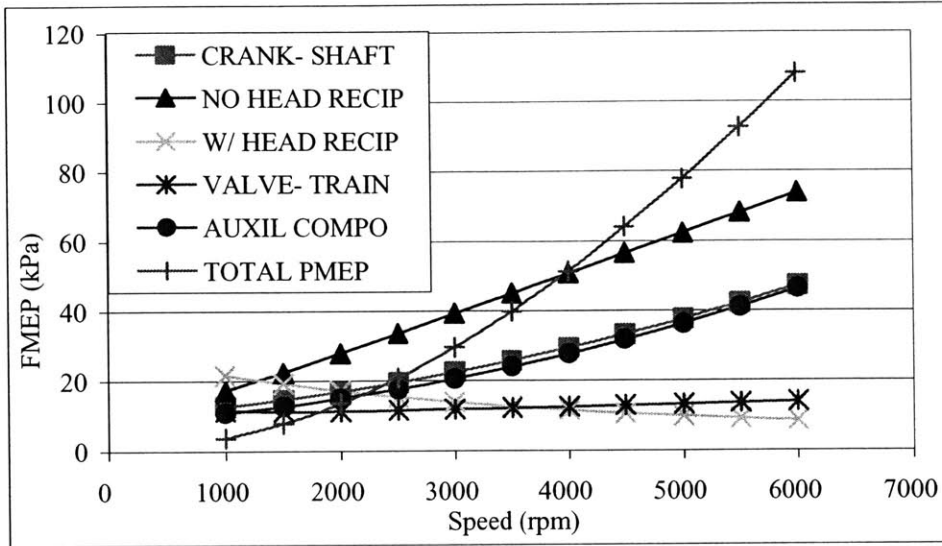


Figure 3-6 Breakdown of friction components in the model

3.3.3 Indicated Fuel Conversion Efficiency

Indicated efficiency is a base parameter used in the BSFC model for the calculation of the BSFC map for a given concept. According to the ideal gas cycle [14], the indicated efficiency is calculated as:

$$\eta_{f,ig} = 1 - \frac{1}{r_c^{\gamma-1}} \quad (21)$$

where r_c is the compression ratio of the engine and γ is the ratio of specific heats. This formula has been used in publications related to engine modeling and represents air as a working fluid inside the engine cylinder. A more accurate model is the air-fuel cycle where the unburned mixture is frozen in composition and the burned gas mixture is in equilibrium. In the ideal gas cycle the indicated efficiency is multiplied by a factor between 0.8 and 0.9 according to Shyler [16]. Heywood [14] suggests that roughly a factor of 0.8 should be used to adjust air-fuel cycle data to account for real engine effects.

A different approach is used here to get a more accurate value for the indicated efficiency throughout the entire engine operating regime. The following equations describe how real engine data was used to obtain values for indicated efficiency.

Brake fuel conversion efficiency is defined as:

$$\eta_{f,b} = \frac{1}{\eta_c \cdot bsfc \cdot Q_{LHV}} \quad (22)$$

where η_c is the combustion efficiency, bsfc is the brake specific fuel consumption in g/kWh and Q_{LHV} is the lower heating value of the hydrocarbon fuel in MJ/kg. Combustion efficiency is strongly dependent on the equivalence ratio as shown by Heywood [14]. For stoichiometric operation it is around 92 to 96 percent. Brake fuel efficiency can also be expressed as:

$$\eta_{f,b} = \eta_{f,ig} \cdot \eta_m \quad (23)$$

where η_m is mechanical efficiency and $\eta_{f,ig}$ is gross indicated fuel conversion efficiency. Mechanical efficiency is defined as:

$$\eta_m = \frac{bmep}{imep_g} \quad (24)$$

where bmep is brake mean effective pressure and imep_g is gross indicated mean effective pressure, respectively defined as:

$$bmep = \frac{6.28 \cdot n_r \cdot Tq}{Vd \cdot n_c} \quad (25)$$

and

$$imep_g = bmep + tfmep \quad (26)$$

where Tq is the torque output of the engine in Nm, n_r is the number of crank revolutions for each power stroke per cylinder (2 for four-stroke cycles), Vd is the cylinder displacement and n_c is the number of cylinders.

Keeping the torque output of the engine constant, which is one of the requirements in the model, bmep can be calculated from (25) and along with imep_g from (26) gives the mechanical efficiency of the engine according to (24). The tfmep in (26) is an output of the friction model discussed earlier in this chapter. Since brake specific fuel consumption for the 2.0 liter engine is known, using (22) with indolene as a fuel (lower heating value of 43.1 MJ/kg) brake fuel

conversion efficiency can be calculated. Knowing mechanical efficiency and brake fuel conversion efficiency, gross indicated efficiency is calculated from (23). The bsfc data for the engine includes enrichment at wide-open throttle (WOT) and gross indicated efficiency must be corrected in that regime for stoichiometric mixture. A correction from the fuel-air cycle data [14] is used to adjust the indicated efficiency for rich operation as shown in Figure 3-7.

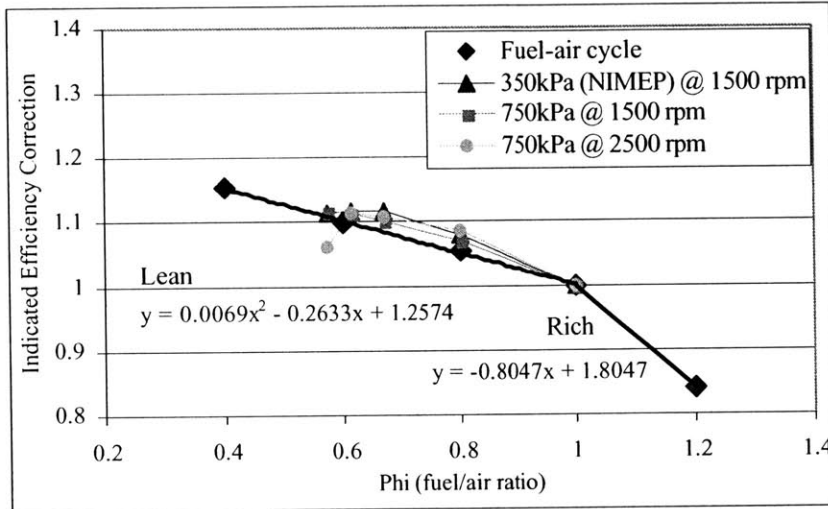


Figure 3-7 Fuel-air cycle efficiency correction for equivalence ratio

3.3.4 Brake Specific Fuel Consumption Model

This model takes indicated efficiency for a baseline engine with stoichiometric mixture and adjusts it for equivalence ratio changes using the correlation shown in Figure 3-7. This correction is based on the fuel-air cycle data and matches well with experimental data presented at the end of Chapter 2, some of which are plotted in Figure 3-7. Fuel-air cycle data are also used to adjust indicated efficiency for changes in compression ratio based on correlation shown in Figure 3-8. Both corrections are relative to the compression ratio of the 2.0 liter engine and stoichiometric equivalence ratio. Two driving parameters presented at the start of this chapter determine indicated efficiency for a new concept. The **plasmatron fraction** determines compression ratio increase (Section 1.2) and equivalence ratio if **engine operation** is lean for maximum efficiency (Section 3.3.4.3).

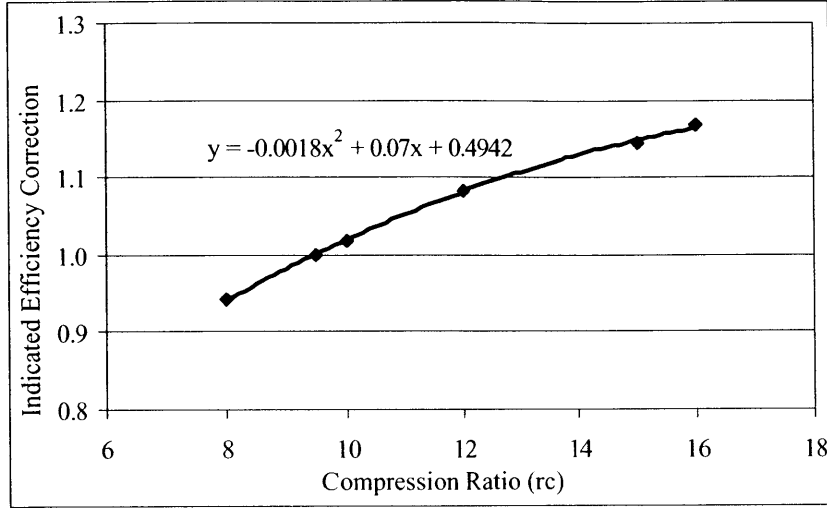


Figure 3-8 Fuel-air cycle efficiency correction for changes in compression ratio.

In the next step, mechanical efficiency is calculated from (24) and used with indicated efficiency in (23) to determine the brake fuel conversion efficiency. Brake mean effective pressure used in (24) is calculated in (25) based on torque and displaced volume. Maximum torque is held constant for a given speed to maintain a constant performance of the vehicle. V_d is the displaced volume of the baseline engine adjusted by the user if the engine concept involves **downsizing**. Gross indicated mean effective pressure is defined in (26) and total friction is calculated in the friction model in (20).

This new brake fuel conversion efficiency is used in a modified (22) to calculate the BSFC for a given load and speed:

$$bsfc = \frac{1}{\eta_c \cdot \eta_{f,b} \cdot \eta_{fs} \cdot Q_{LHV}} \quad (27)$$

where η_{fs} is the efficiency of the fuel system, introduced by Smaling [9] that accounts for the plasmatron conversion efficiency:

$$\eta_{fs} = R_p \cdot \left(\frac{(1 - R_p)}{R_p} + 1.1458 - 0.3134 \cdot (O/C) \right) \quad (28)$$

This equation is a weighted average of plasmatron efficiency and 100%, representing the rest of the system, based on the plasmatron fraction. Plasmatron efficiency comes from (2) with mass flow rates of reactants and products from (1) expressed in terms of oxygen to carbon ratio (O/C). Product mass flow rates for plasmatron are calculated from atom balance equations based on the one-step chemical reaction shown in (1). For the purpose of this modeling study, an O/C ratio of 1.1 is used which corresponds to 80% plasmatron conversion efficiency.

After bsfc is calculated for all of the points on the 12 by 12 load and speed matrix, this matrix becomes the new BSFC map. In this process most of the calculations are straightforward with the exception of pumping friction calculation. This calculation requires intake pressure, which is calculated using volumetric efficiency.

3.3.4.1 Volumetric Efficiency Correction

Volumetric efficiency is an important parameter in the BSFC model since it is used to calculate the intake pressure required to produce the desired torque. Knowing the brake specific fuel consumption on the WOT torque line for the baseline engine, volumetric efficiency correction can be calculated. Brake power, P_b , in kW is related to the torque as:

$$P_b = \frac{4 \cdot \pi \cdot Tq \cdot N}{2000 \cdot 60} \quad (29)$$

where N is engine speed in revolutions per minute. Mass flow rate of fuel required to produce this torque is:

$$\dot{m}_{fuel} = \frac{P_b}{\eta_{f,b} \cdot Q_{LHV} \cdot \eta_c} \quad (30)$$

Brake fuel efficiency is calculated in (22) knowing brake specific fuel consumption for a given torque and speed. Combustion efficiency increases with air and EGR dilution. For lean operation combustion efficiency is increased to around 98 percent [14]. The mass flow rate of air is calculated as:

$$\dot{m}_{air} = \dot{m}_{fuel} \cdot (A/F) \quad (31)$$

where A/F is the air-fuel ratio of the charge mixture. Enrichment of 10 to 20 percent is common on the WOT torque curve for maximum output. Volumetric efficiency [14] is defined as:

$$\eta_{vol} = \frac{2 \cdot \dot{m}_{air}}{V_d \cdot N \cdot \rho_{a,i}} \quad (32)$$

where $\rho_{a,i}$ is the manifold air density. Taylor [17] defines ideal volumetric efficiency:

$$\eta_{vol,ideal} = \frac{\left(1 + \gamma(r_c - 1) - \frac{p_e}{p_i}\right)}{\gamma(r_c - 1)} \quad (33)$$

and

$$\eta_{vol} = \eta_{vol,ideal} \cdot fn(N) \quad (34)$$

where p_e is the exhaust back pressure in kPa. Using torque data at WOT, brake power is calculated in (29). (30) and (31) are used to calculate mass flow rate of air, which is used to obtain volumetric efficiency from (32). The speed correction function is obtained by combining (32) and (34). It is used along with (33) for calculation of volumetric efficiency for the entire engine map of a concept that is being evaluated according to (34). Volumetric efficiency data for different concepts is presented in Chapter 4 along with other important engine parameters.

3.3.4.2 Manifold Air Pressure

Using equation 32 and adjusting it for EGR:

$$\dot{m}_{air} + \dot{m}_{egr} = \frac{\eta_{vol} \cdot V_d \cdot N \cdot \rho_{a,i}}{2} \quad (35)$$

Treating this as an ideal gas mixture:

$$\dot{m}_{air} = (1 - EGR) \cdot \frac{p_i \cdot \eta_{vol} \cdot V_d \cdot N}{2 \cdot R \cdot T_{manifold}} \quad (36)$$

or

$$P_i = \frac{2 \cdot \dot{m}_{air} \cdot R \cdot T_{manifold}}{(1 - EGR) \cdot \eta_{vol} \cdot V_d \cdot N} \quad (37)$$

where \dot{m}_{air} is the total mass air flow consumption of the engine. According to Shyler [16], who uses the same formula for calculation of manifold intake pressures in his model, when compared to experimental data the intake pressures calculated from (37) are in very good agreement for a range of different EGR settings, loads and speeds. Since p_i is used to calculate η_{vol} in (33) and (34), and also in (32) to calculate \dot{m}_{air} , the BSFC model includes a number of iterations that converge into a final p_i value for a given load and speed. This value is used to calculate the pumping work in the friction model, required for calculation of the new bsfc.

3.3.4.3 Empirical Relationships from Experimental Data

Experimental data presented in Chapter 2 were used to determine the dilution point where peak efficiency and lean limit occur. If the **engine operation** variable is set for lean operation at maximum efficiency, TDP value is determined where peak efficiency occurs. This variable can also be set for a particular equivalence ratio at which the engine operates. In this case, TDP is calculated based on equivalence ratio only, whereas otherwise equivalence ratio is adjusted to match the TDP determined by the relationship in (38) or (39). The following relationships were derived from efficiency and combustion stability data and are presented in Figure 3-9:

$$TDP_{peak_efficiency} = 1.5 + \frac{0.1}{15} R_p \quad (38)$$

$$TDP_{lean_limit} = 1.605 + \frac{0.107}{15} R_p \quad (39)$$

The two relationships are presented as independent of load and speed since TDP of peak efficiency and lean limit did not change more than 3 percent for different load or speed operating conditions. TDP where peak efficiency occurs was determined by curve fitting experimental data and the lean limit was determined by 3 percent COV of NIMEP.

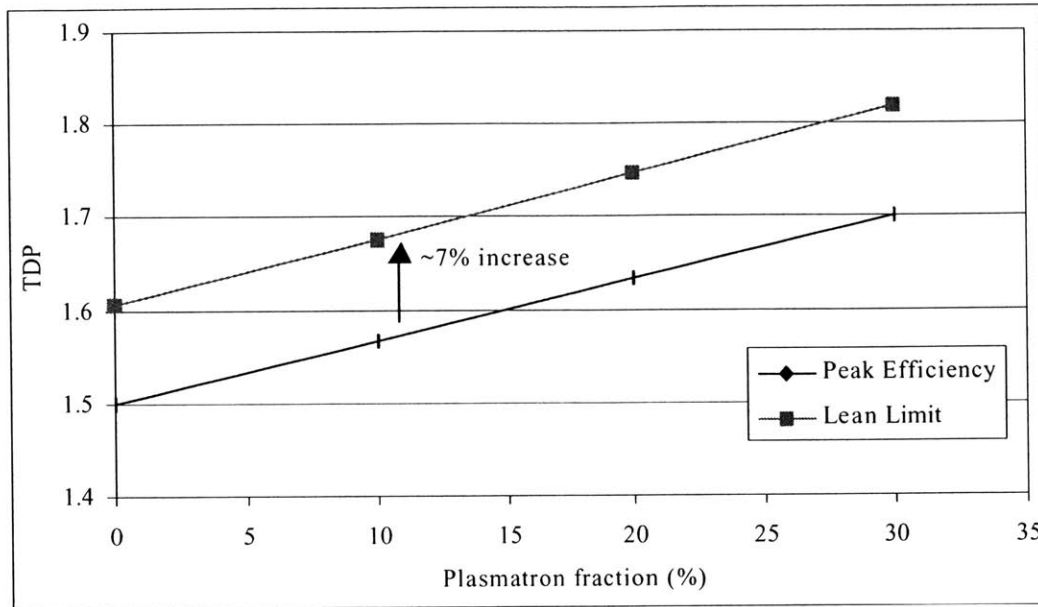


Figure 3-9 Data derived TDP - plasmatron fraction correlation

3.3.5 Boost

If the intake pressure that is required for a given load and speed, as calculated in the BSFC model, is higher than the maximum obtainable from a naturally aspirated operation, boosting is required. There are two options that user can specify under the **cylinder charging** parameter that can provide the required boost: turbocharger and mechanical supercharger. In both cases a heat exchanger or intercooler is used to cool the charge after compression prior to entry to the cylinder to further increase air density.

3.3.5.1 Turbocharging

Energy available in the engine's exhaust stream is used to drive the turbine, which drives the compressor, which raises the inlet fluid density prior to entry to each engine cylinder. A single shaft connects the compressor and the turbine. Performance maps were supplied by BorgWarner Turbo Systems and are shown in Figure 3-10 and 3-11. The compressor map covers a large range of pressure ratios, which is necessary since downsizing is one of the options in this engine simulation. The smaller the engine displacement, for equivalent performance, the higher the intake pressures will be. In Figure 3-10, the pressure ratio is plotted versus the corrected volume flow rate based on a reference temperature.

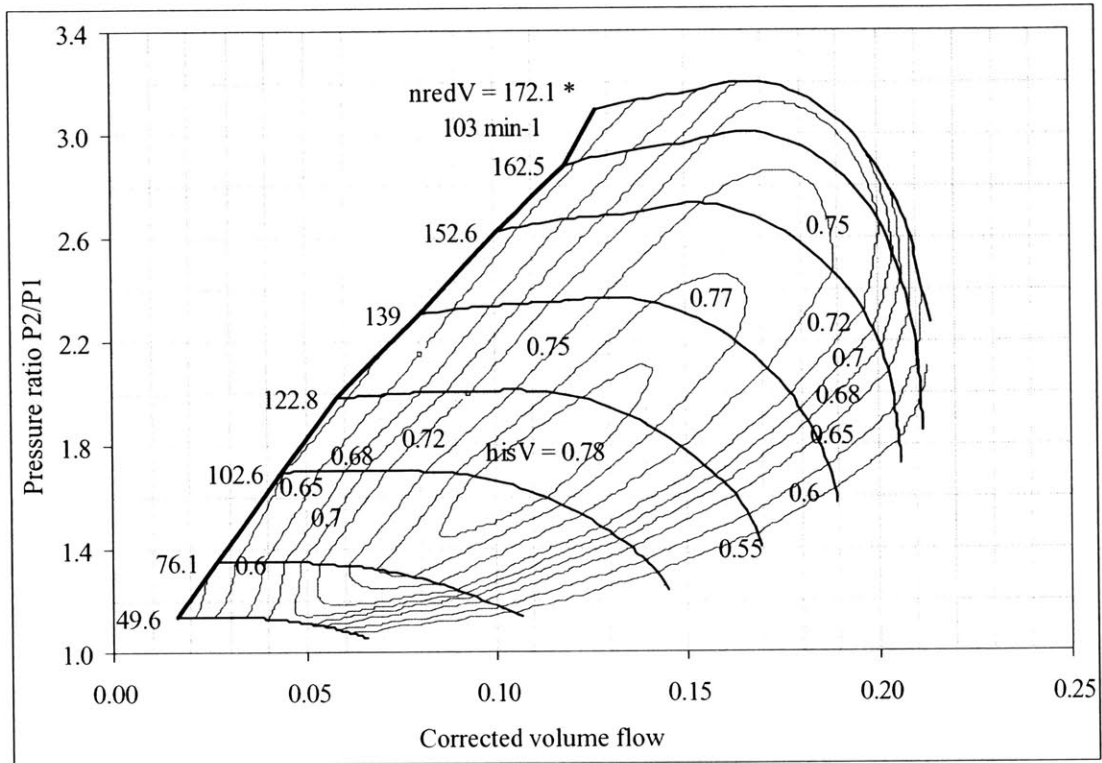


Figure 3-10 Performance map for a Borg Warner compressor K06

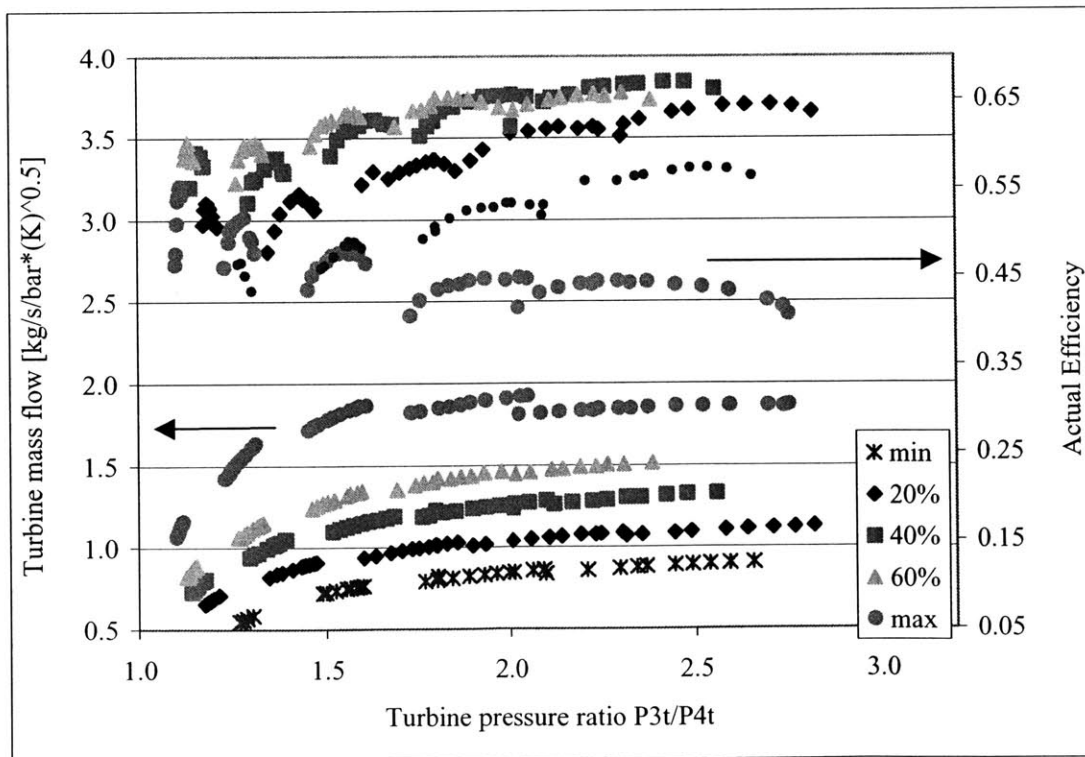


Figure 3-11 Performance map for a Borg Warner Variable Geometry Turbine

Figure 3-11 shows the performance for a variable geometry turbine (VGT). Variable geometry allows the turbine to cover a broader range of operation. For example: the same pressure ratios can be achieved for quite a range of mass flows across the turbine. However, the turbine efficiency is lower in the extreme blade positions. Efficiency plotted in this figure is the combined turbine and mechanical shaft efficiency. A number of different curves are plotted with each curve representing a different blade angle.

Once the required intake pressure is calculated in the BSFC model it is used along with the charge temperature and mass flow rate of air to calculate the pressure drop across the turbine. Pressure drop across the turbine is used in the friction model along with the intake pressure.

Power required to run the compressor based on the first law of thermodynamics is:

$$-\dot{W}_{compressor} = \dot{m}_{air} \cdot c_{p_air} \cdot (T_2 - T_1) \quad (40)$$

where T_1 is the compressor inlet temperature and T_2 is the outlet temperature. The second law is used to determine compressor isentropic efficiency and when substituted into previous equation we get:

$$-\dot{W}_{compressor} = \frac{\dot{m}_{air} \cdot c_{p_air} \cdot T_1}{\eta_c} \left(\left(\frac{p_2}{p_1} \right)^{(\gamma_a - 1)/\gamma_a} - 1 \right) \quad (41)$$

where γ_a is the specific heat ratio of air and η_c is the isentropic efficiency of the compressor. γ_a and c_{p_air} are functions of compressor inlet temperature but since this is atmospheric γ_a and c_{p_air} are constant. Isentropic efficiency for the compressor comes from the map in Figure 3-10 and depends on the pressure ratio and the volume flow rate. Similarly, for the turbine:

$$\dot{W}_{turbine} = \dot{m}_{exh} \cdot c_{p_exh} \cdot (T_3 - T_4) \quad (42)$$

where T_3 is the exhaust gas temperature at the exit of the exhaust port, just before the turbine inlet, and T_4 is the exhaust temperature at the turbine exit. Using the turbine isentropic efficiency:

$$\dot{W}_{turbine} = \dot{m}_{exh} \cdot c_{p_exh} \cdot T_3 \cdot \eta_t \left(1 - \left(\frac{P_4}{P_3} \right)^{(\gamma_e - 1)/\gamma_e} \right) \quad (43)$$

where P_3 is the pressure at the turbine inlet and P_4 is the pressure at the exit. P_4 is calculated in the friction model as a function of the exhaust mass flow rate and temperature and represents the atmospheric pressure plus the pressure drop in the rest of the exhaust system. c_{p_exh} and γ_e are temperature dependent, while the turbine isentropic efficiency is determined by the mass flow rate of exhaust and the turbine pressure ratio. Since the turbine provides the work required to drive the compressor:

$$-\dot{W}_{compressor} = \dot{W}_{turbine} \quad (44)$$

Calculation of P_3 from this equation would require a number of iterations, not included in this model, since the speed at which the turbocharger shaft rotates is also used to obtain turbine and compressor efficiencies. Once P_3 is calculated the pressure drop across the turbine is known. This is used in the friction model, output of which drives mechanical efficiency, which determines the new brake fuel conversion efficiency. This efficiency is then used to calculate the new intake pressure and the process continues until the model converges.

Exhaust temperature is needed in (43) to calculate P_3 . For the purpose of this work exhaust temperature is determined from the energy balance on the engine:

$$\eta_c \cdot \dot{m}_{fuel} \cdot Q_{LHV} = \eta_{f,b} \cdot \dot{m}_{fuel} \cdot Q_{LHV} + \eta_{loss} \cdot \dot{m}_{fuel} \cdot Q_{LHV} + \left(\dot{m}_{exh} \cdot c_{p_exh} \cdot T_{exh} - \dot{m}_{air} \cdot c_{p_air} \cdot T_{charge} \right) \quad (45)$$

where η_{loss} accounts for heat losses to the coolant and oil and can be defined as:

$$\eta_{loss} = \frac{Q}{\dot{m}_{fuel} \cdot Q_{LHV}} \quad (46)$$

with, Q related to speed as

$$Q = \int \dot{Q} dt \propto \dot{Q} \cdot \frac{2}{N} \quad (47)$$

The rate of heat loss can be expressed with Prandtl and Reynolds numbers as:

$$\dot{Q} = C \cdot \text{Re}^{0.8} \cdot \text{Pr}^{0.4} \propto \text{Re}^{0.8} \propto \left(\frac{\rho \cdot u \cdot L}{\mu} \right)^{0.8} \quad (48)$$

where

$$u \propto N \quad \text{and} \quad \rho \propto \dot{m}_{fuel} \propto BMEP \quad (49) \quad (50)$$

Combining all these relationships into one simple correlation we get:

$$\eta_{loss} = \frac{Q}{\dot{m}_{fuel} \cdot \dot{Q}_{LHV}} \propto \frac{(BMEP \cdot N)^{0.8}}{BMEP \cdot N} = (BMEP \cdot N)^{-0.2} \quad (51)$$

Constants were determined by matching this correlation to the Ford engine data.

Stoichiometric exhaust temperature is determined from (45) and corrected for lean or EGR operation if required. The correlations for lean and EGR adjustments of exhaust temperature were presented in the results section of Chapter 2 in Figures 2-22 and 2-23 respectively. The correlation equations are displayed in the two figures.

Charge temperature model developed by Smaling [9] is used to calculate T_{charge} in (45). The resulting temperature takes into account the hot plasmatron gas that is mixed with air before it enters into the engine. The only adjustment made to that model was that the incoming air temperature was changed from ambient to the temperature after the intercooler if boosting is required:

$$T_{charge} = \frac{\sum_{i=1}^7 m_{X_i} \cdot c_{P,X_i} \cdot T_{plasmatron} + \sum_{i=1}^2 m_j \cdot c_{P,X_j} \cdot T_{manifold}}{\sum_{i=1}^7 m_{X_i} \cdot c_{P,X_i} + \sum_{i=1}^2 m_{X_i} \cdot c_{P,X_j}} \quad (52)$$

with

$$\left\{ \begin{array}{l} \chi_j \in (N_2, O_2) \\ \chi_i \in (H_2O, H_2, CO, CO_2, N_2, C_7H_{14}, C_2H_2, O_2, CH_4) \end{array} \right.$$

3.3.5.2 Mechanical Supercharging

A compressor driven by power taken from the engine provides the compressed air. Based on the required pressure from the BSFC model, the work required to supply this pressure is calculated and added to the auxiliary mean effective pressure in the friction model. The same formula for the work done by the compressor (41) applies here to determine the work required to supply the desired intake pressure:

$$scmep = \frac{\dot{W}_{compressor}}{V_d \cdot n_c} \quad (47)$$

Figure 3-12 shows the performance map for a compressor used in this simulation.

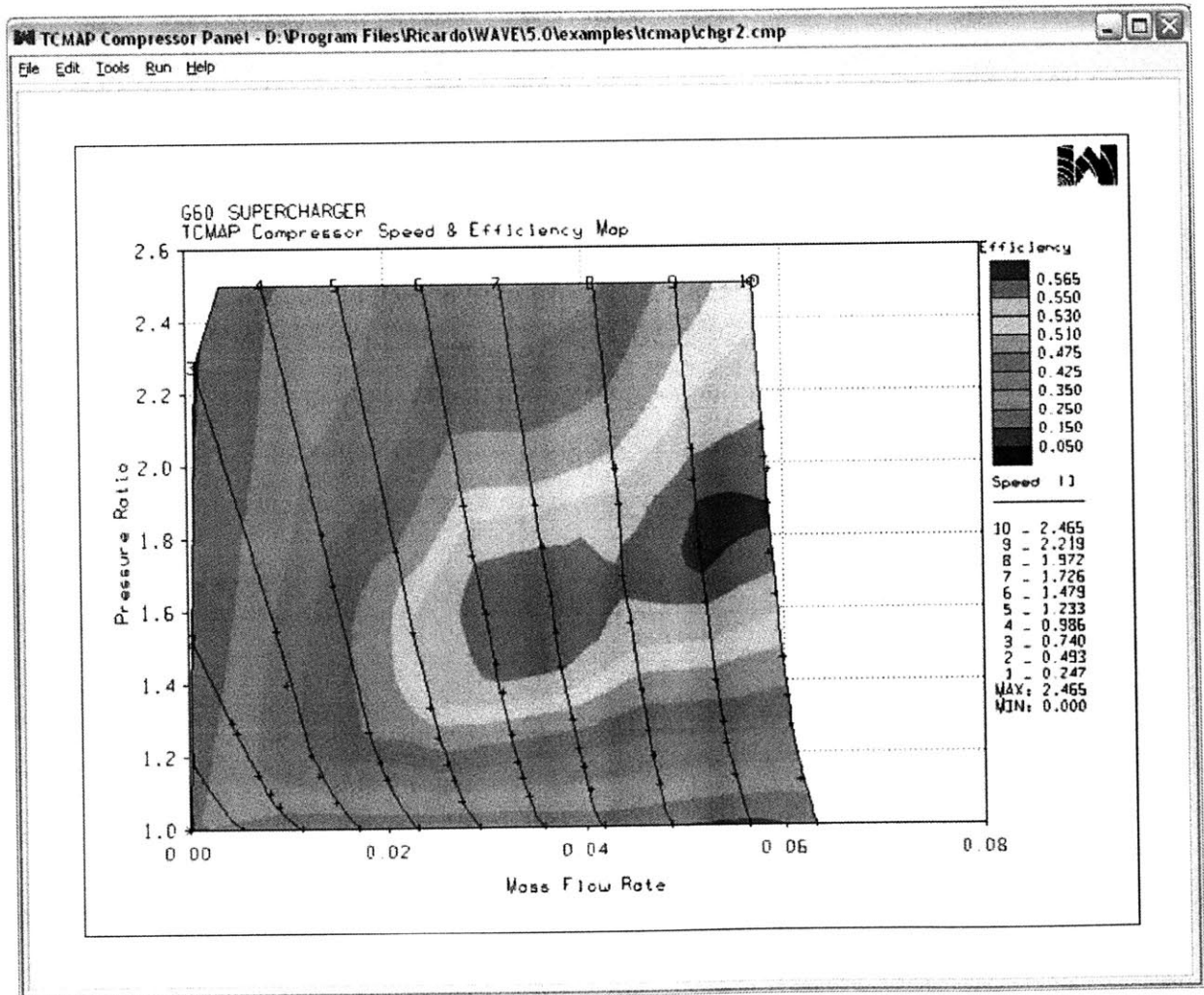


Figure 3-12 Supercharger performance map from Wave

3.3.6 NOx model

A model was developed to generate NOx emissions index map based on load and speed. NOx emissions index represents NOx mass flow rate in exhaust as a percentage of the fuel mass flow rate. It is a common parameter for presentation of emissions data in the automotive industry. The model is calibrated with data from the 2.0 liter engine and adjusted for air or EGR dilution accordingly. Additionally, a temperature correction factor, introduced by Smaling [9] is used to correct emissions for higher inlet charge temperatures:

$$M_T = 0.00445 * T_{charge} - 0.341 \quad (48)$$

3.3.6.1 Engine data

Ford data at part load with no EGR were analyzed and correlations were developed to model NOx emissions index based on load and speed. Figure 3-13 shows the NOx emissions index trends with load and speed. This data is adjusted to match the actual engine data and extrapolations are used for speeds higher than 4000 rpm. The actual correlation used in the model is presented at the bottom of Figure 3-13. Figure 3-14 shows the NOx emissions index map for the baseline concept.

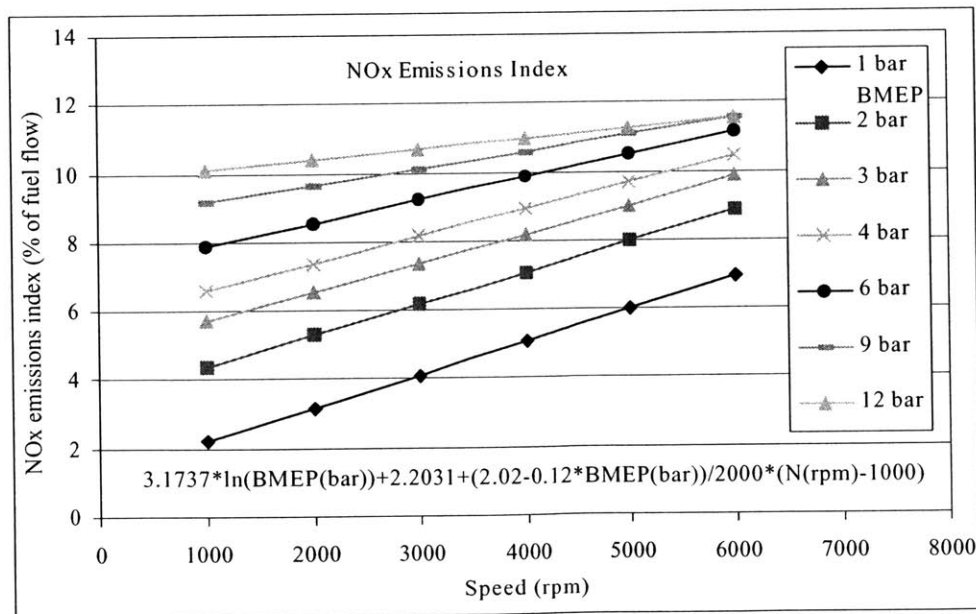


Figure 3-13 NOx emissions index model as a function of load and speed

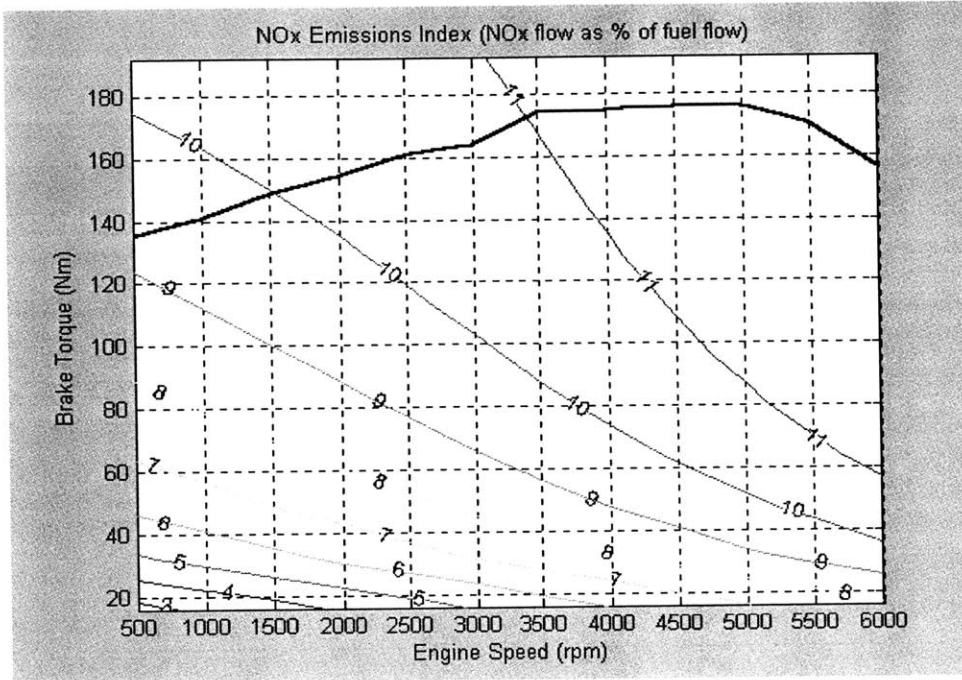


Figure 3-14 NOx emissions index map for baseline engine

3.3.6.2 Dilution correction

Figure 3-15 shows the NOx emissions index correction factors for EGR and air dilution. These two correlations are based on experimental data presented in Chapter 2. The actual emissions do vary with load and speed as seen in experimental results, but when normalized to stoichiometric operation for a particular load and speed with no EGR, the curves look similar. When plotted on a semi-logarithmic scale versus TDP there is a linear decrease in NOx emissions after a certain TDP value. For air dilution this value is around 1.25 and for EGR it is around 1.18. Due to this phenomenon, the correction factors for EGR and air are composed of two curves each, to better match the experimental results. All the correlations are presented in Figure 3-15. BSNOx emissions are calculated as:

$$BSNOx = NOx_{index} \cdot BSFC = (NOx_{index_baseline} \cdot M \cdot M_T) \cdot BSFC \quad (49)$$

where BSFC in g/kWh is calculated in (27), $NOx_{index_baseline}$ in percent is calculated from formula in Figure 3-13 based on load and speed, and M and M_T are dimensionless dilution and temperature correction factors shown in Figure 3-15 and equation (48) respectively.

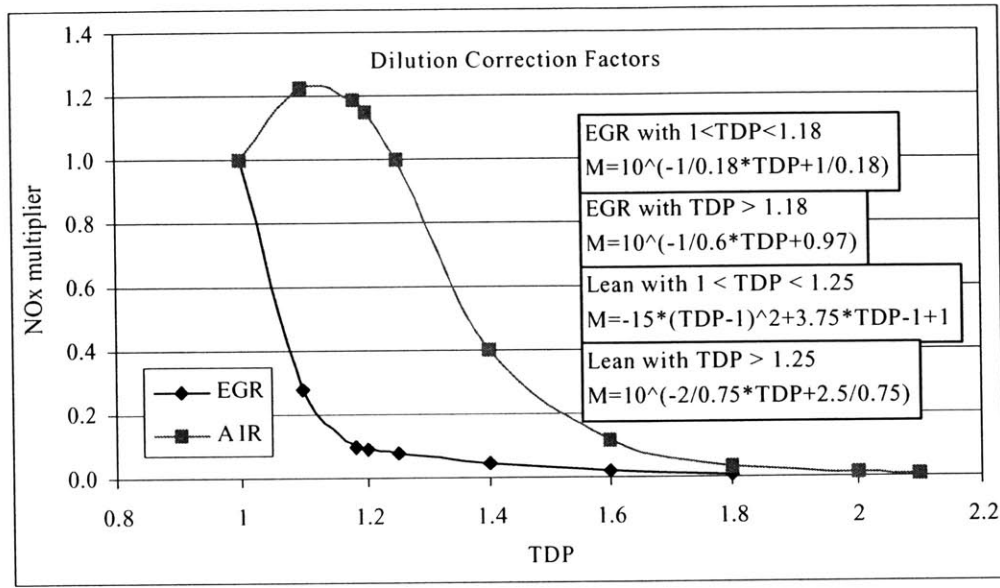


Figure 3-15 Dilution correction factors for NOx emissions

3.4 Concepts of Interest

The objective of this thesis is to develop a model for evaluation of fuel economy benefits and NOx engine out emissions for a lean boosted plasmatron-engine concept. To evaluate the benefits, a **baseline** case is simulated first for comparison purposes. This entails naturally aspirated operation with a stoichiometric mixture without any plasmatron addition or EGR. Then, **lean boost** concept with a turbocharger and constant 20 percent plasmatron gas addition throughout the entire operating range is investigated. Since the production version of the baseline engine uses some EGR for NOx emission control, a third case is evaluated with 10% **EGR** at part load. This model allows for different amounts of plasmatron for different operating points, but for simplicity plasmatron fractions are held constant since it is not clear what amounts should be used in what operating regime.

A downsizing study is also performed for lean boost concept. The cylinder displacement is downsized in 10% increments until a max BMEP of 19 bar is reached which is the limit of modern turbocharged engines (Subaru WRX-STi). Typical maximum value of bmeP for turbocharged production engines is around 16 bar.

(This page was intentionally left blank.)

CHAPTER 4 DISCUSSION OF RESULTS

Three different concepts are evaluated and engine maps of the following parameters are presented:

- mechanical efficiency
- gross indicated efficiency
- brake fuel efficiency
- BSFC
- manifold air pressure (MAP)
- BSNO_x
- volumetric efficiency
- exhaust pressure
- exhaust temperature

4.1 Introduction of Concepts

Baseline Concept

This concept involves naturally aspirated engine operating at stoichiometry with no EGR dilution. This is a concept that others are compared to for evaluation of fuel economy improvement and NO_x emissions reduction.

10% EGR Concept

This concept is identical to the baseline concept except that it operates with 10 percent EGR dilution at part load. This concept more accurately portrays the actual vehicle modeled in this study because the 2.0 liter Ford Zetec engine does use some EGR at part load for NO_x emission control but detailed data were not available.

Lean Boost Concept

This concept involves lean operation for maximum efficiency with constant 20 percent plasmatron addition. The engine is downsized by 20 percent and turbocharged.

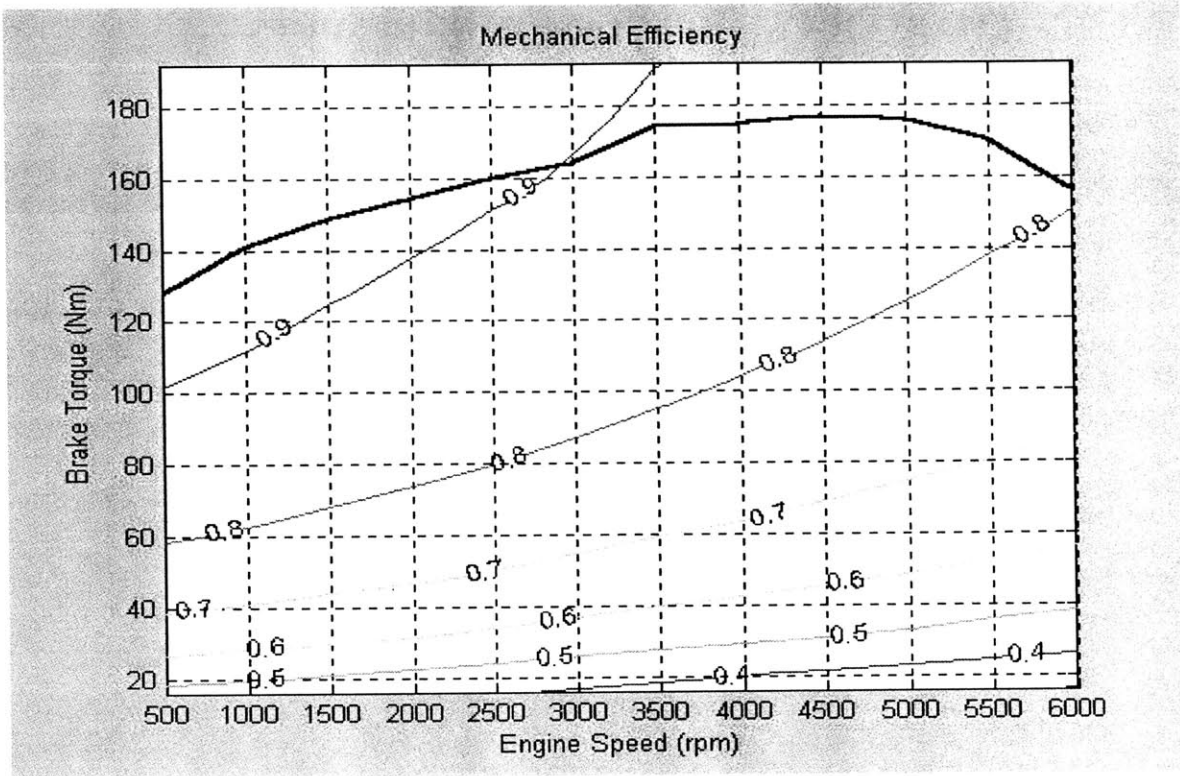


Figure 4-1 Baseline: Mechanical Efficiency

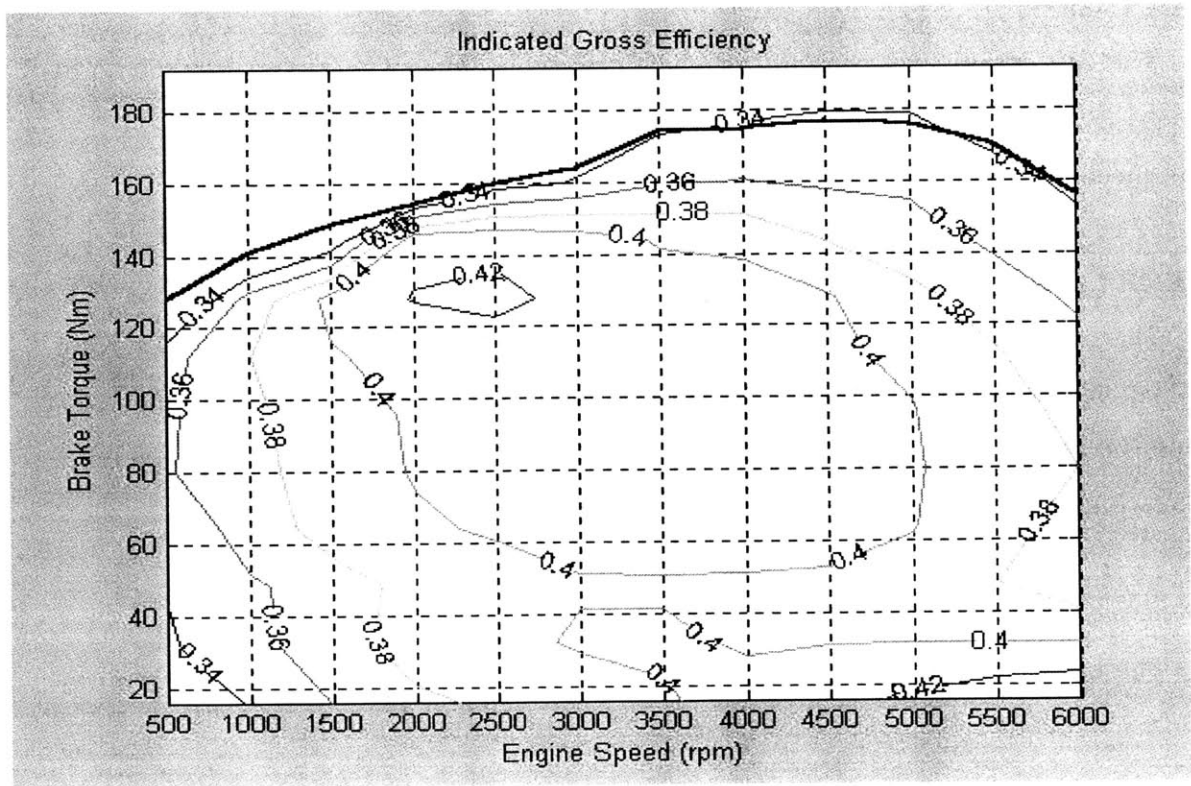


Figure 4-2 Baseline: Gross Indicated Efficiency

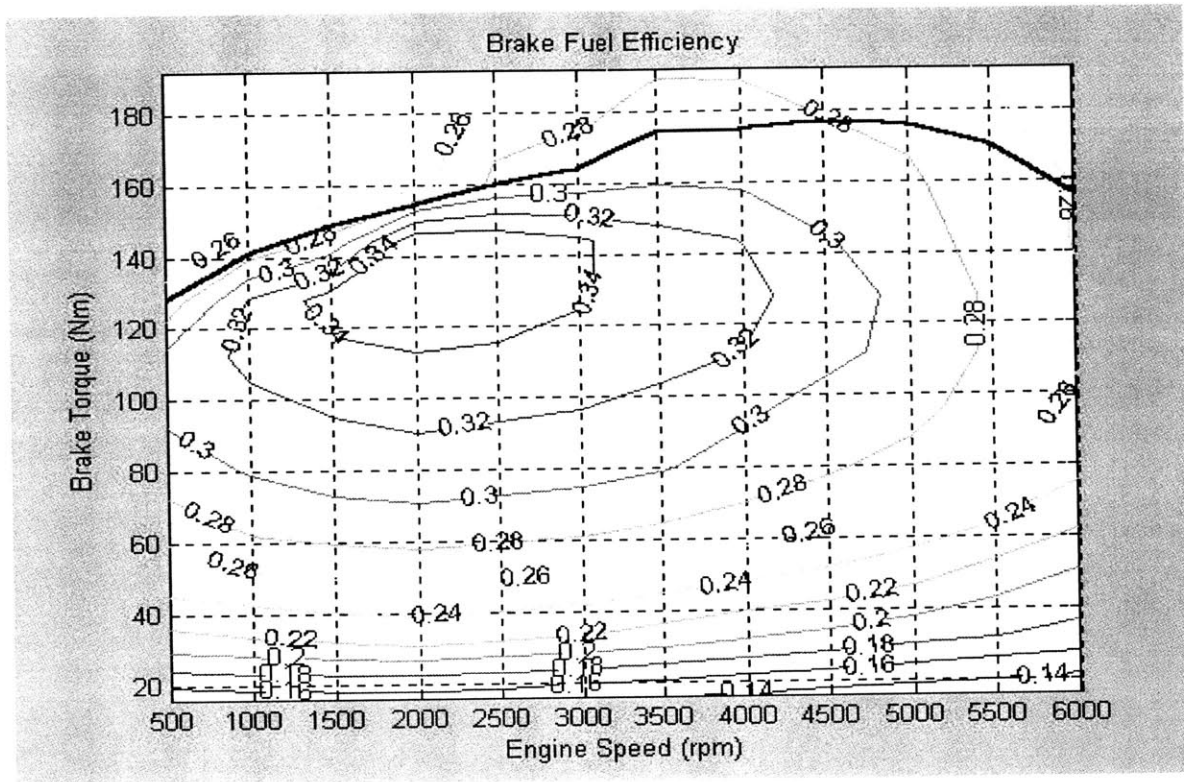


Figure 4-3 Baseline: Brake Fuel Efficiency

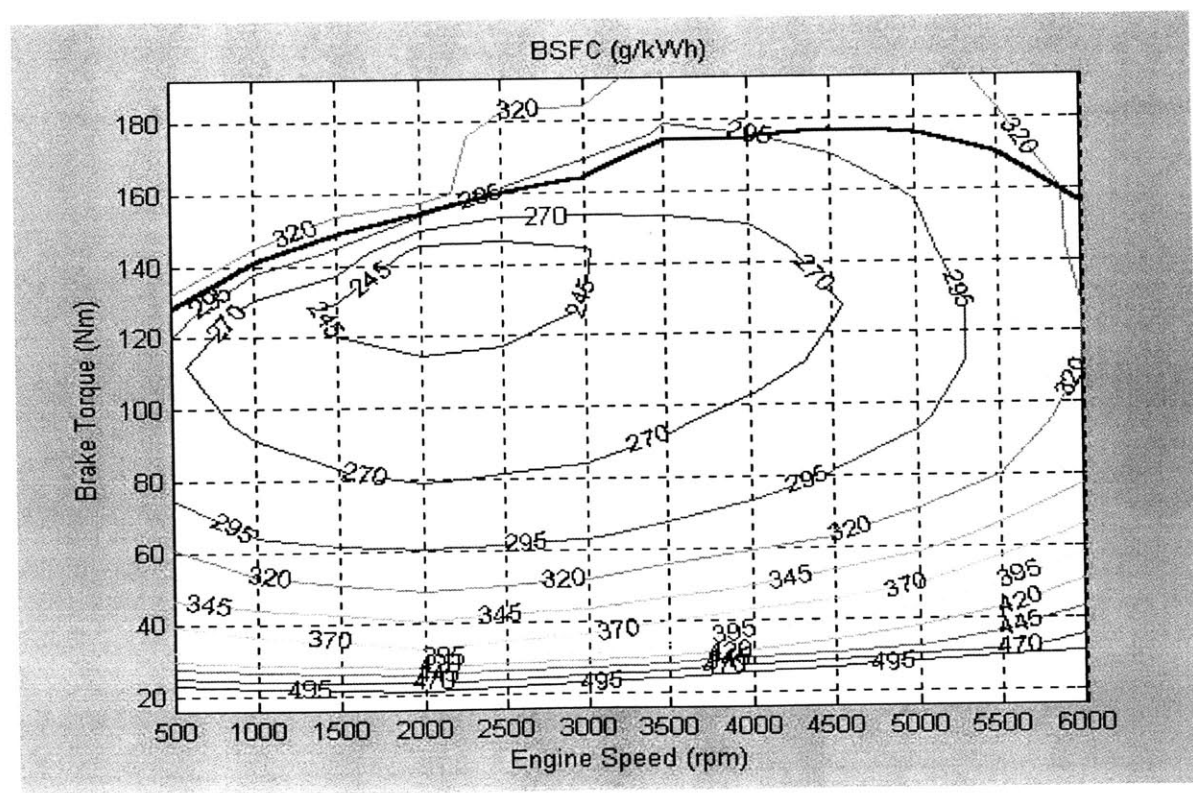


Figure 4-4 Baseline: BSFC

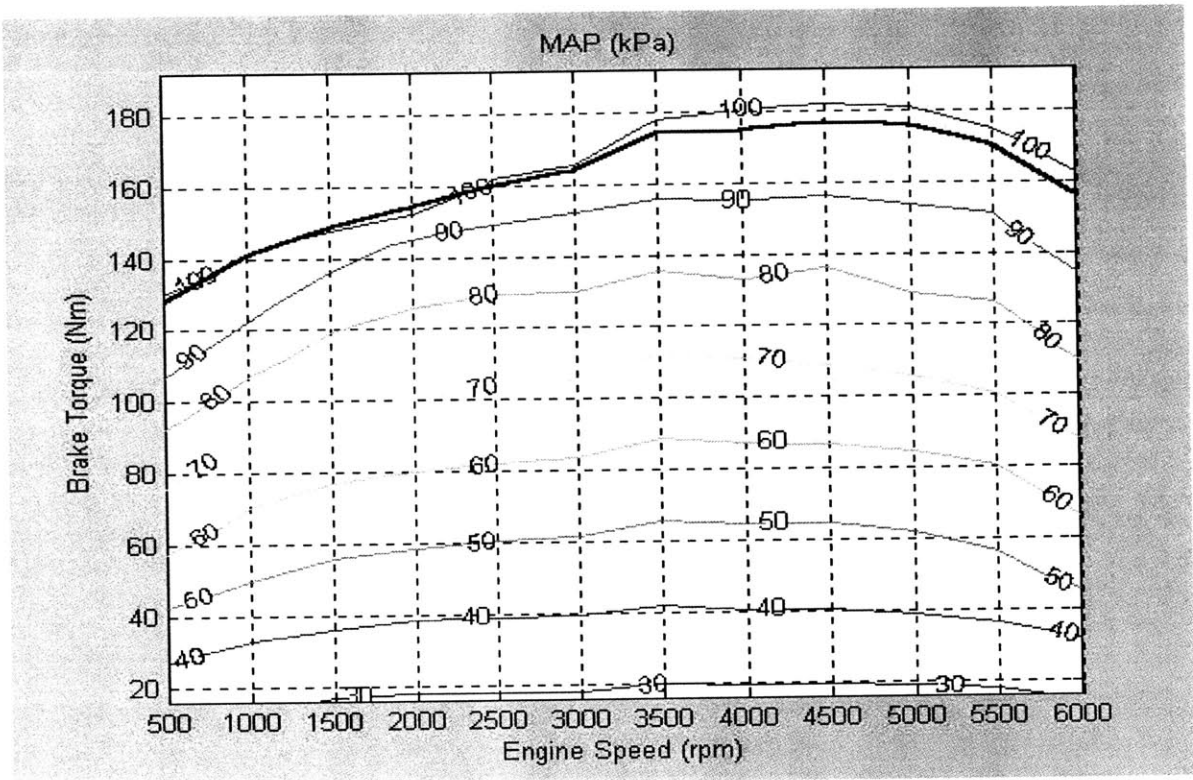


Figure 4-5 Baseline: MAP

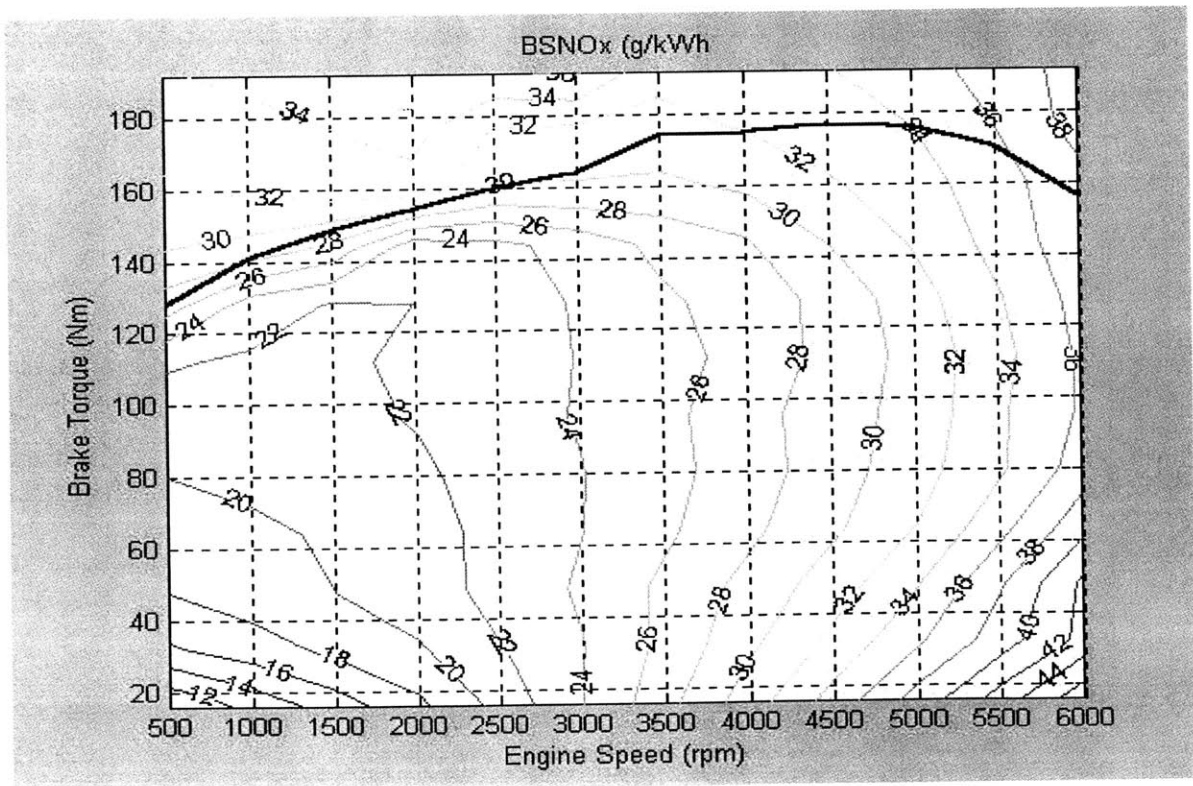


Figure 4-6 Baseline: BSNO_x

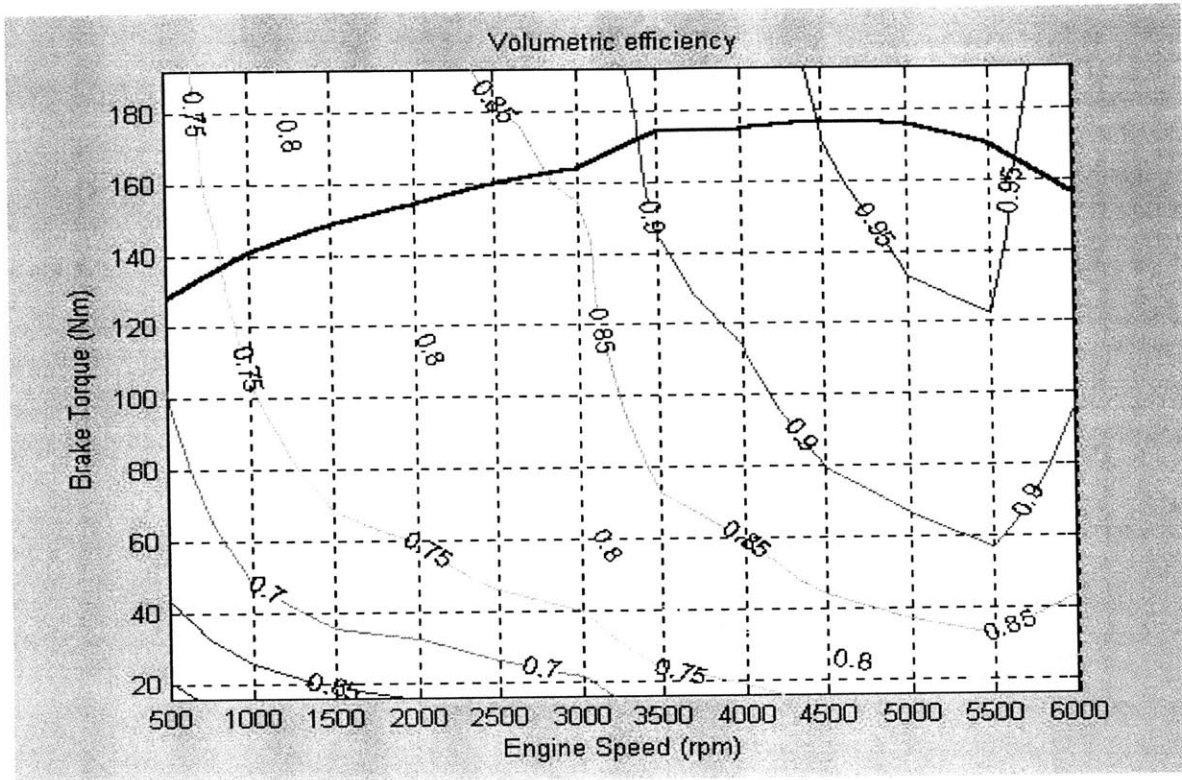


Figure 4-7 Baseline: Volumetric Efficiency

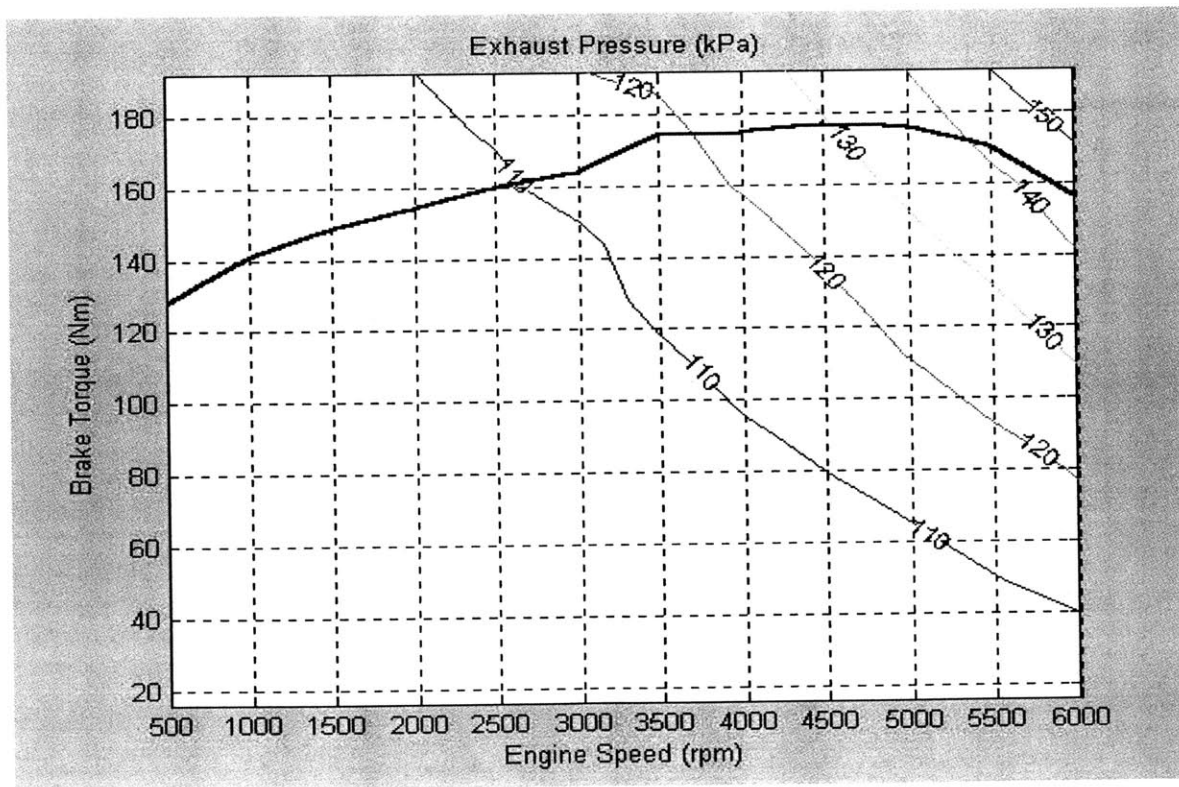


Figure 4-8 Baseline: Exhaust Pressure

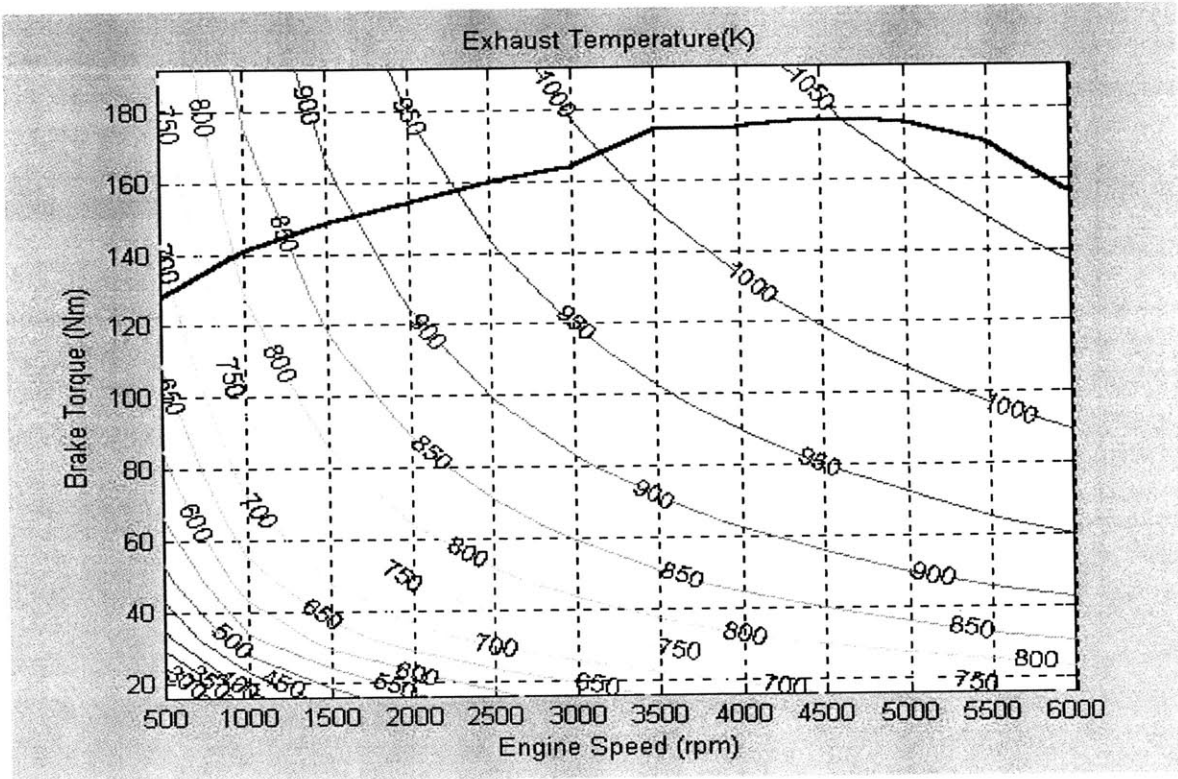


Figure 4-9 Baseline: Exhaust Temperature

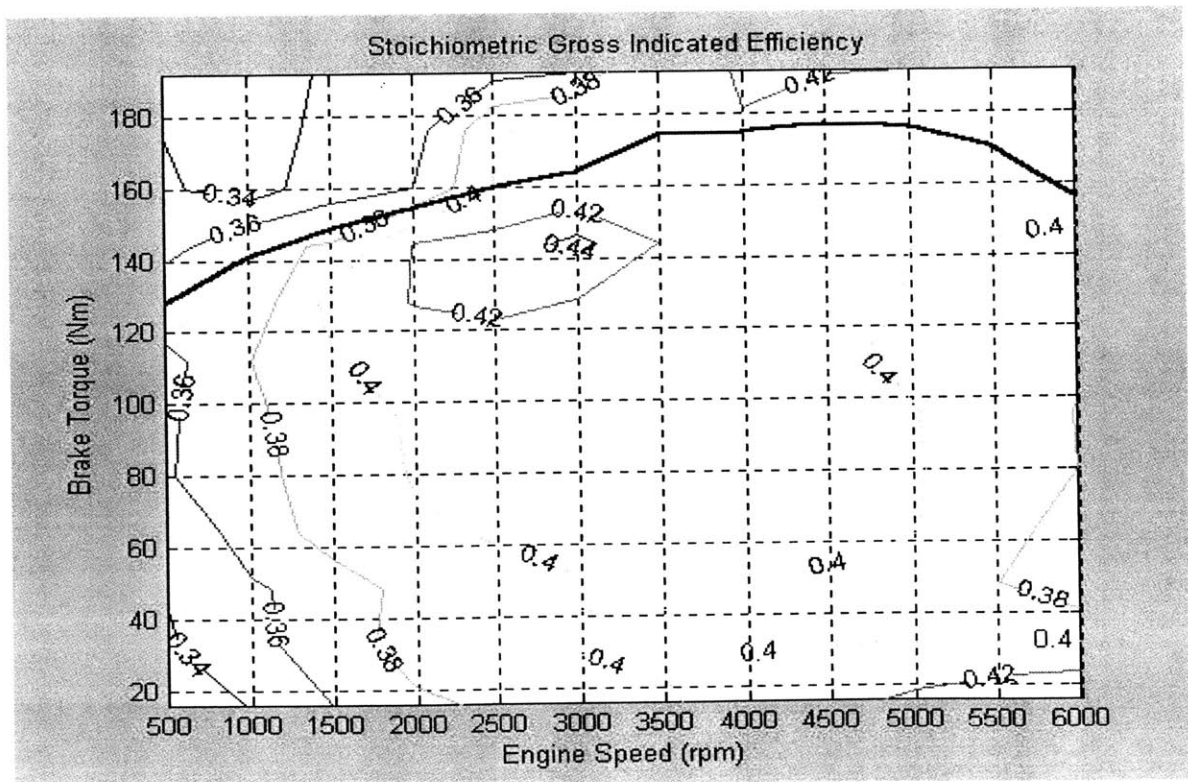


Figure 4-10 Baseline: Stoichiometric Gross Indicated Efficiency

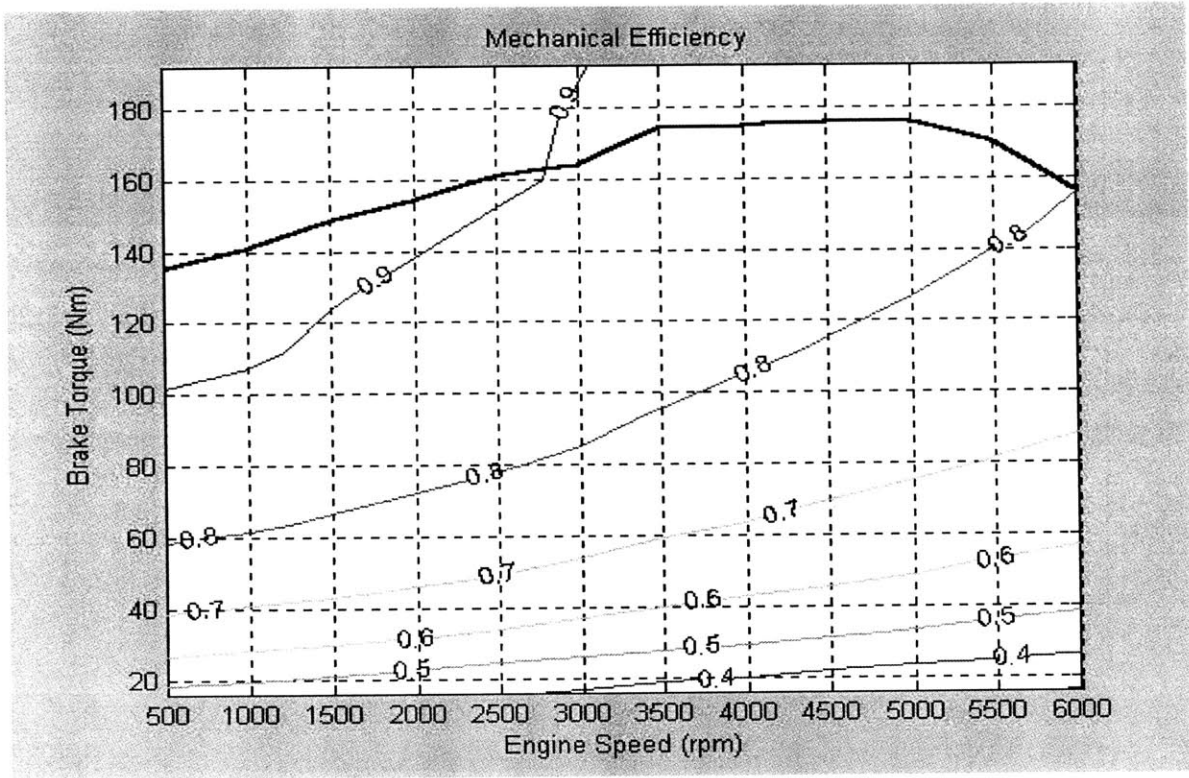


Figure 4-11 10% EGR: Mechanical Efficiency

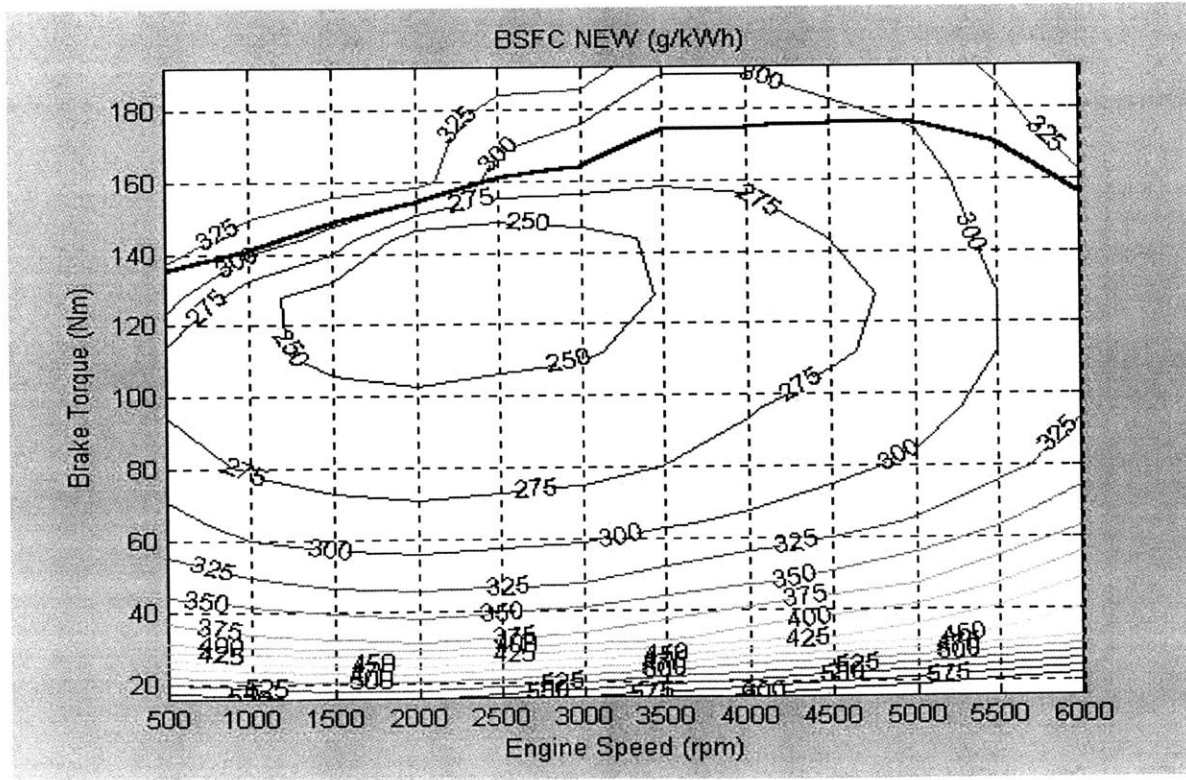


Figure 4-12 10% EGR: BSFC

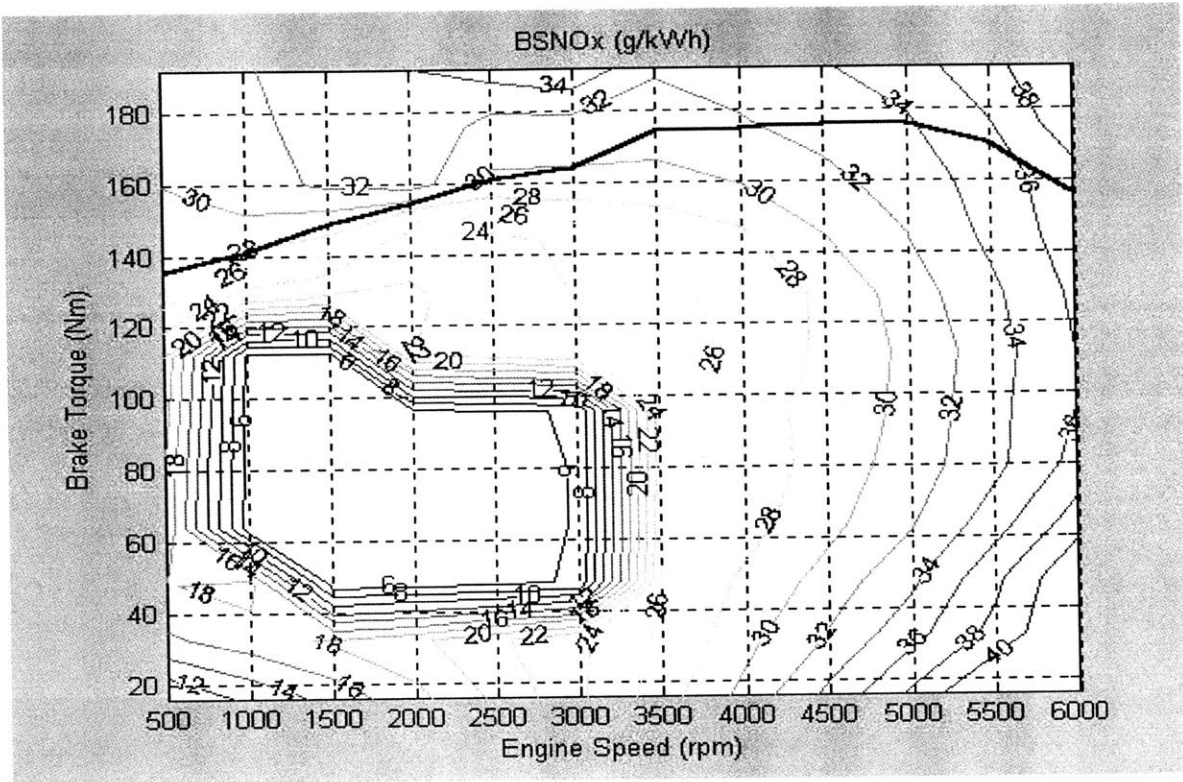


Figure 4-13 10% EGR: BSNOx

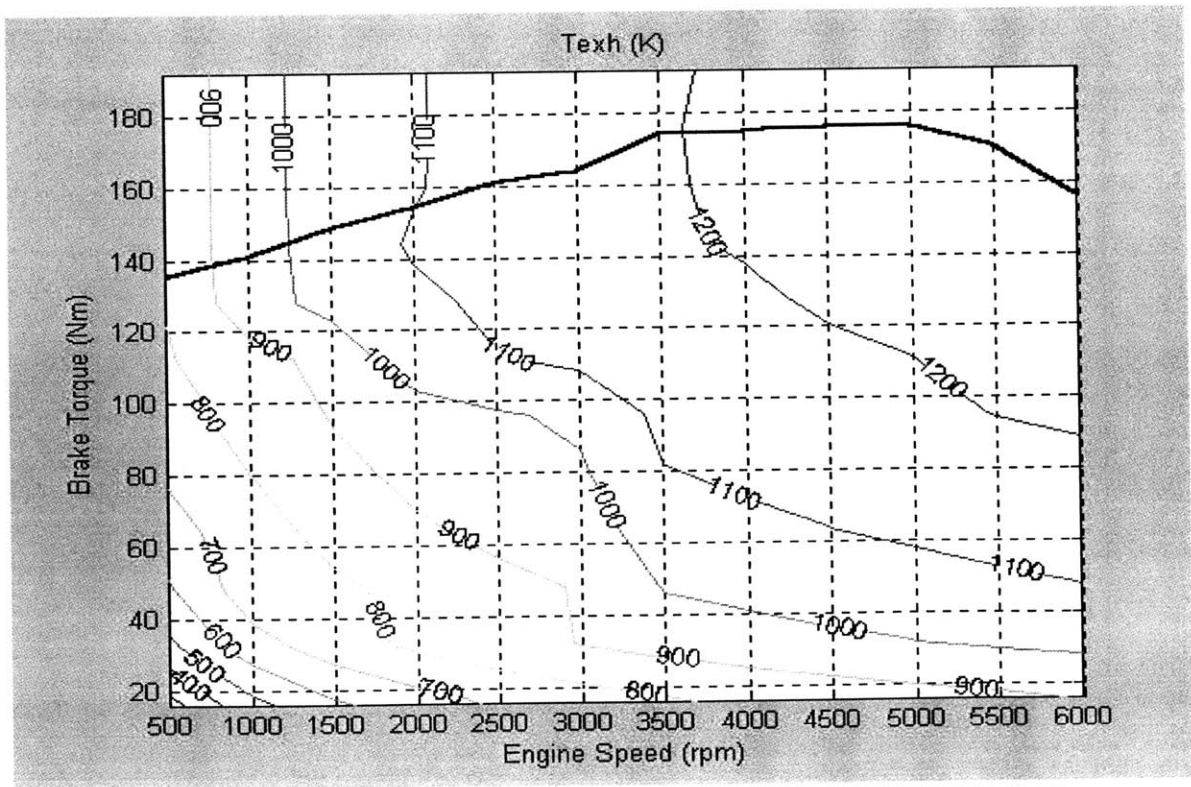


Figure 4-14 10% EGR: Exhaust Temperature

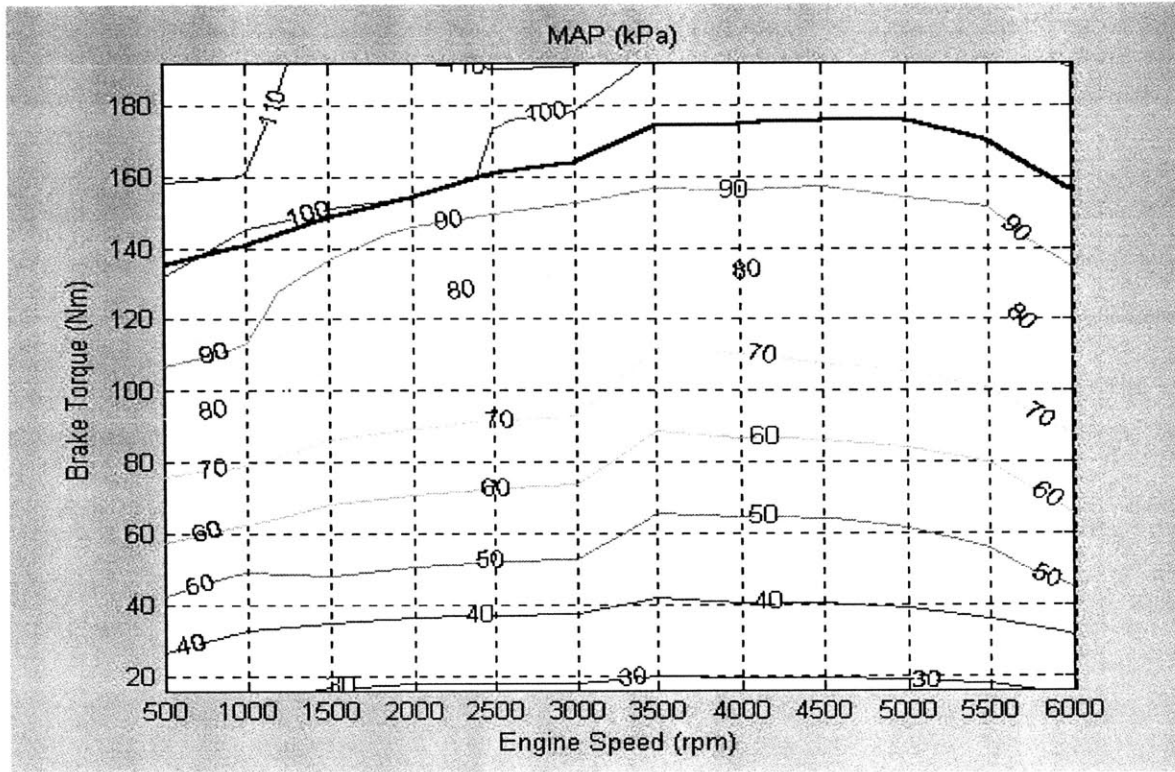


Figure 4-15 10% EGR: MAP

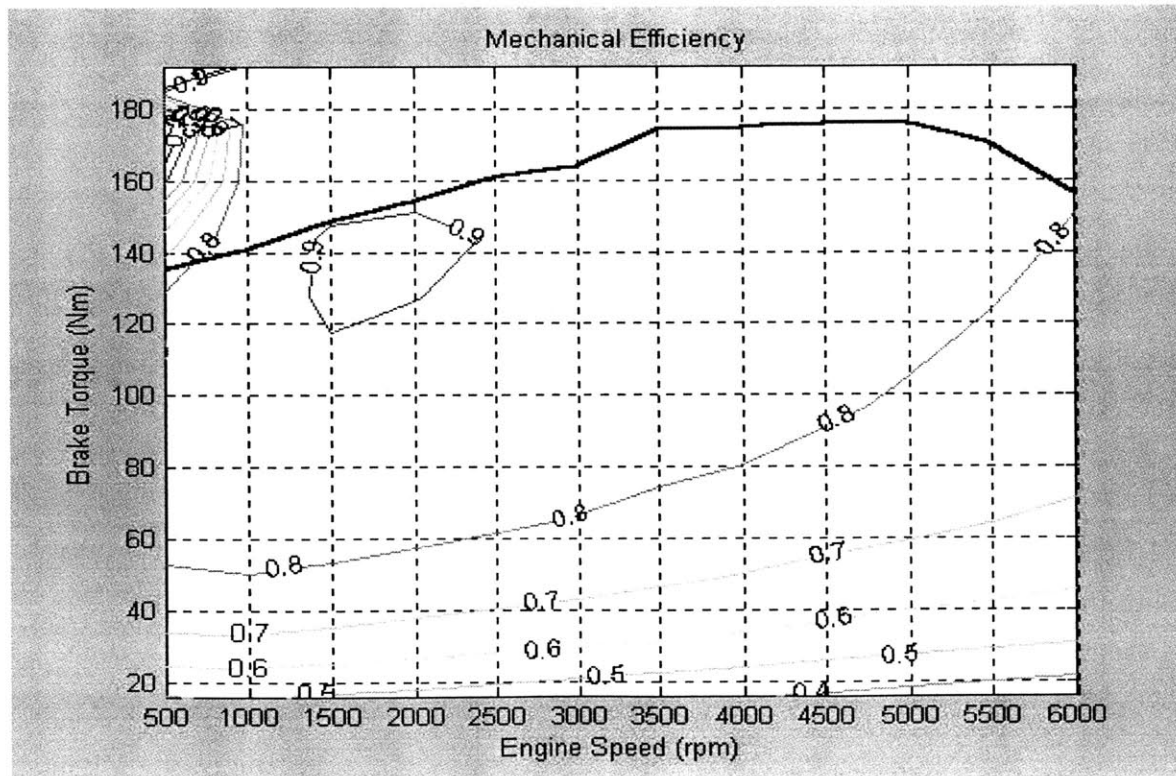


Figure 4-16 Lean Boost: Mechanical Efficiency

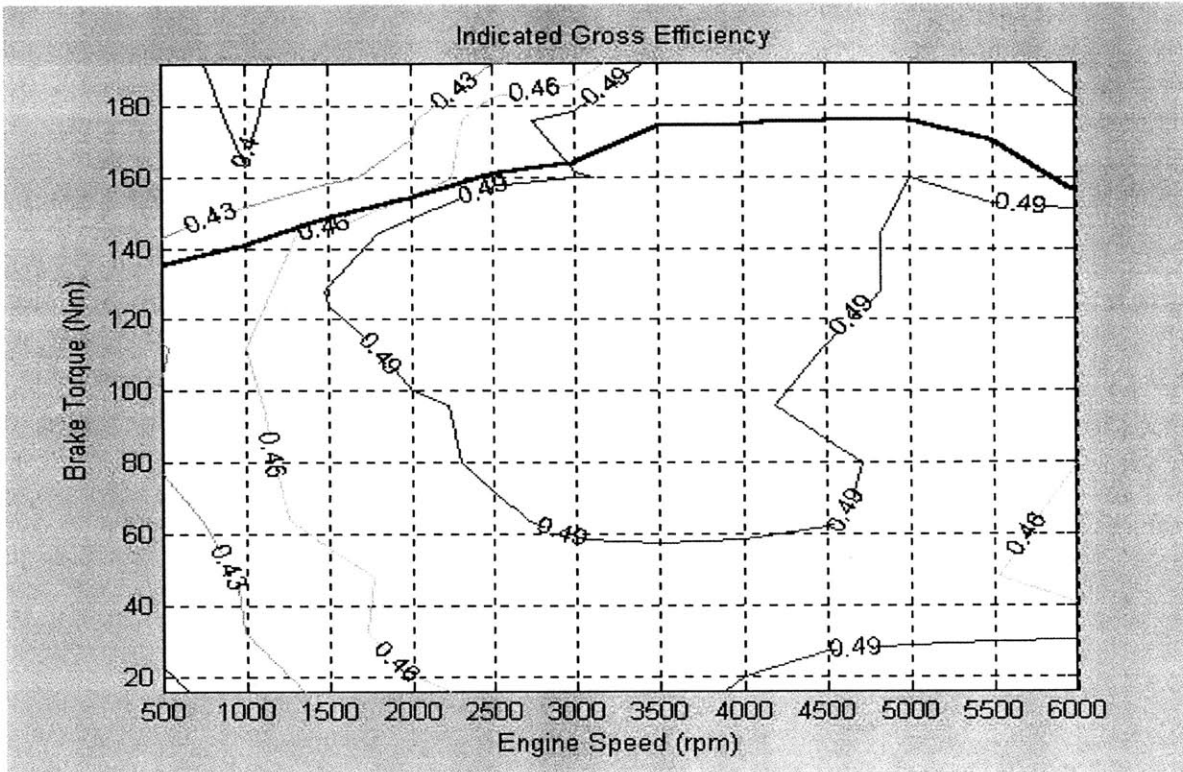


Figure 4-17 Lean Boost: Gross Indicated Efficiency

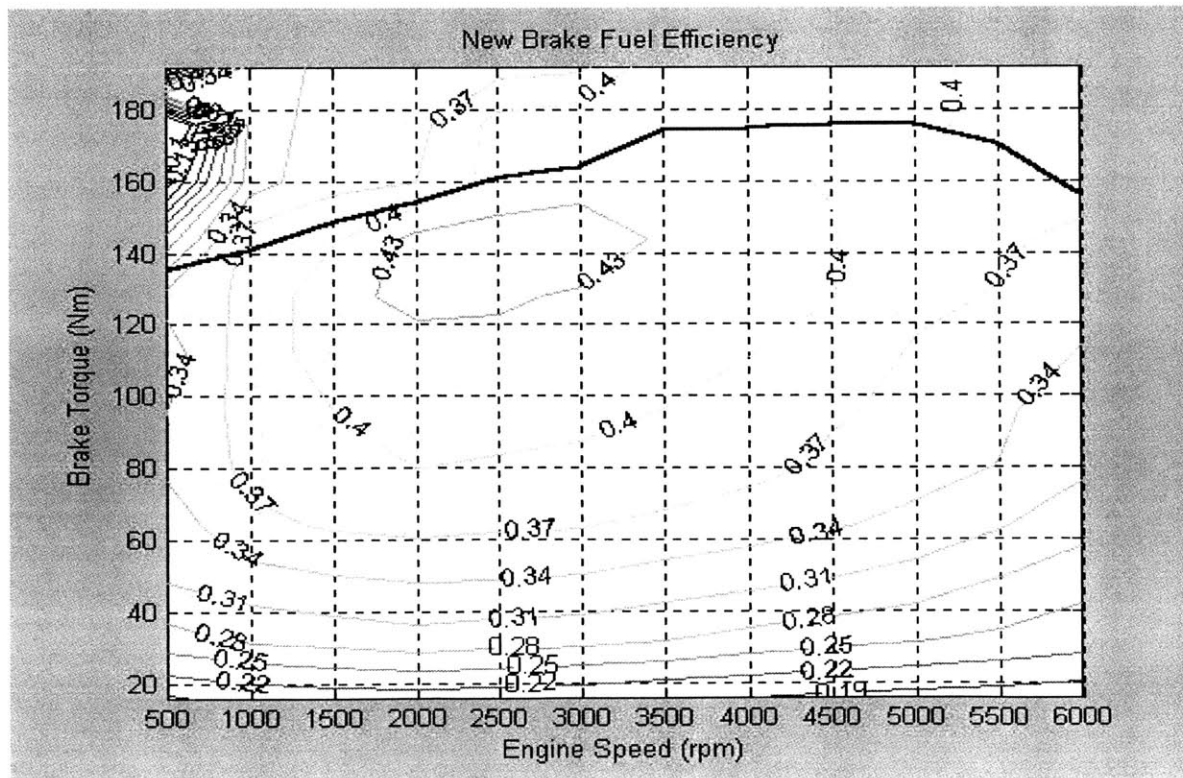


Figure 4-18 Lean Boost: Brake Fuel Efficiency

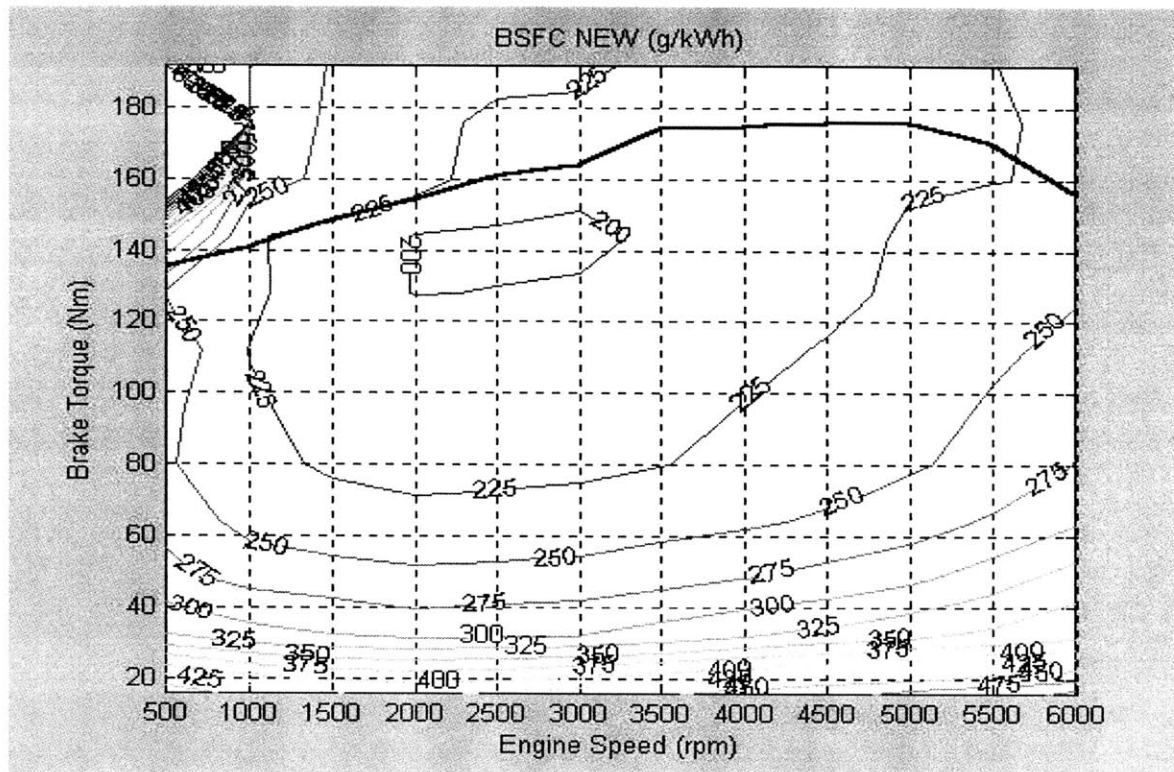


Figure 4-19 Lean Boost: BSFC

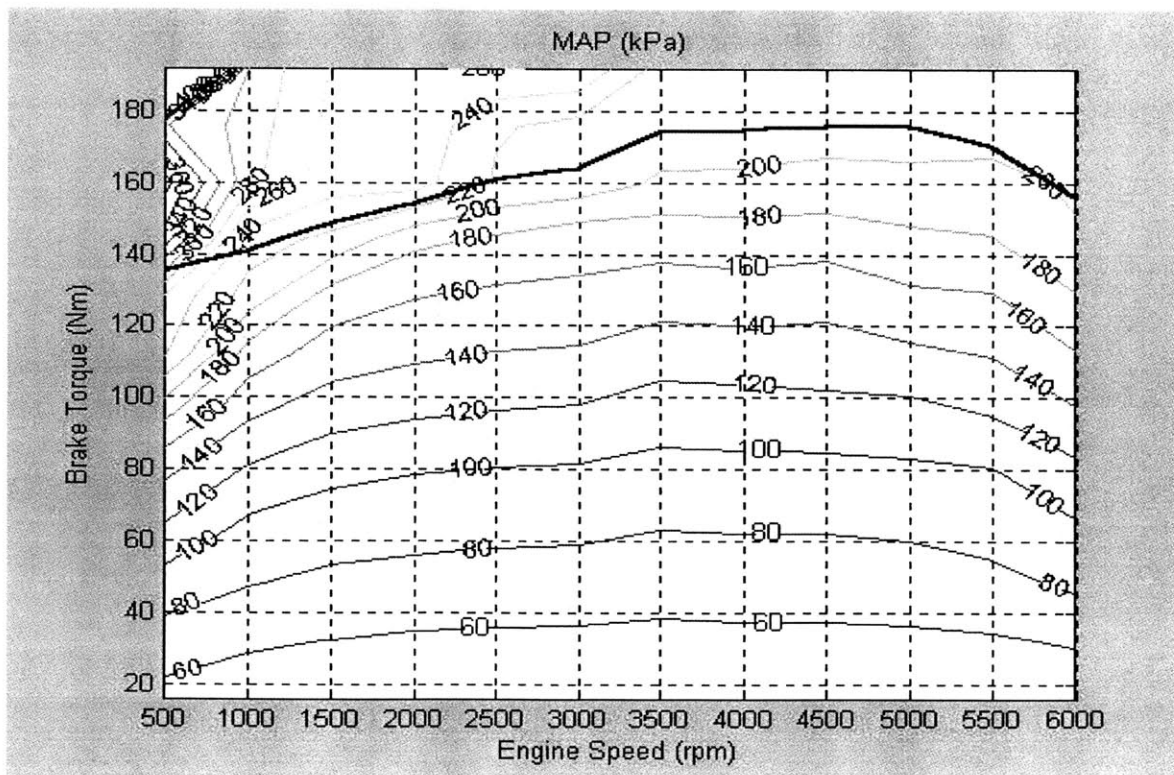


Figure 4-20 Lean Boost: MAP

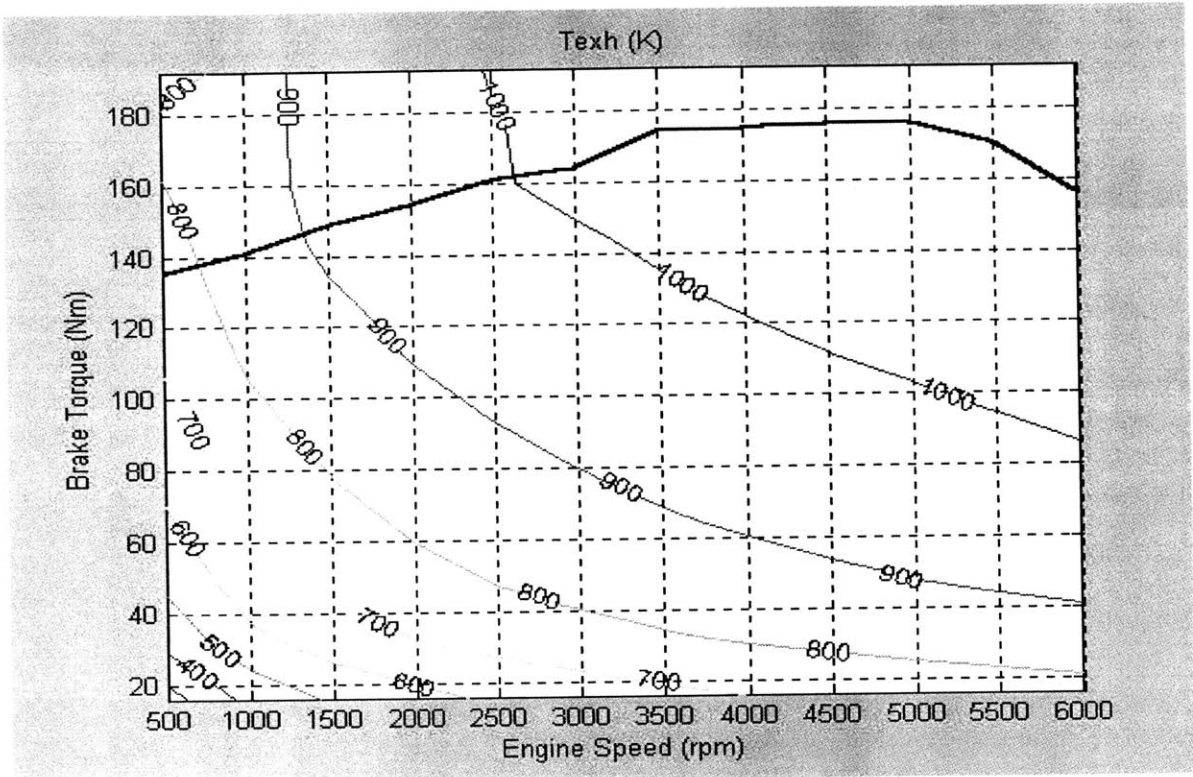


Figure 4-21 Lean Boost: Exhaust Temperature

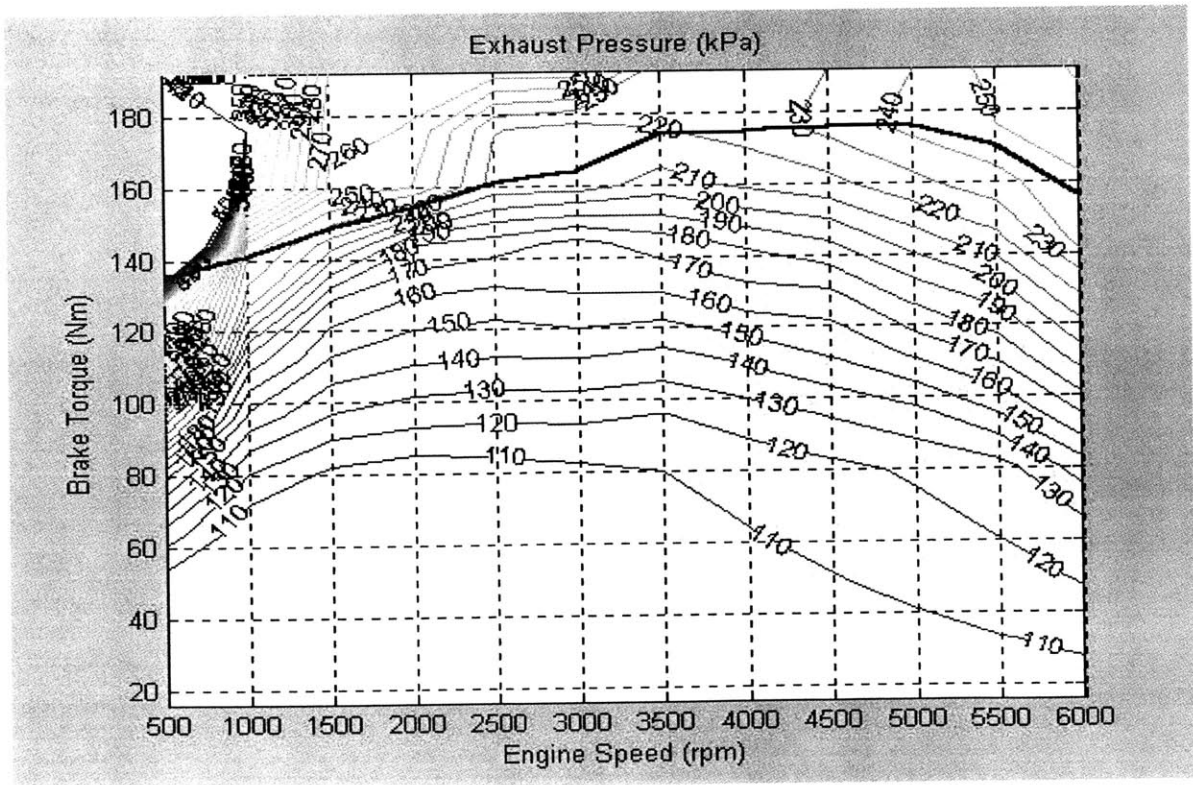


Figure 4-22 Lean Boost: Exhaust Pressure

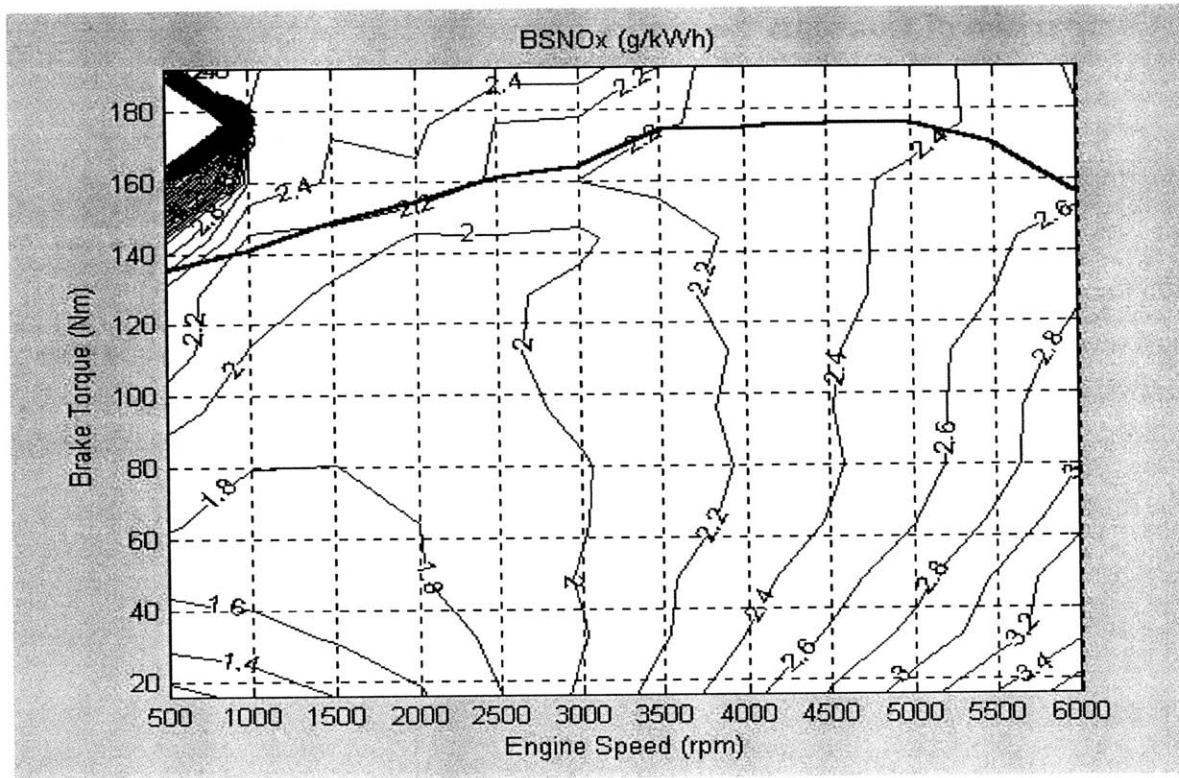


Figure 4-23 Lean Boost: BSNOx

There is not a significant variation in parameters between the Baseline and 10% EGR concepts. The major difference is in the BSNOx due to EGR dilution at part load for emission control. This difference can be seen when comparing Figures 4-13 and 4-6. EGR presence also influences MAP (Figure 4-15) and exhaust temperature (Figure 4-14).

Most of the parameters change when comparing Baseline concept to Lean Boost. Mechanical efficiency in Figure 4-16 is higher due to turbocharging. MAP and exhaust pressures are raised substantially (Figures 4-20 and 4-22). Indicated efficiency (Figure 4-17) is increased due to the presence of plasmatron gas that allows for compression ratio increase and very lean operation. Combined benefits of mechanical and indicated efficiency are seen in brake fuel efficiency improvement in Figure 4-18. Very high dilution causes a dramatic decrease in BSNOx (Figure 4-23).

4.2 Comparison of Concepts

Lean Boost concept is compared to Baseline and 10% EGR concepts to evaluate the fuel economy improvement and reduction in engine out NOx emissions. When compared to the Baseline concept there is a 24.4 percent fuel economy improvement (Figure 4-24) and 91 percent reduction in NOx emissions (Figure 4-25). A comparison between Lean Boost and 10% EGR concept shows a fuel economy improvement of 22.7 percent and 82.6 percent reduction in NOx emissions (Figure 4-26).

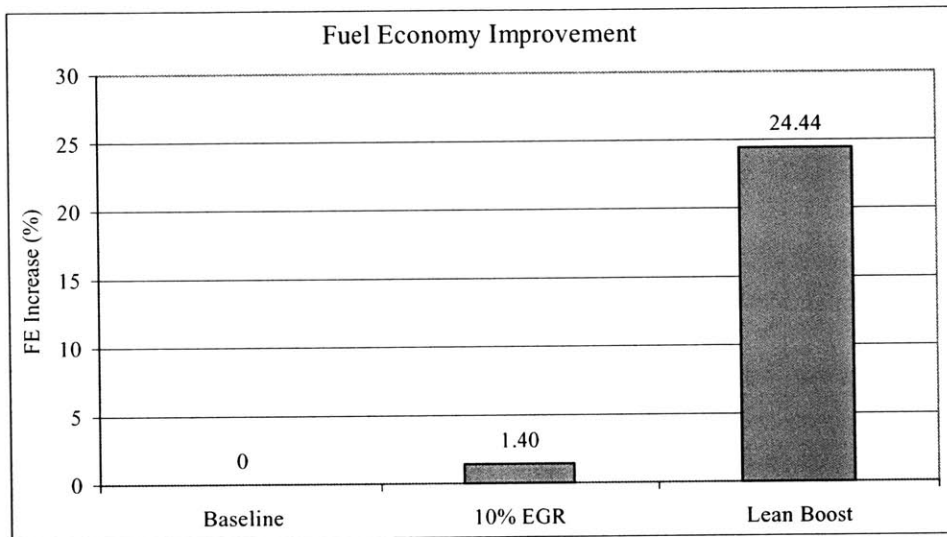


Figure 4-24 Fuel economy comparison of all three concepts

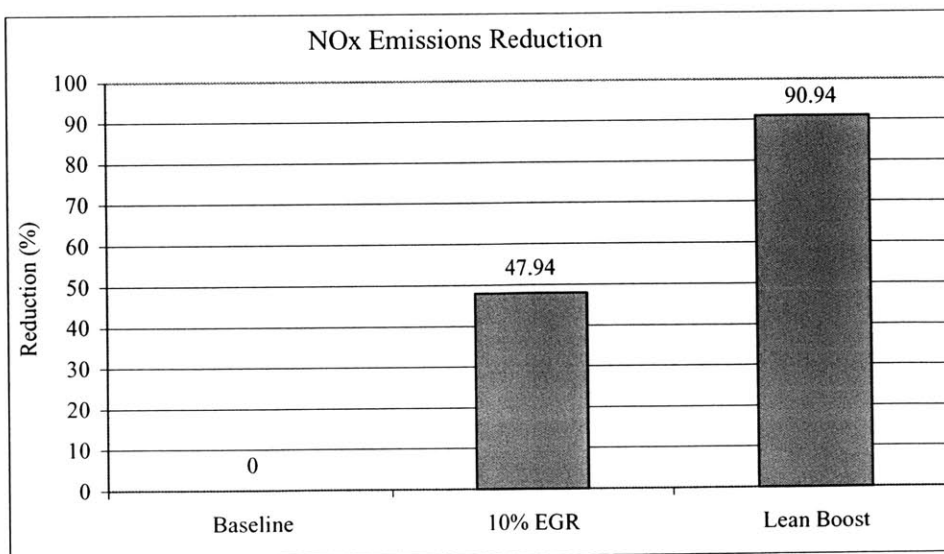


Figure 4-25 NOx emissions comparison of all three concepts

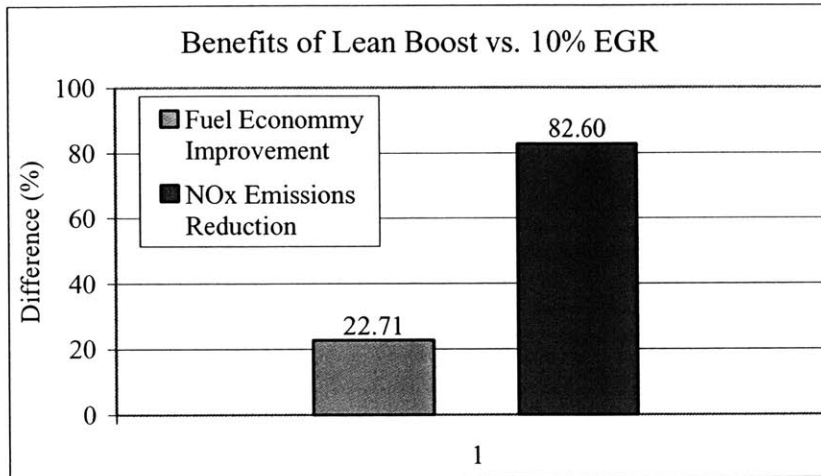


Figure 4-26 Benefits of Lean Boost vs 10% EGR

4.3 Downsizing Effect on Fuel Economy

Lean Boost engine concept is downsized in 10 percent increments until a maximum BMEP of 19 bar is reached which is the limit of a good turbocharged production engine. Fuel economy improvement for different percent reduction in engine displacement is presented in Figure 4-27. A linear increase in fuel economy improvement is observed when engine displacement is reduced while performance is kept constant. Fuel economy improvement around 3.33 percent is observed for every 10 percent reduction in engine size.

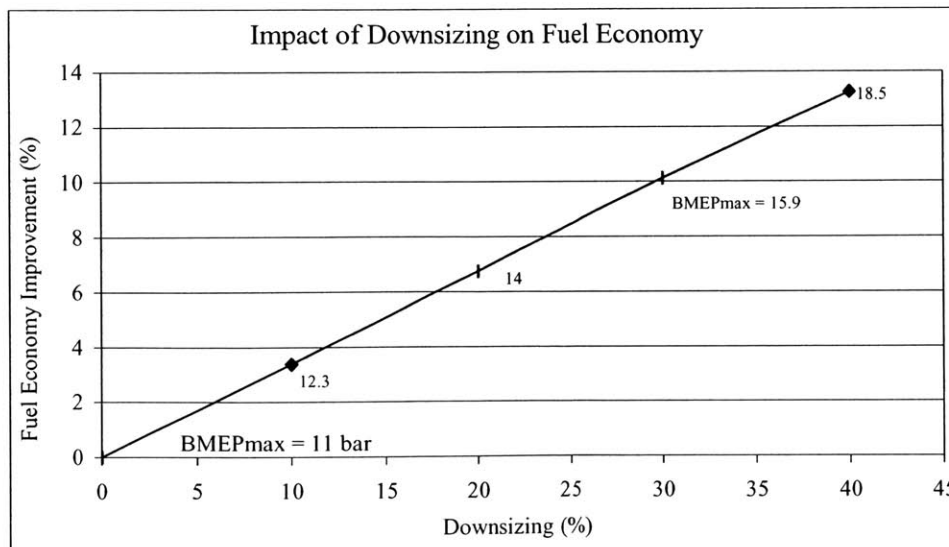


Figure 4-27 Impact of downsizing on fuel economy

(This page was intentionally left blank.)

CHAPTER 5 CONCLUSIONS

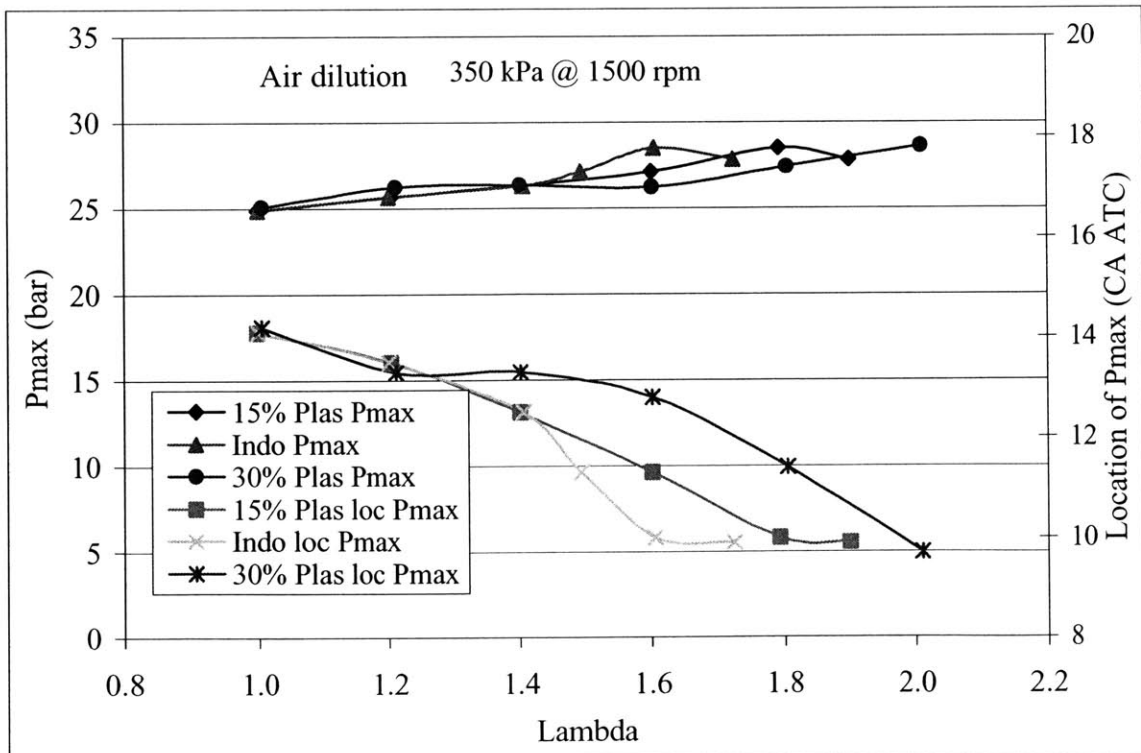
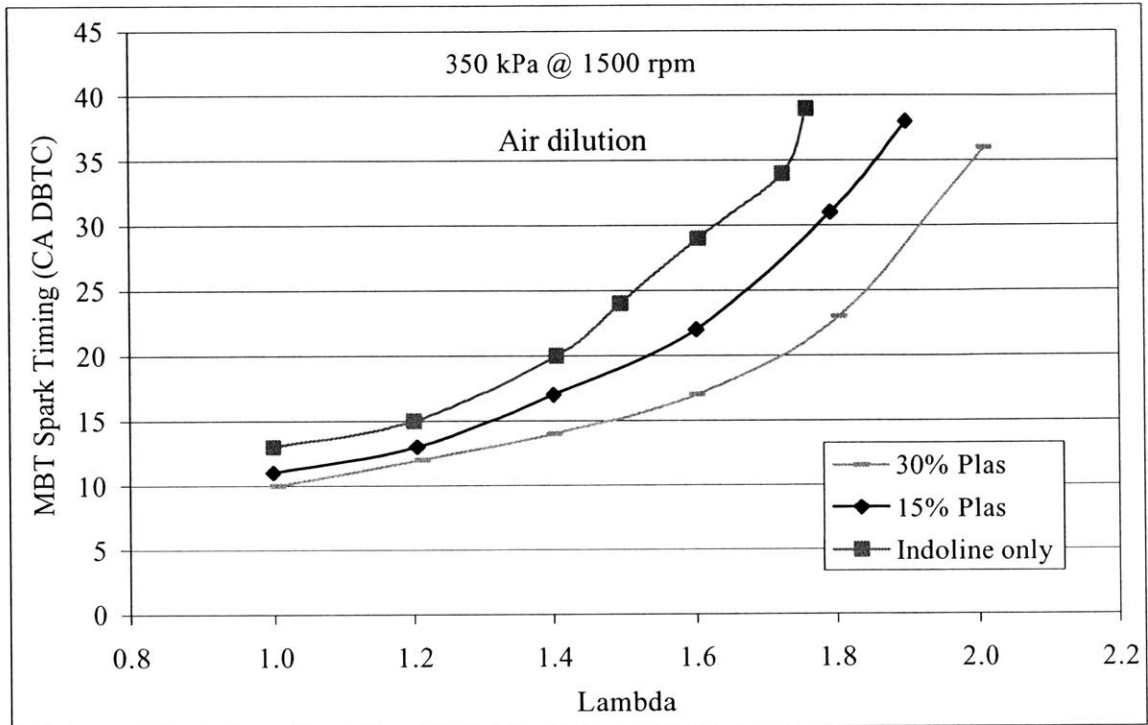
- A set of models, part physical and part empirical, have been combined to develop this engine simulation. Experimental data along with production engine data were used to calibrate this model. For a stoichiometric naturally aspirated operation with no hydrogen addition the simulation matches the production engine data very well. Experimental data were used to develop correlations for lean operation with various amounts of hydrogen addition. Turbocharger model was incorporated to allow high boost pressures that are required for very lean operation. This model was used for evaluation of fuel economy benefits and NO_x emissions reduction of lean boosted operation with hydrogen addition.
- Lean boosted operation with 20 percent reformat gas addition and 20 percent reduced engine displacement has significant fuel economy increase (24 percent), while the NO_x engine out emissions are reduced by 91 percent when compared to a naturally aspirated stoichiometric concept with no downsizing and no EGR dilution or plasmatron addition. There are still significant fuel economy benefits, approximately 23%, when 20 percent downsized, lean boosted operation with 20 percent reformat gas addition is compared to a naturally aspirated stoichiometric concept with 10 percent EGR dilution at part load for NO_x emissions control, which is more representative of the production vehicle. In this comparison NO_x emissions are reduced by 83%.
- There are still a number of issues that this model does not address in enough detail and thus the results might be optimistic. Knock constraint at low speed and maximum BMEP must be modeled in greater detail before this concept can be optimized. The model could also be improved by backing up the empirical correlations with theoretical models such as in-cylinder combustion model for efficiency and emissions. The next step would be to optimize the amount of plasmatron to be used for particular operating conditions to provide feedback for optimization of plasmatron design and operation. If EGR is used instead of, or along with, air for dilution, the relative amounts of EGR or air need to be determined to adequately reduce NO_x emissions for different operating conditions.

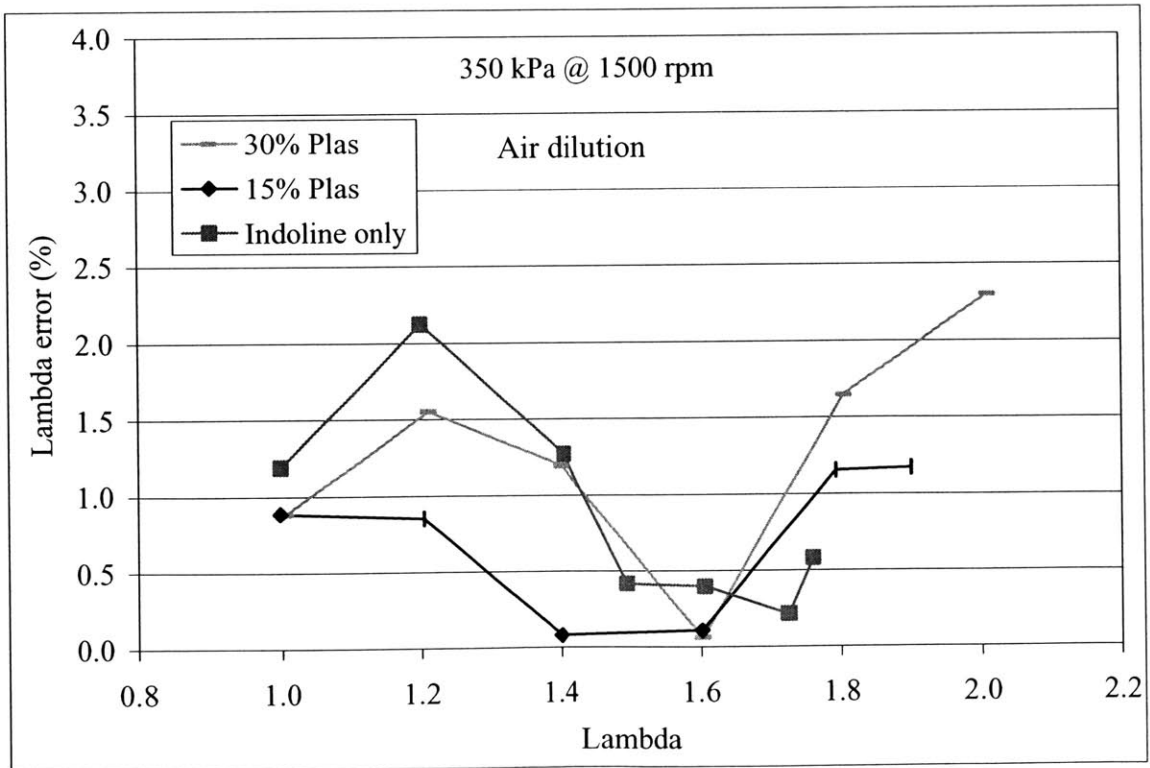
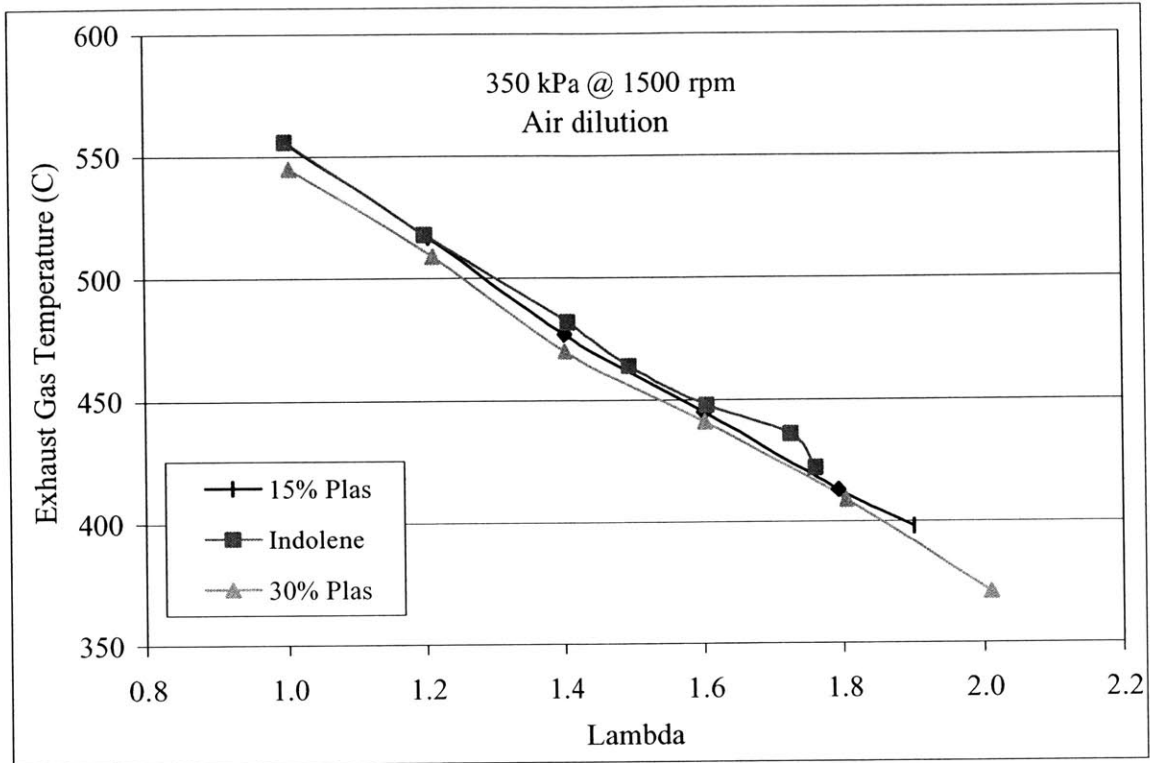
REFERENCES

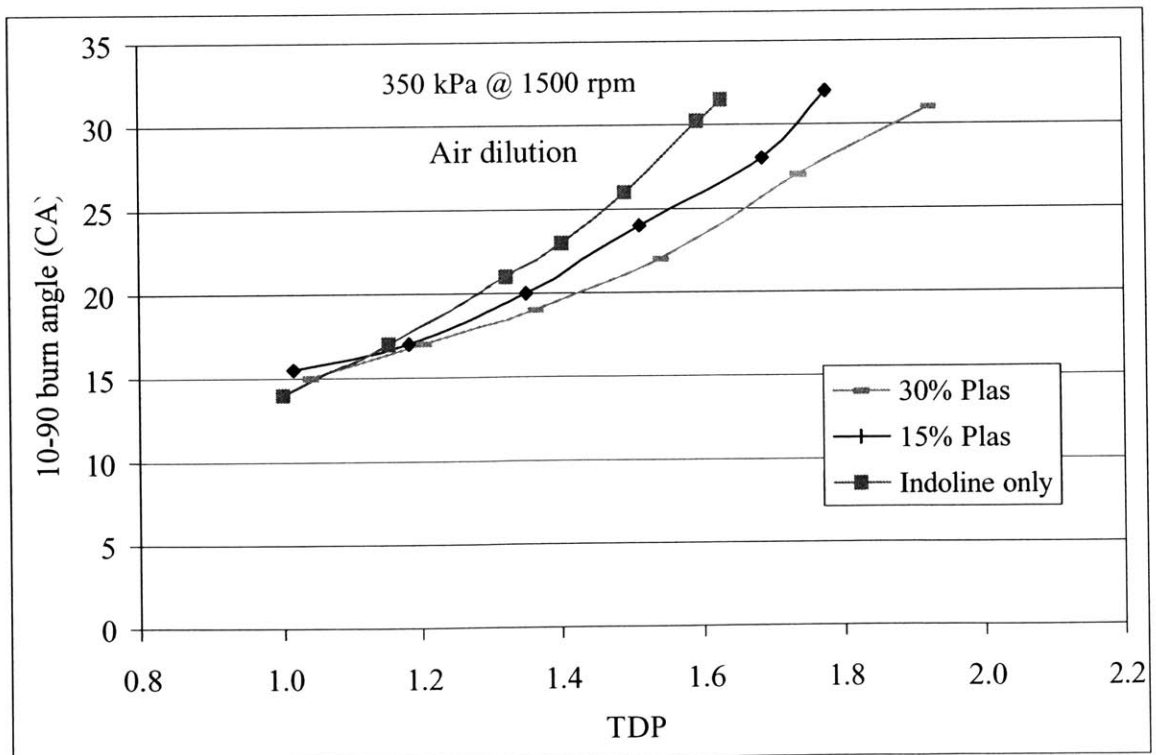
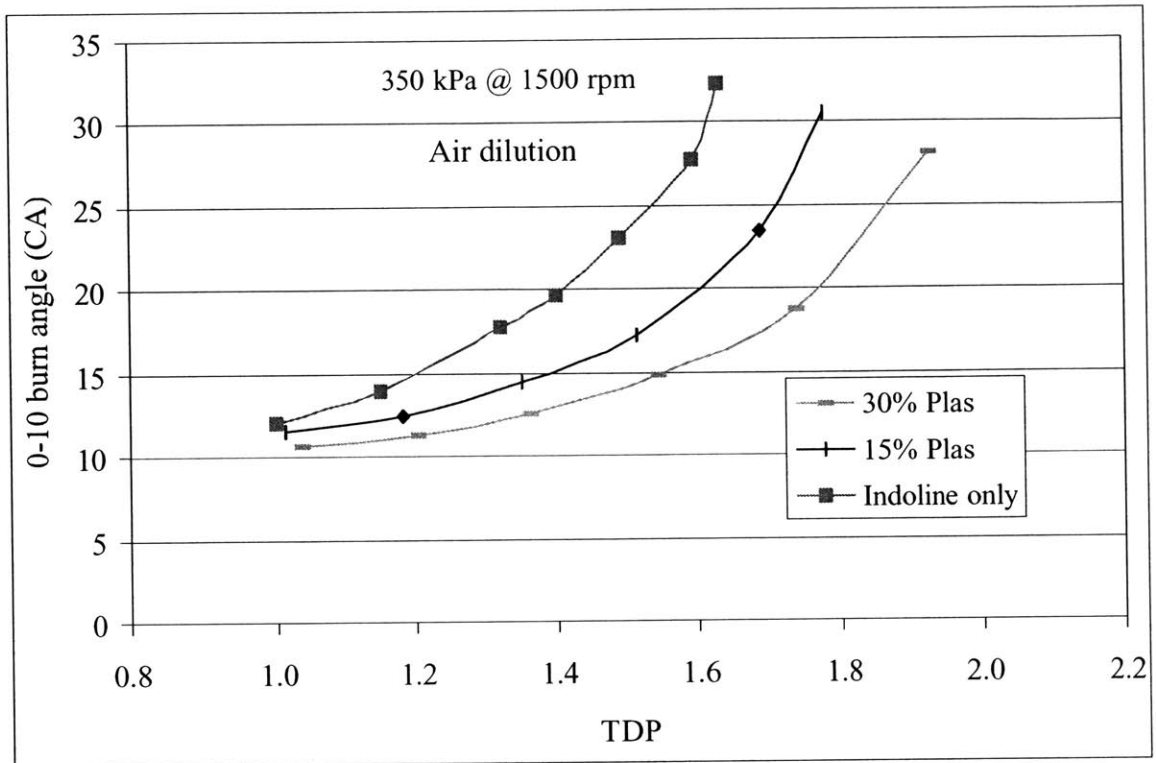
- 1 Glassman, I., Combustion, Academic Press, Inc., California, 1996.
- 2 Tully, E., Heywood, J., "Lean Burn Characteristics of a Gasoline Engine Enriched with Hydrogen from a Plasmatron Fuel Reformer" SAE 2003-01-0630.
- 3 Gruden, D. and Hahn, R., "Performance, Exhaust Emission and Fuel Consumption of IC Engine Operation with Lean Mixtures," I Mech. E Publication (C111/79), 1979.
- 4 Topinka, J., Gerty, M., Heywood, J., Keck, J., "Knock Behavior of a Lean-Burn, H₂ and CO Enhanced, SI Engine Concept," SAE 2004-01-0975.
- 5 Kalghatgi, G.T., "Fuel Anti-Knock Quality-Part I: Engine Studies," SAE 2001-3584.
- 6 Russ, S., "A Review of the Effect of Engine Operating Conditions on Borderline Knock," SAE 960497.
- 7 Green, J., Domingo, N., Storey, J., Wagner, R., Armfield, J., Bromberg, L., Cohn, D., Rabinovich, A., Alexeev, N. "Experimental Evaluation of SI Engine Operation Supplemented by Hydrogen Rich Gas from a Compact Plasma Boosted Fuel Reformer," SAE 2000-01-2206.
- 8 Quader, A., Kirwan, J., Grieve, "Engine Performance and Emissions Near the Dilute Limit with Hydrogen Enrichment Using an On-Board Reforming Strategy," SAE 2003-01-1356.
- 9 Smaling, R., *System Architecture Selection in a Multi-disciplinary System Design Optimization Framework*, M.S. Thesis, MIT, May 2003.
- 10 Chevron Phillips UTG-96, Certificate of Analysis.
- 11 Cheung, H. and Heywood, J., "Evaluation of a One-Zone Burn Rate Analysis Procedure Using Production SI Engine Pressure Data," SAE 932749, 1993.
- 12 Chun, K. and Heywood, J., "Estimating Heat-Release and Mass-of-Mixture Burned from Spark-Ignition Engine Pressure Data," *Combustion Science and Technology*, Vol. 54, pp 133-143, 1987.
- 13 www.ctts.nrel.gov/analysis/
- 14 Heywood, J.B., Internal Combustion Engine Fundamentals, McGraw-Hill, New York, 1988.

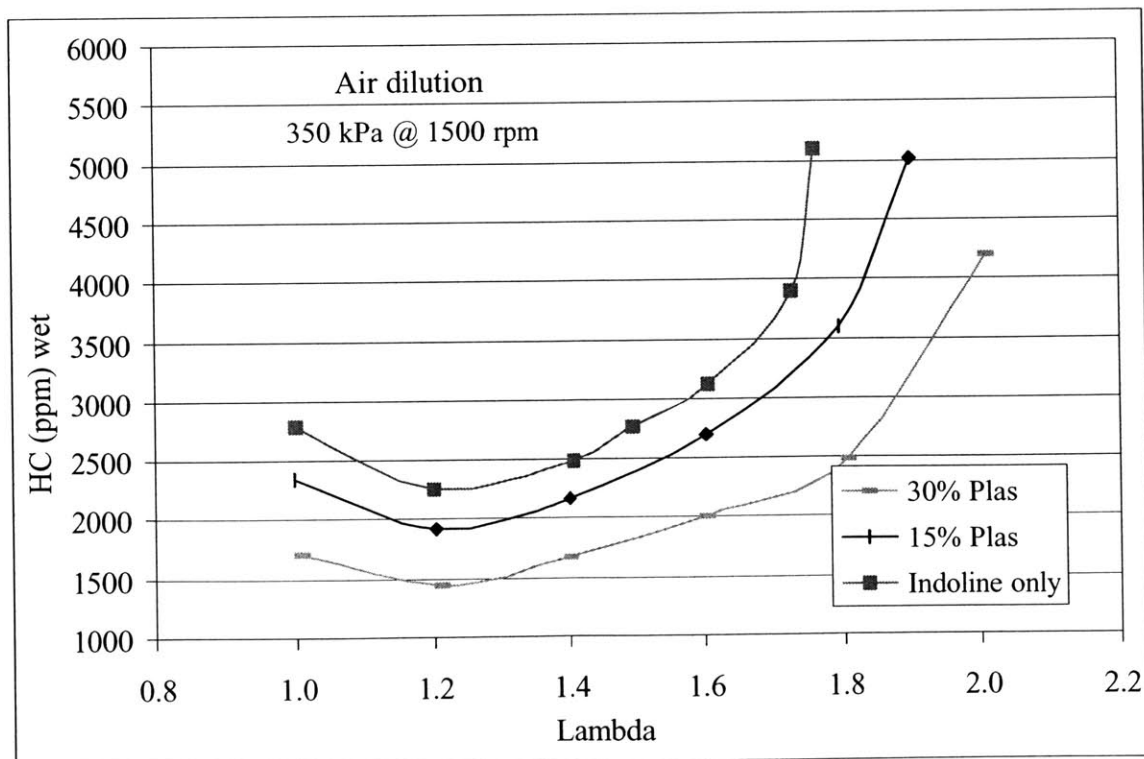
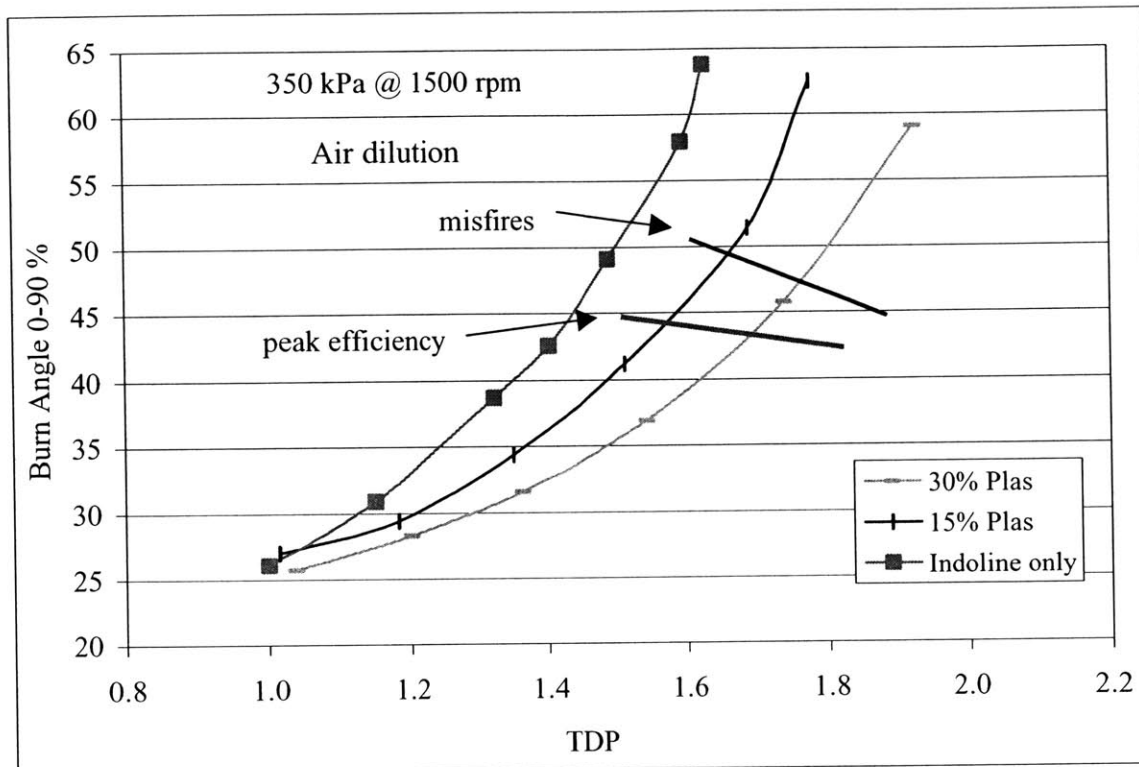
- 15 Sandoval, D. and Heywood, J.B., "An Improved Friction Model for Spark-Ignition Engines," SAE 2003-01-0725.
- 16 Shyler, P. and Chick, J., "A Method of Predicting Brake Specific Fuel Consumption Maps," SAE 1999-01-0556.
- 17 Taylor, C.F., The Internal Combustion Engine in Theory and Practice, Volume Thermodynamics, Fluid Flow, Performance, MIT Press, 2nd Edition, 1985.

APPENDIX A: Experimental data for 350 kPa NIMEP @ 1500 rpm

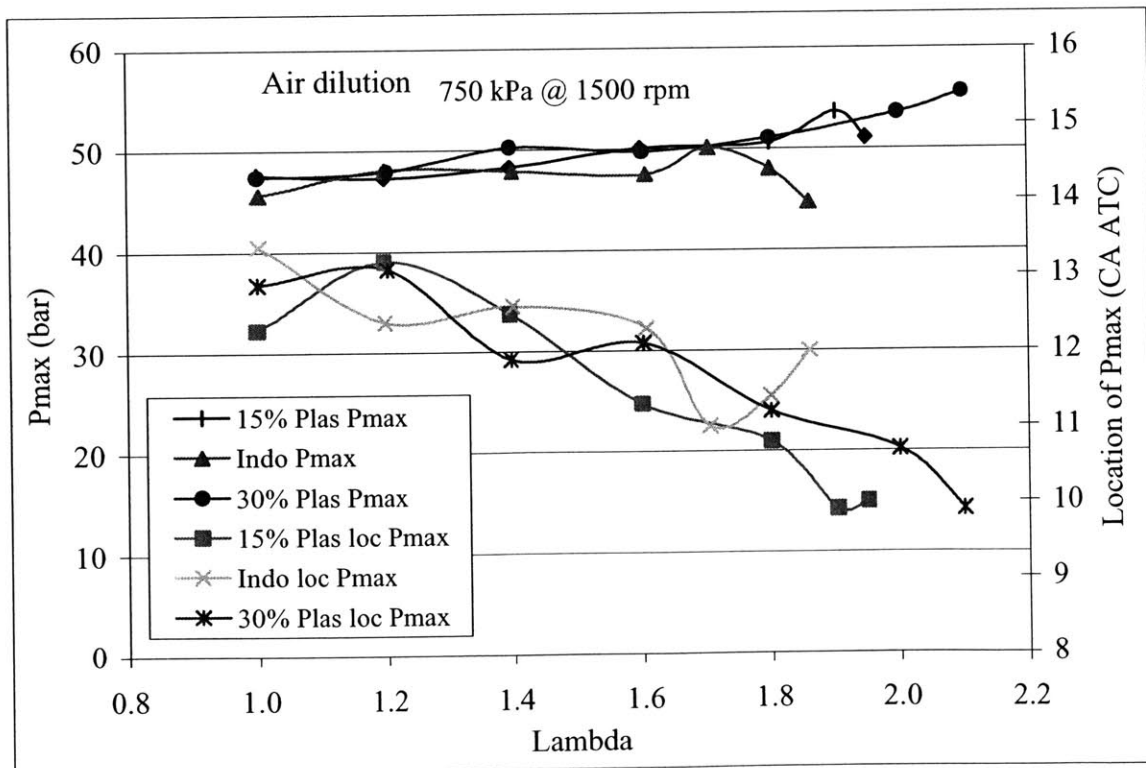
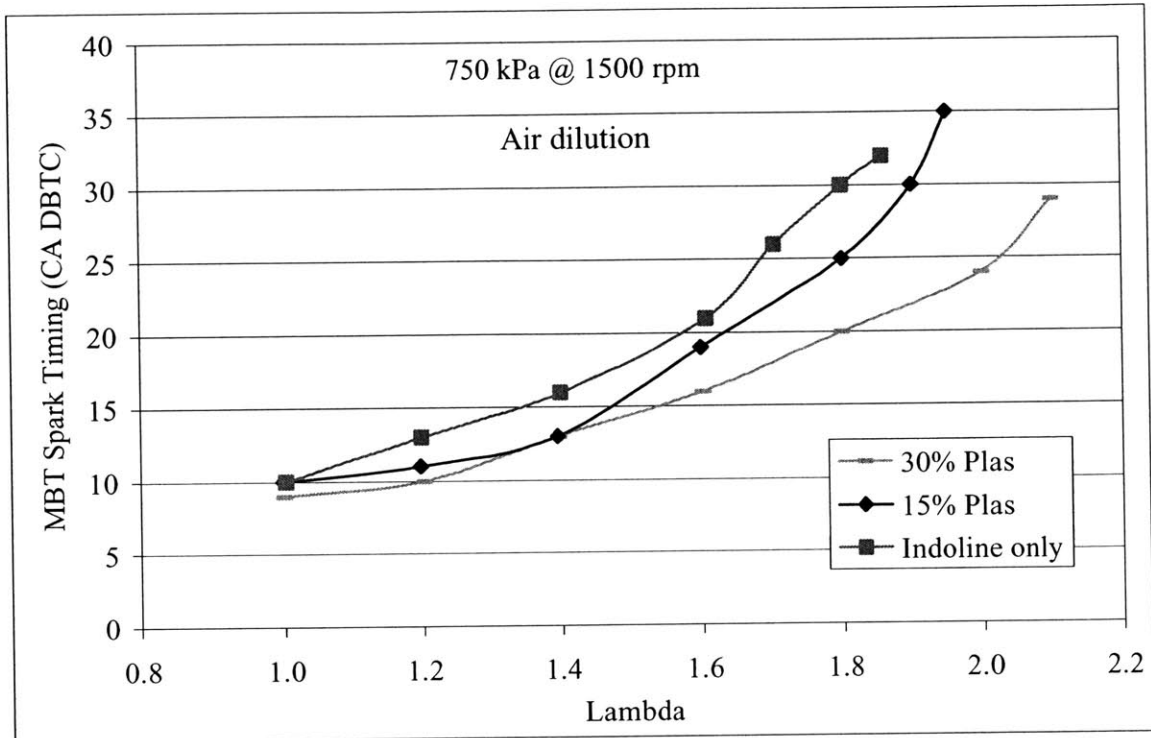


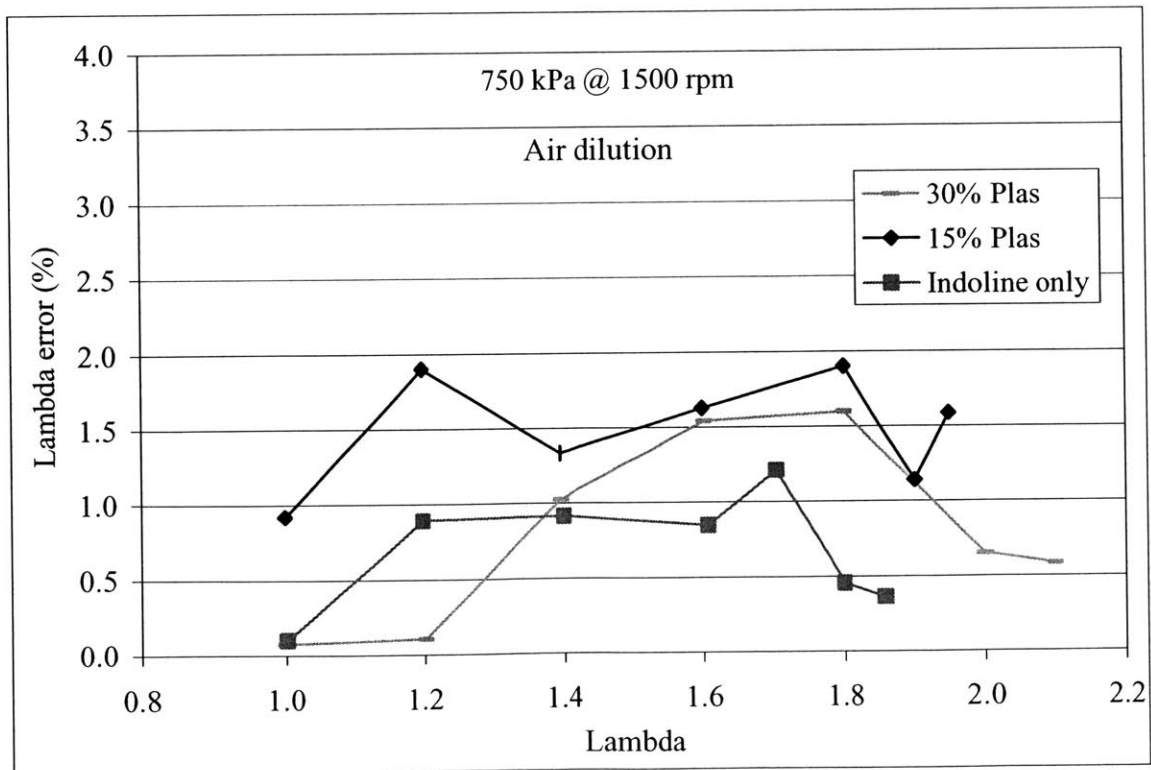
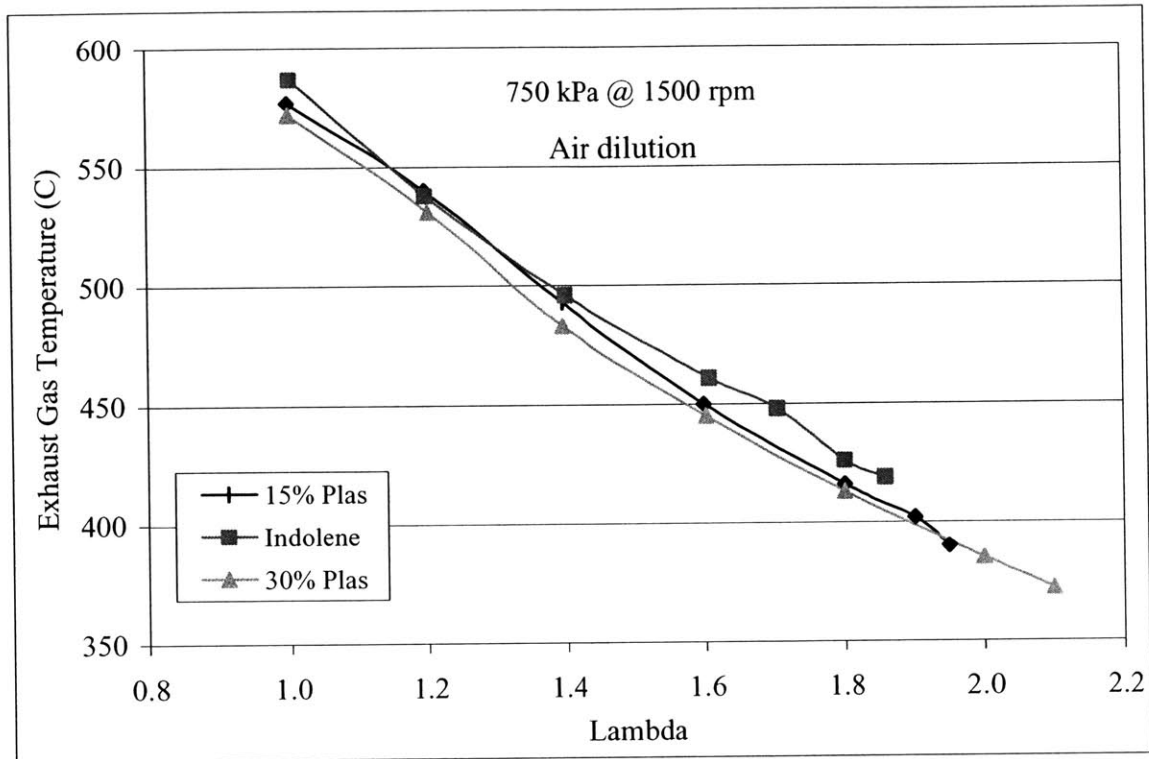


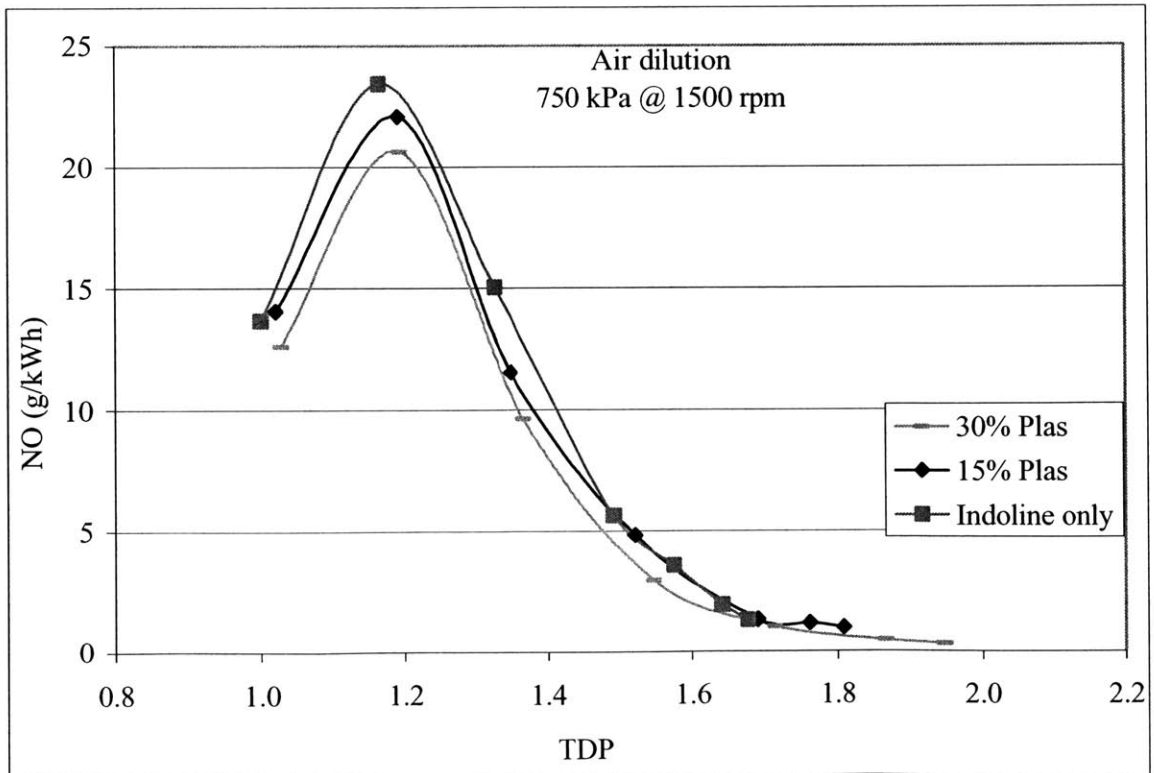
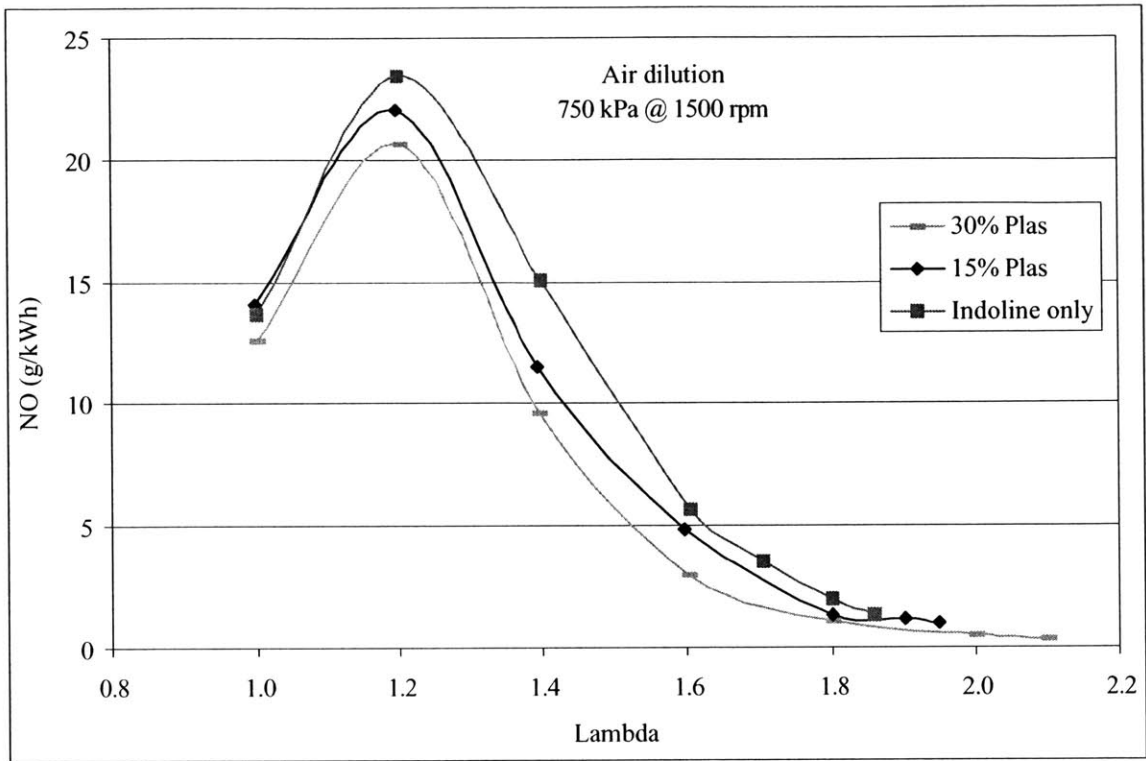


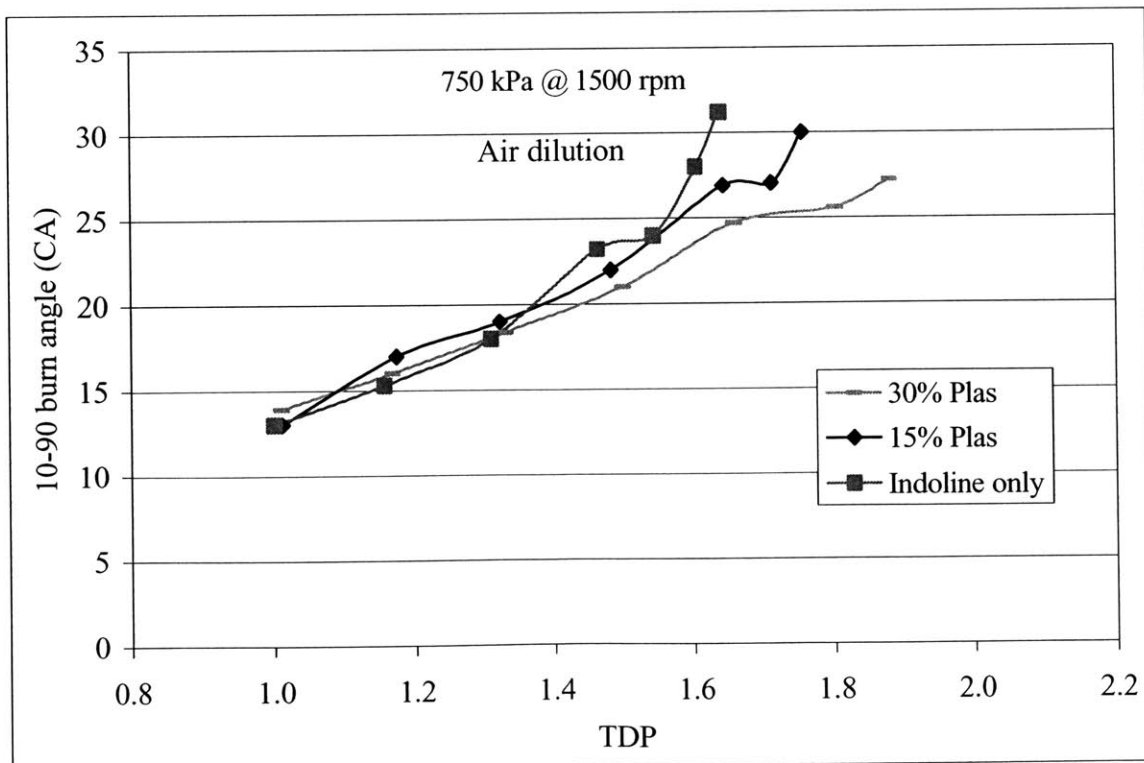
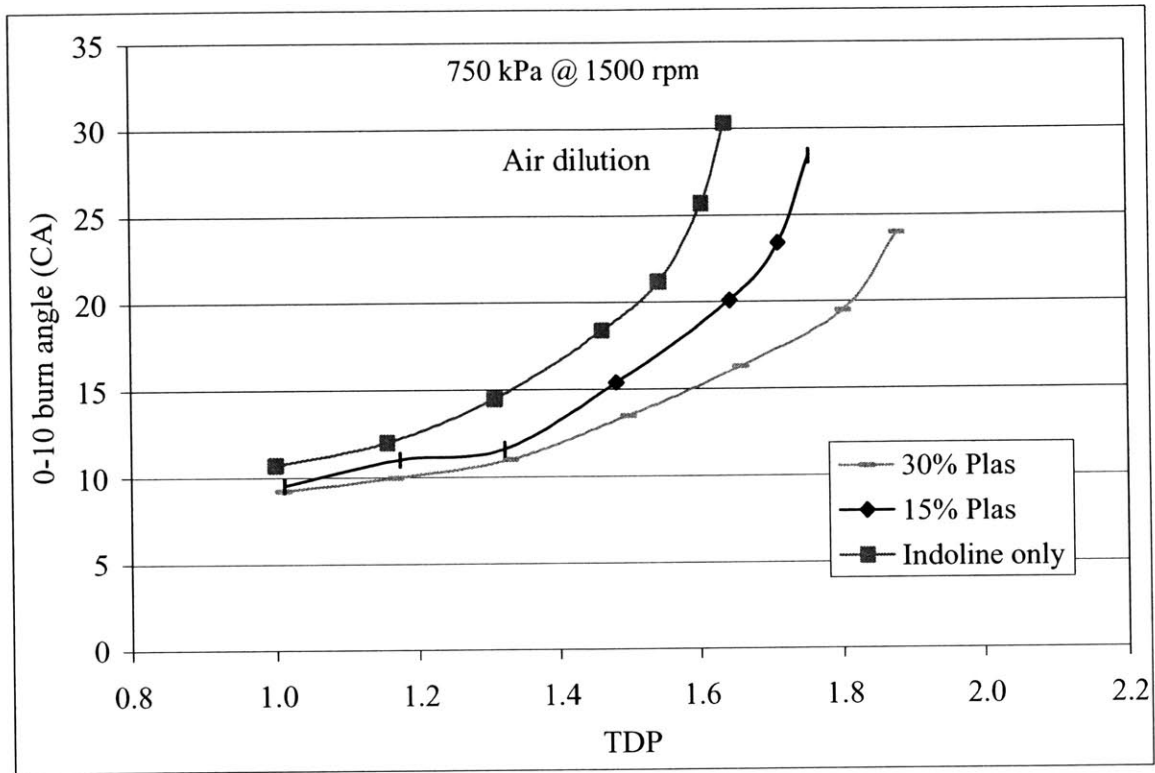


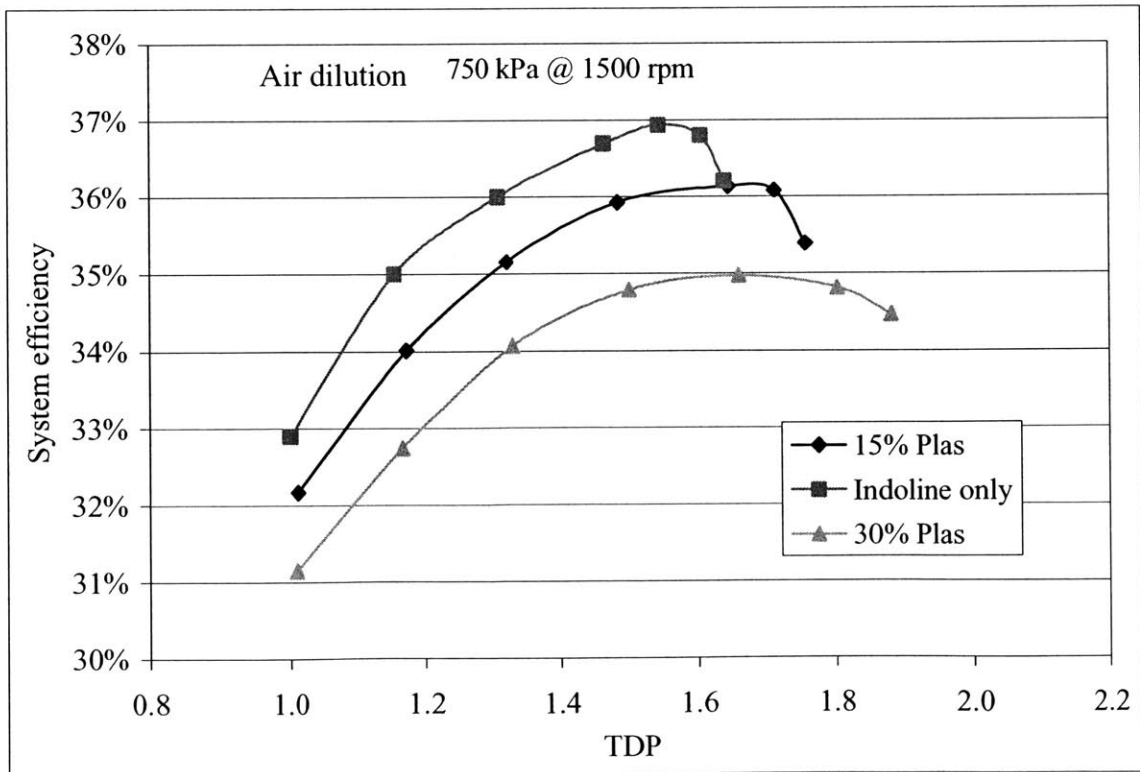
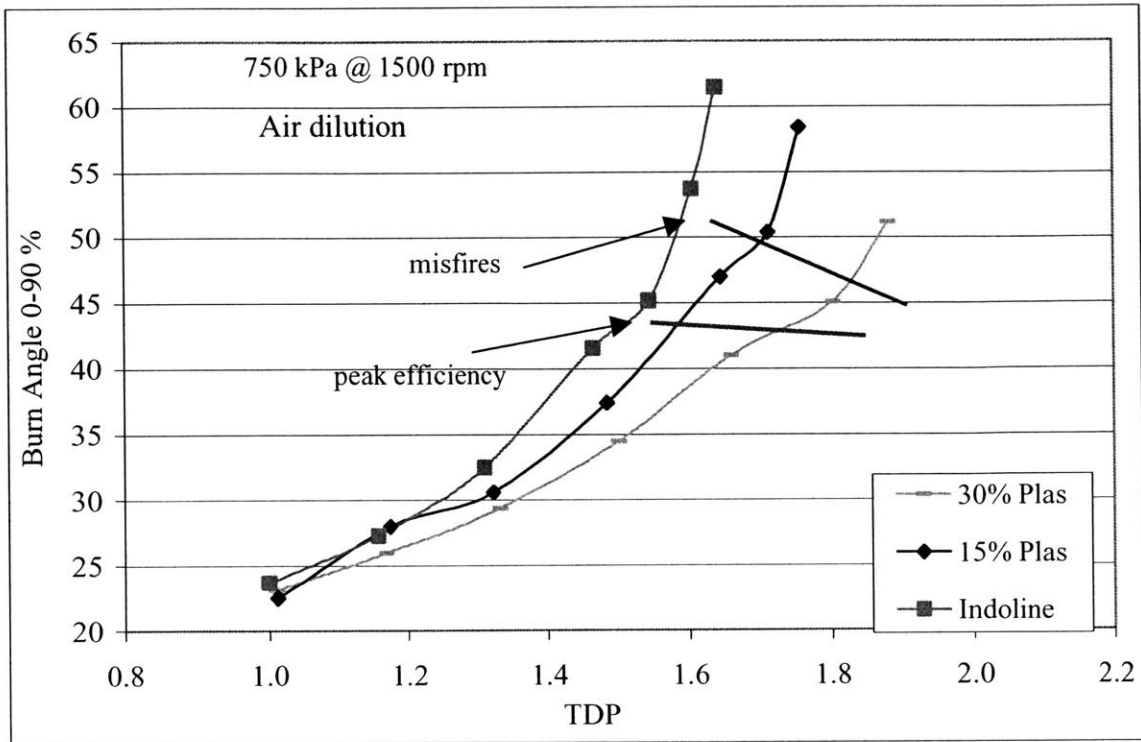
APPENDIX B: Experimental data for 750 kPa NIMEP @ 1500 rpm



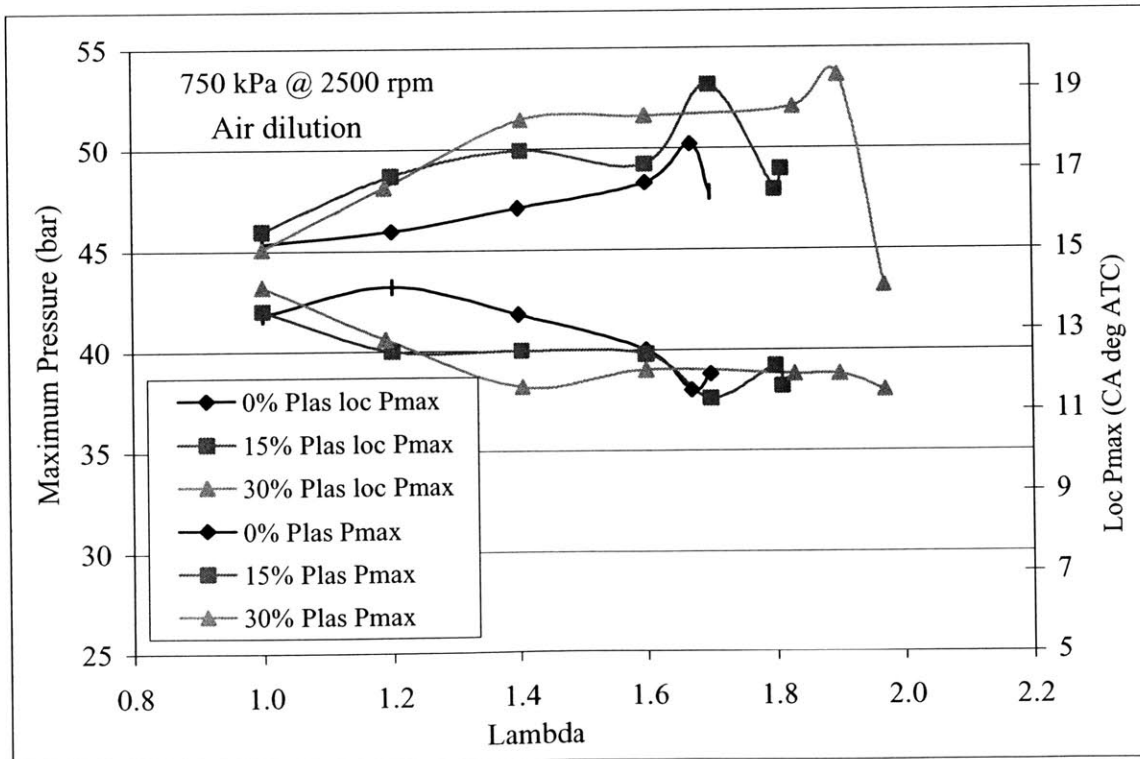
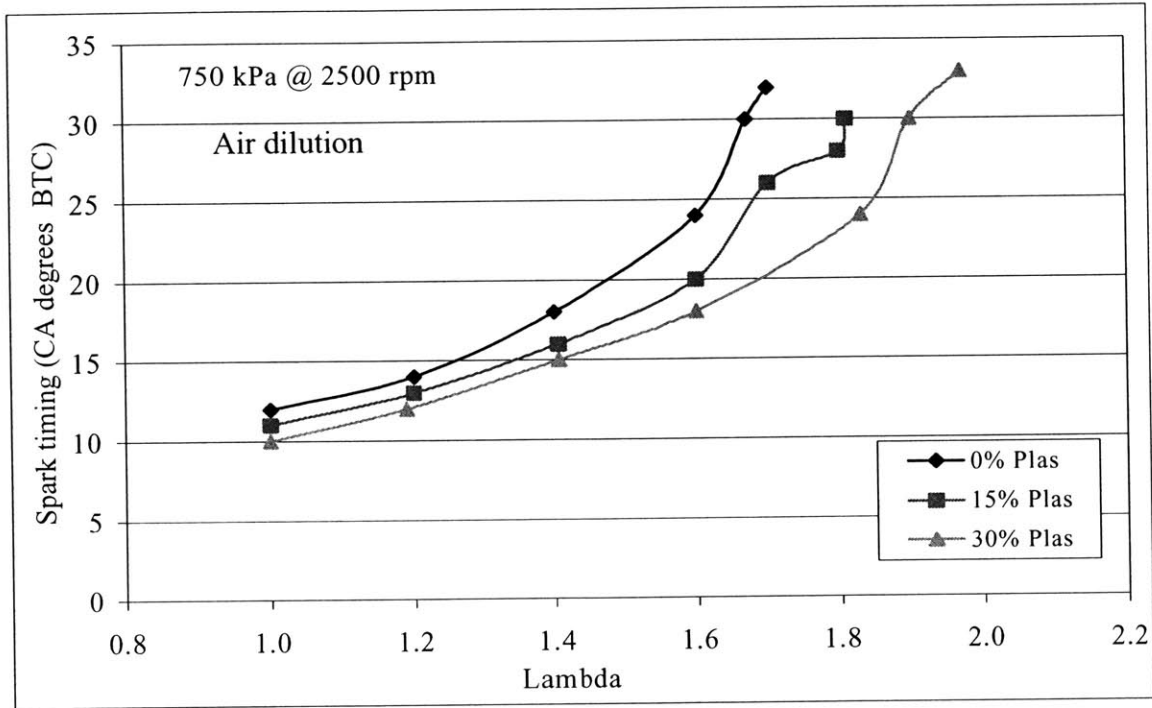


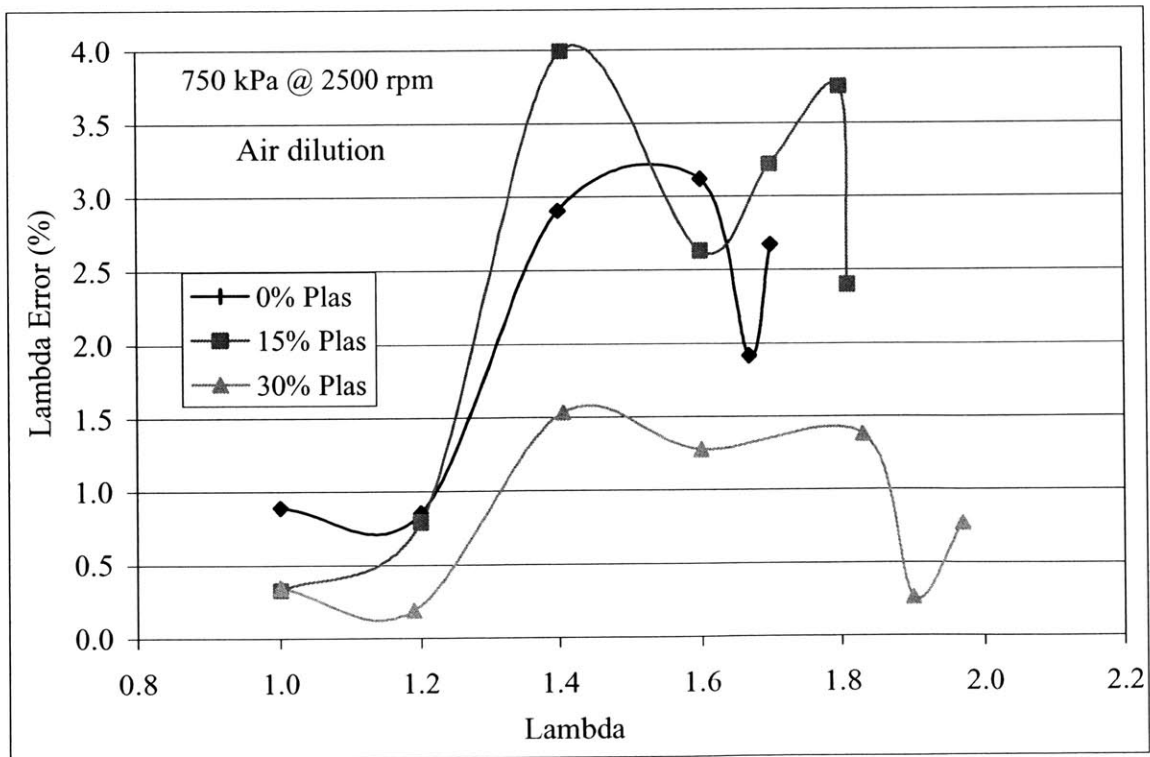
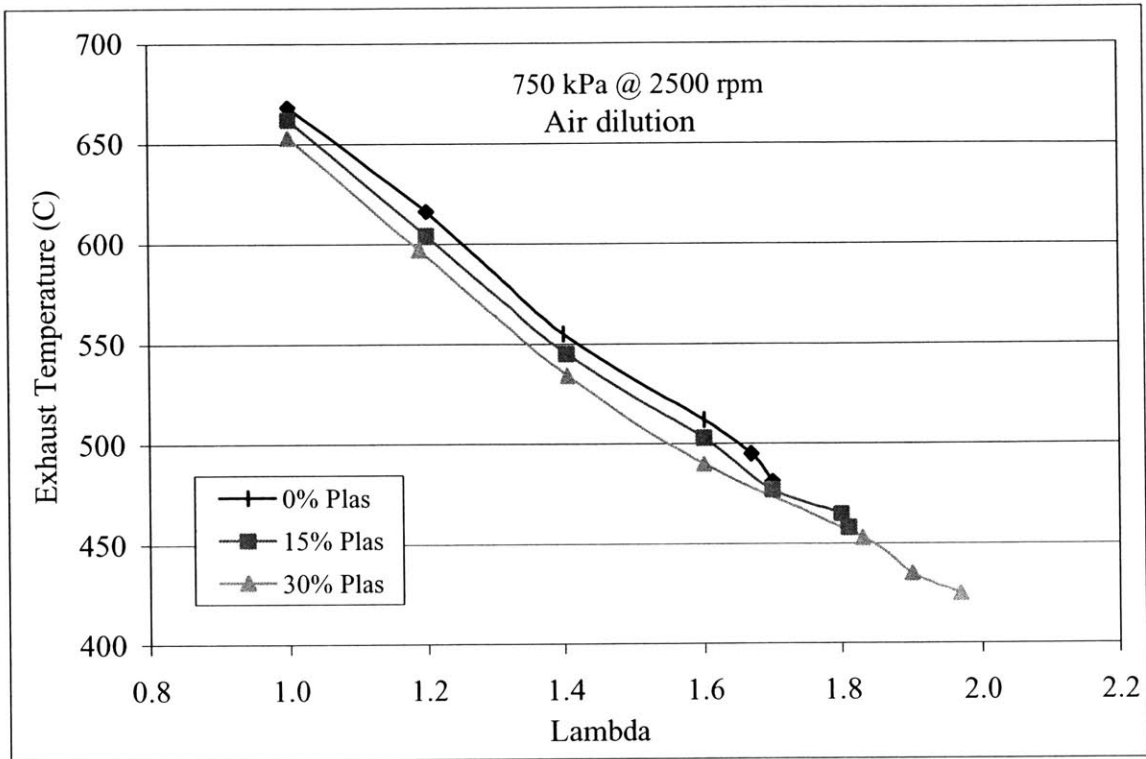


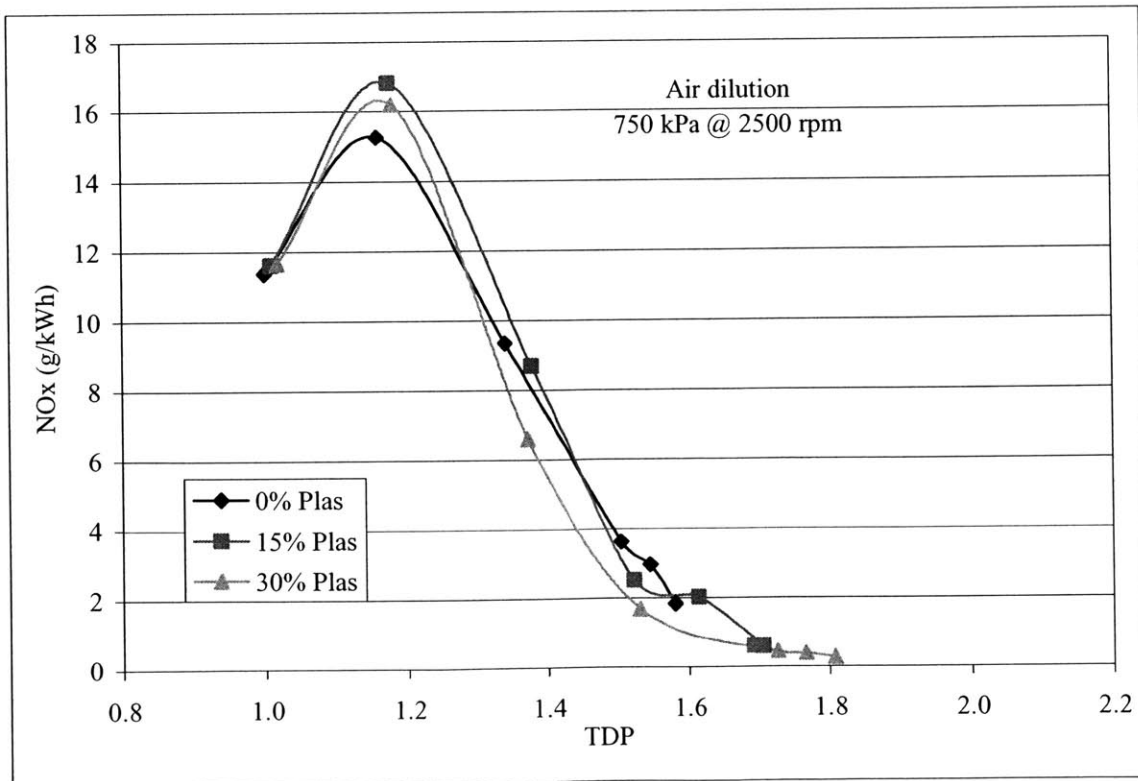
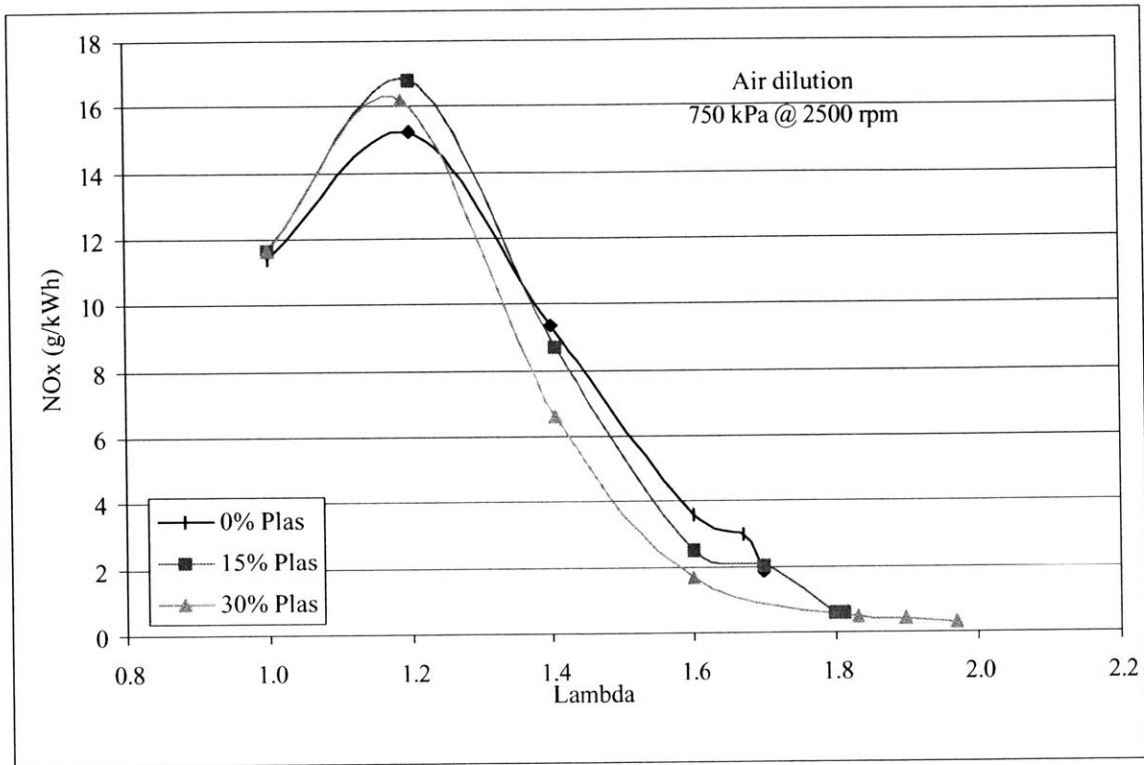


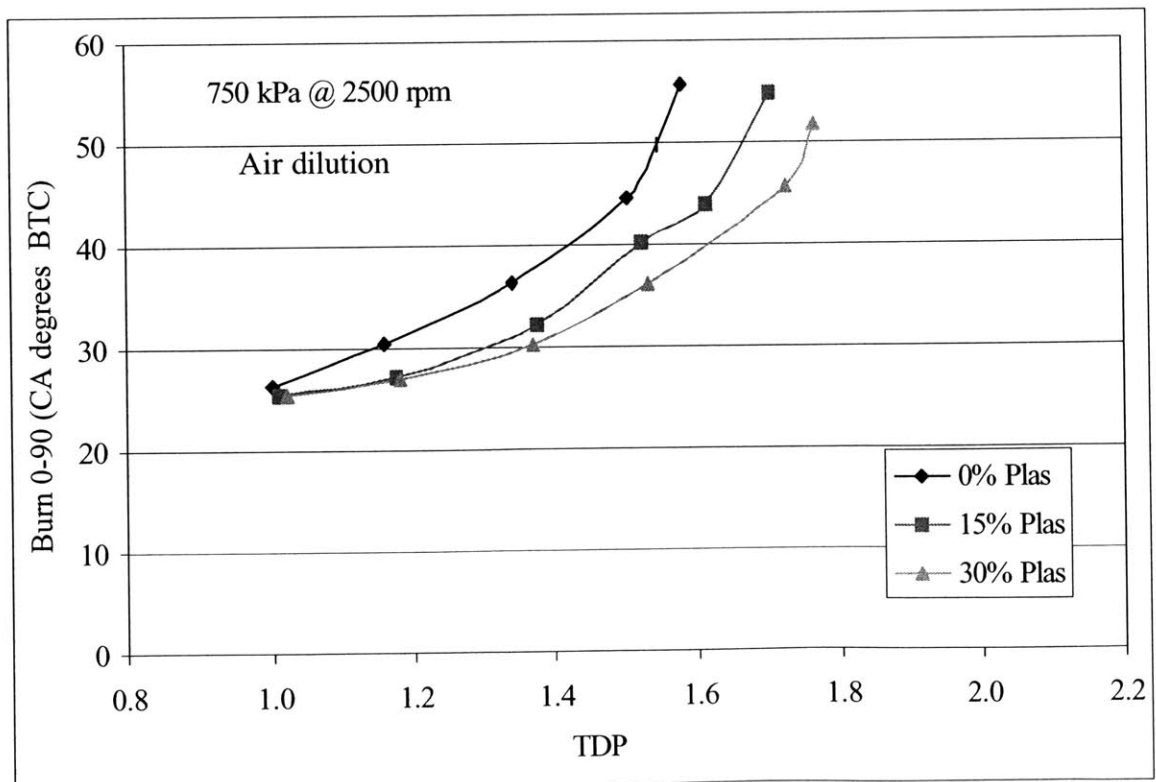
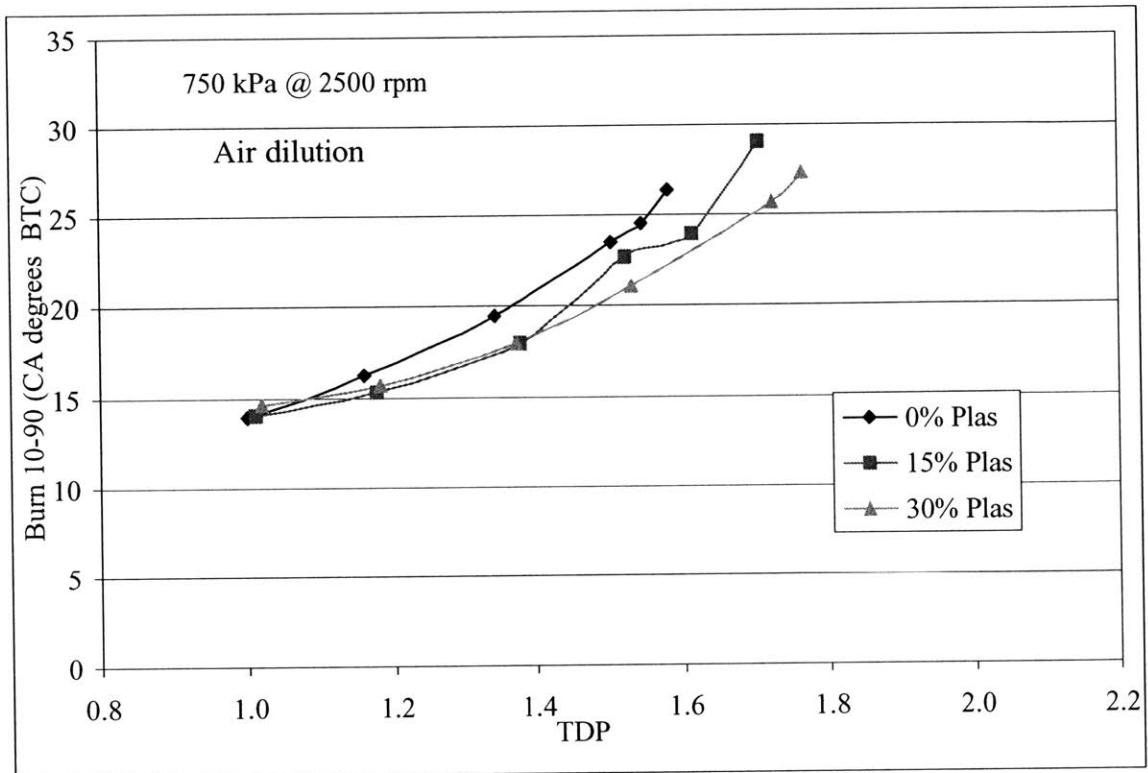


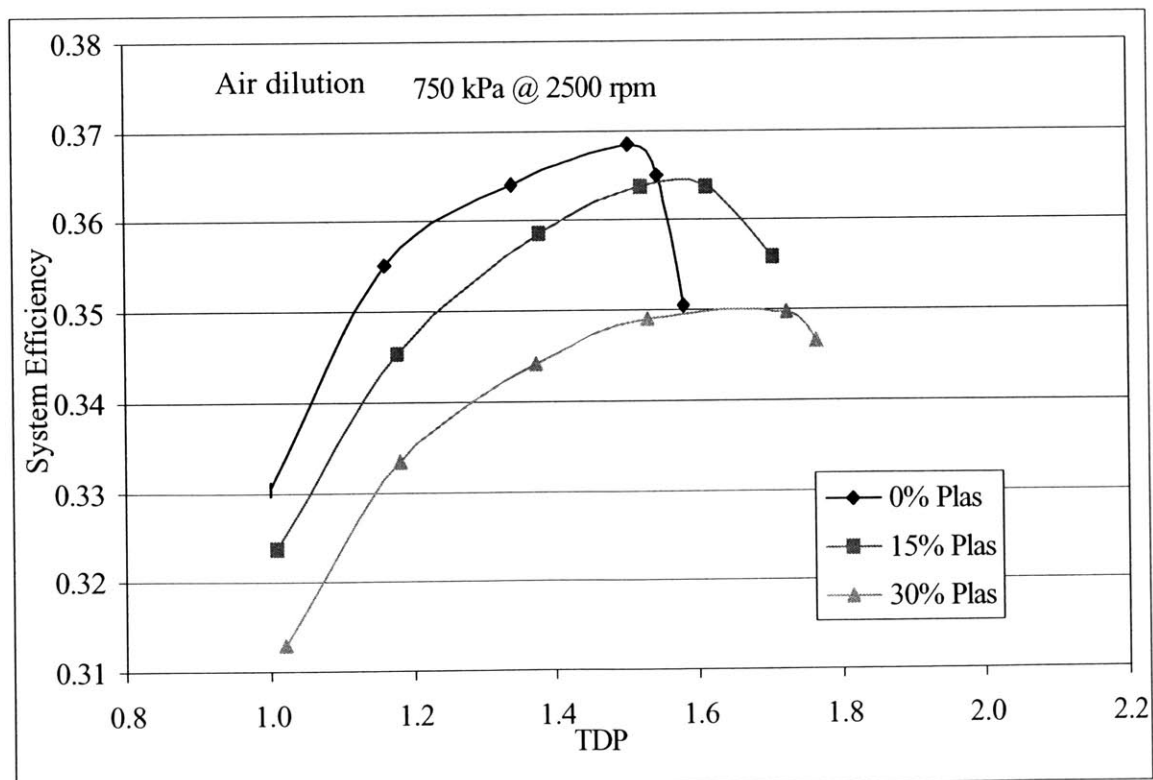
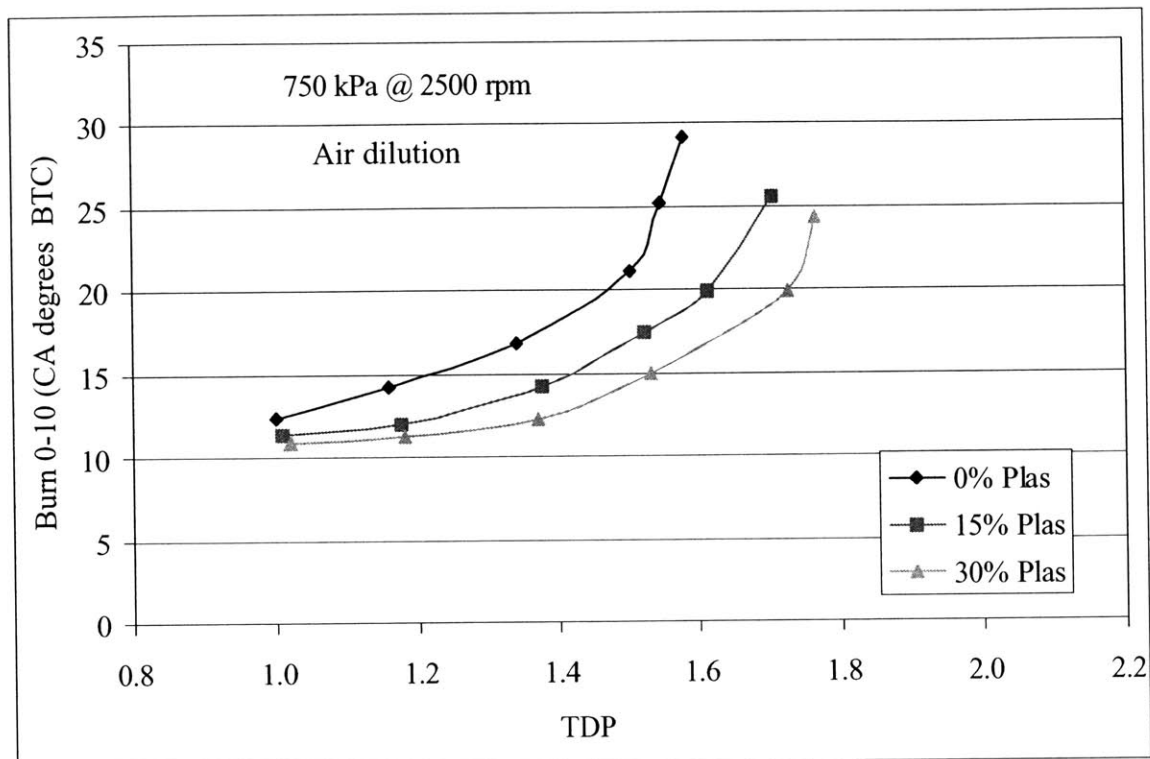
APPENDIX C: Experimental data for 750 kPa NIMEP @ 2500 rpm



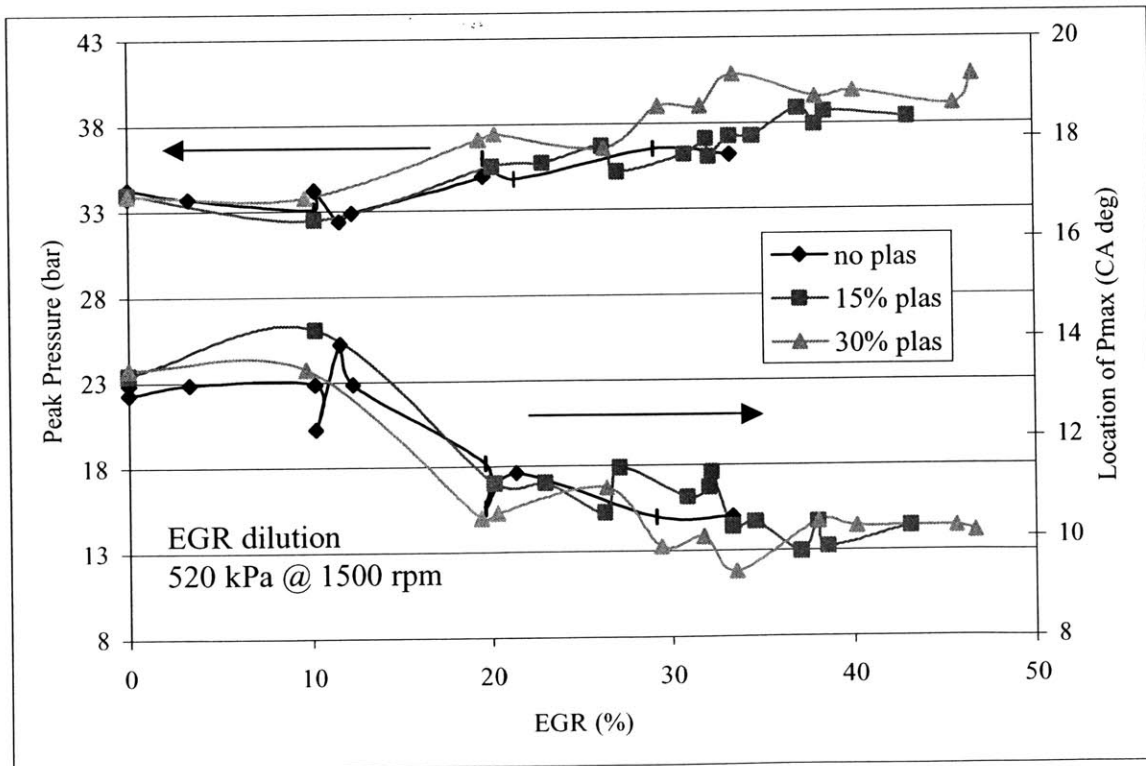
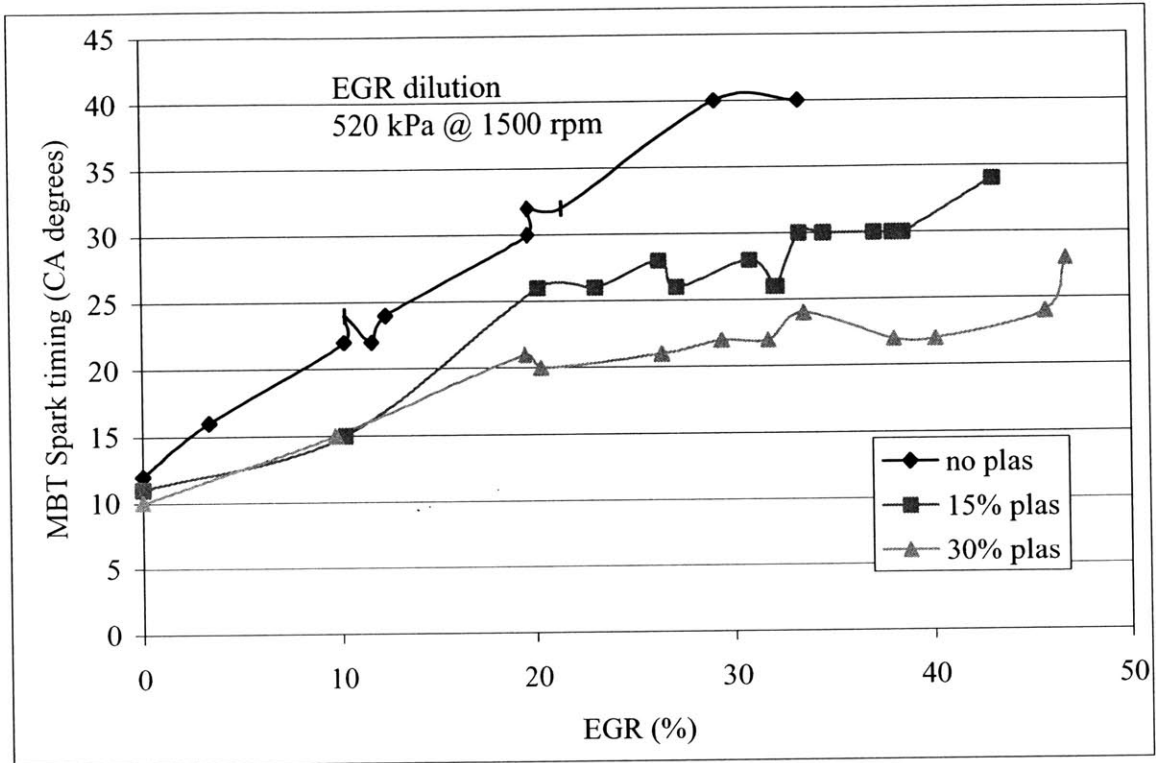


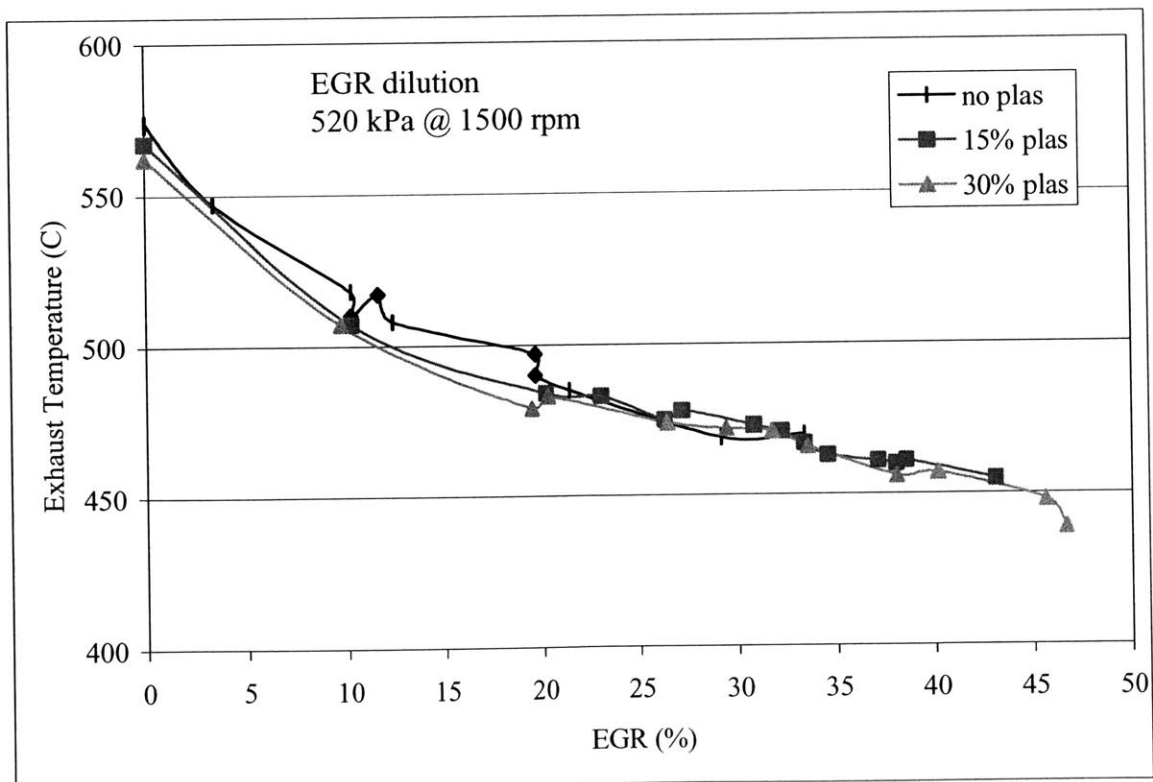
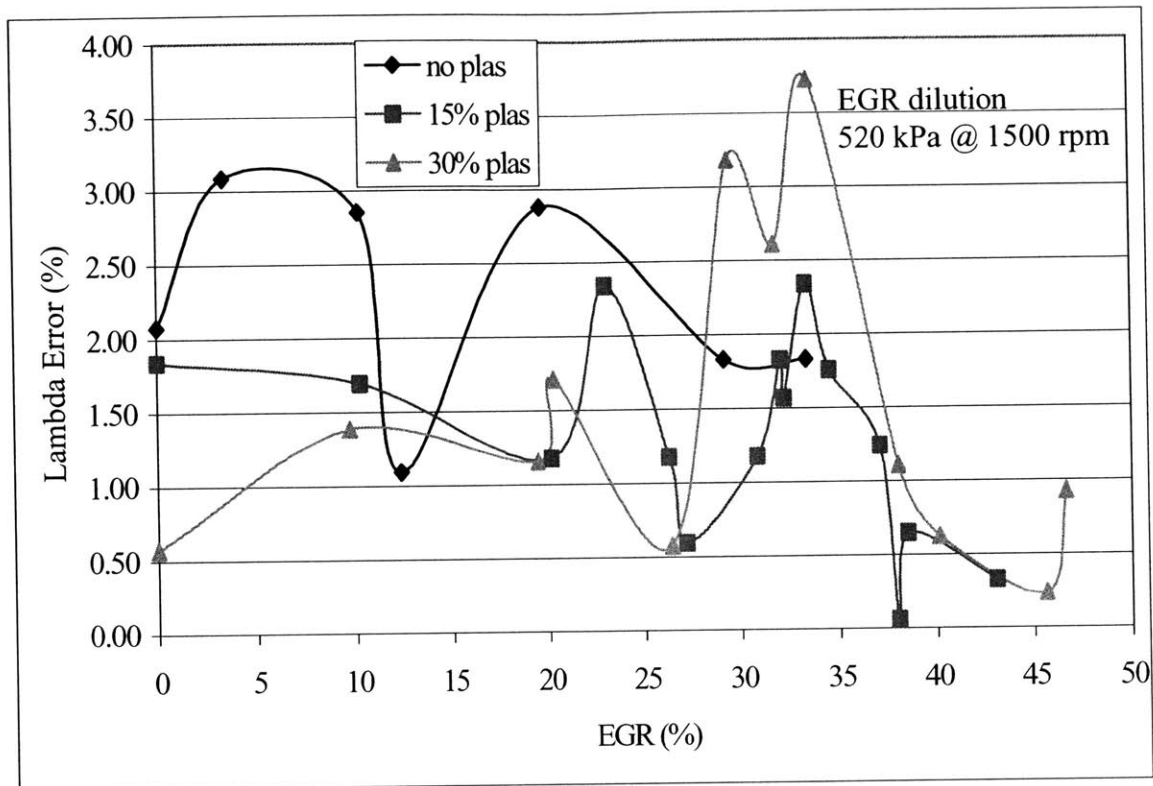


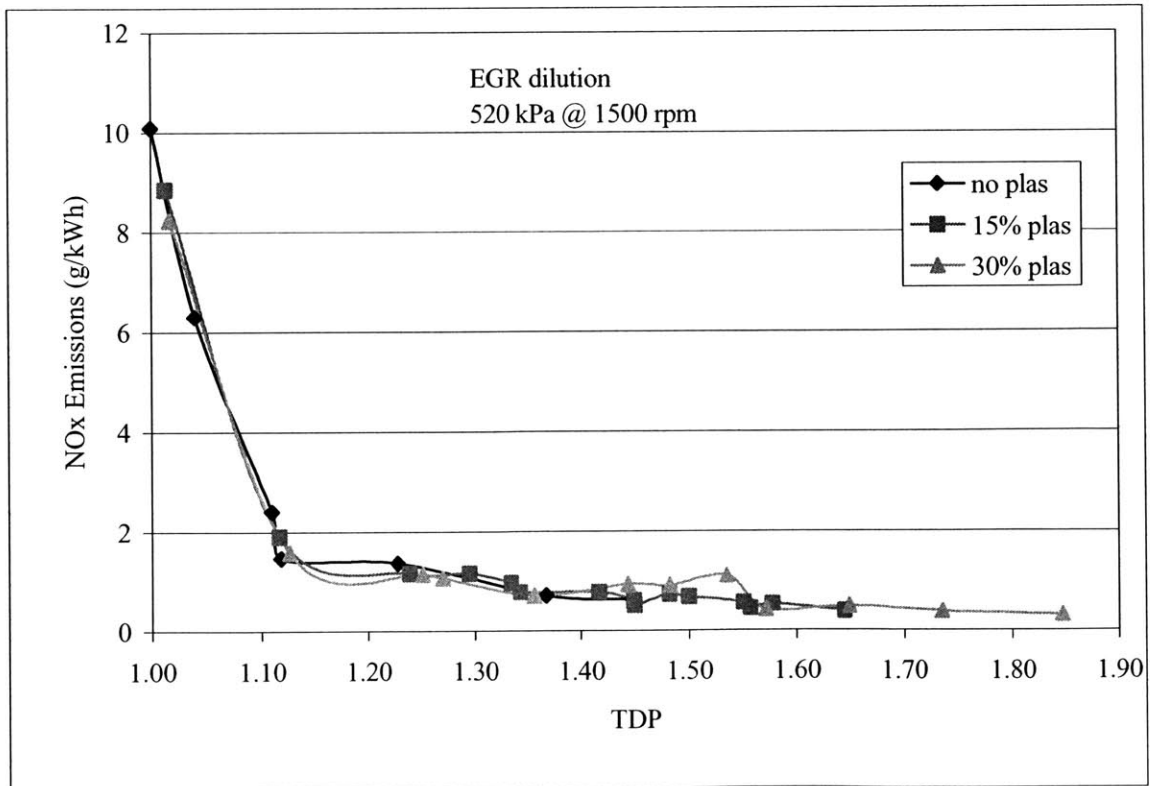
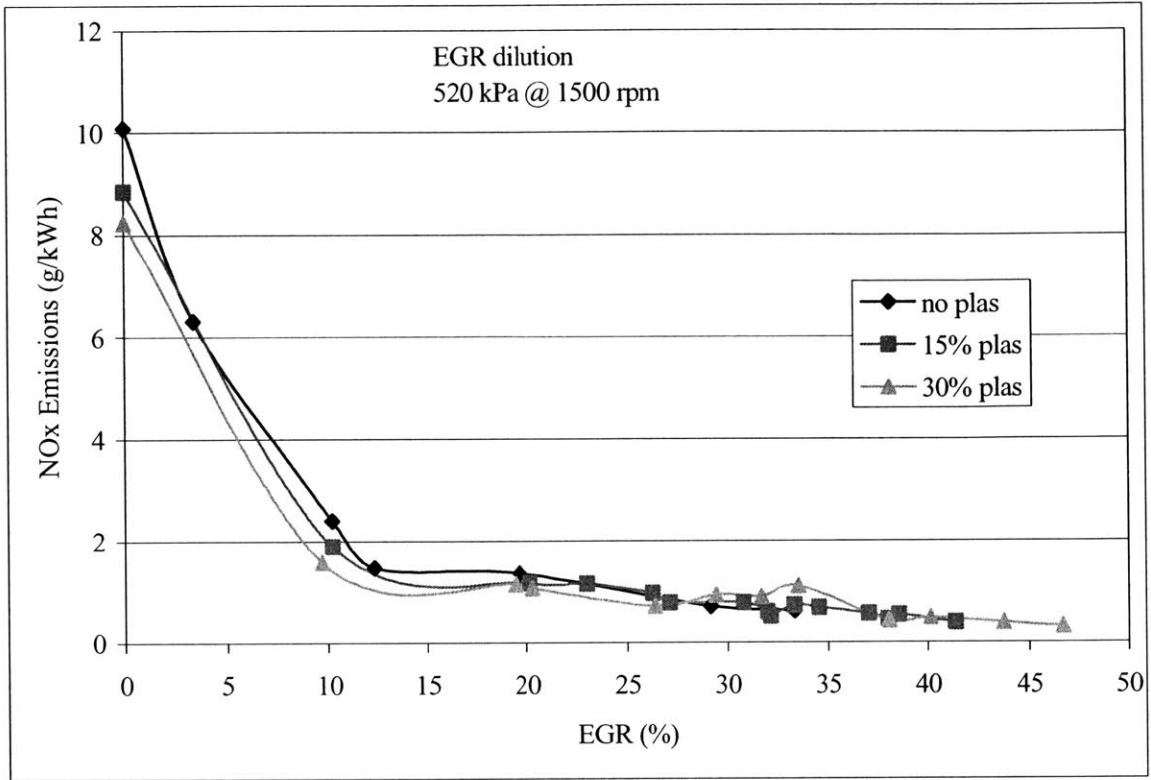


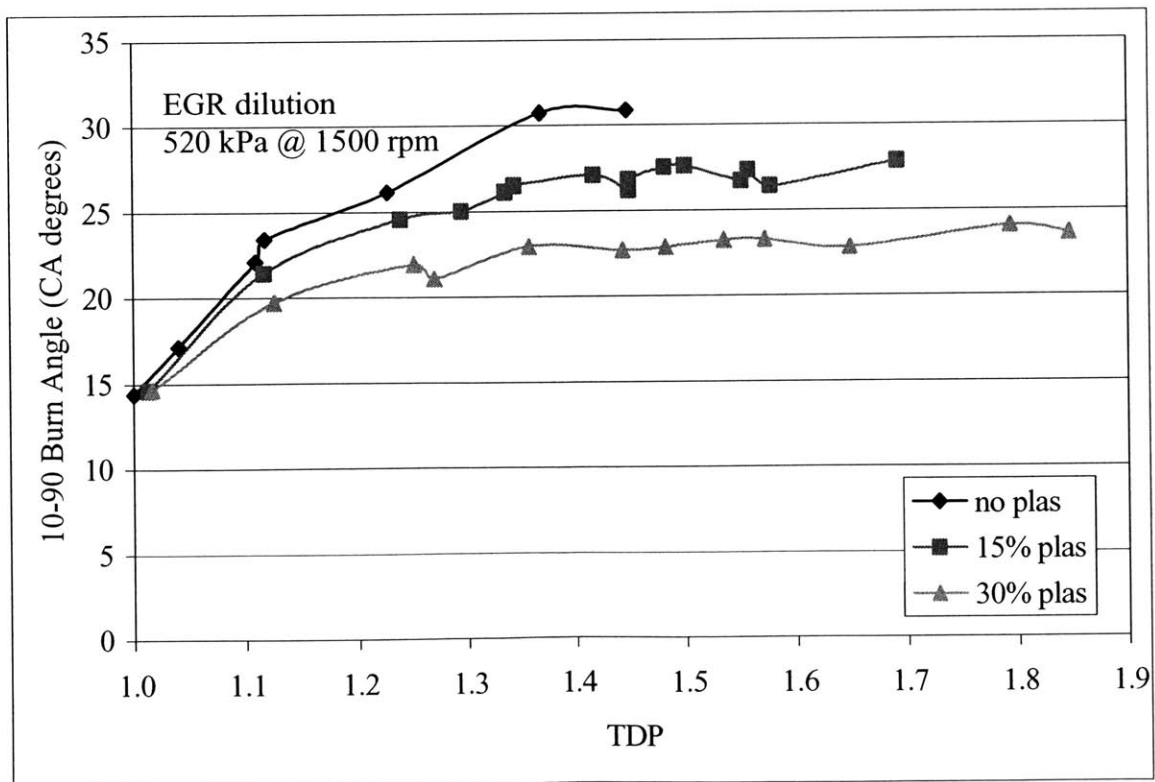
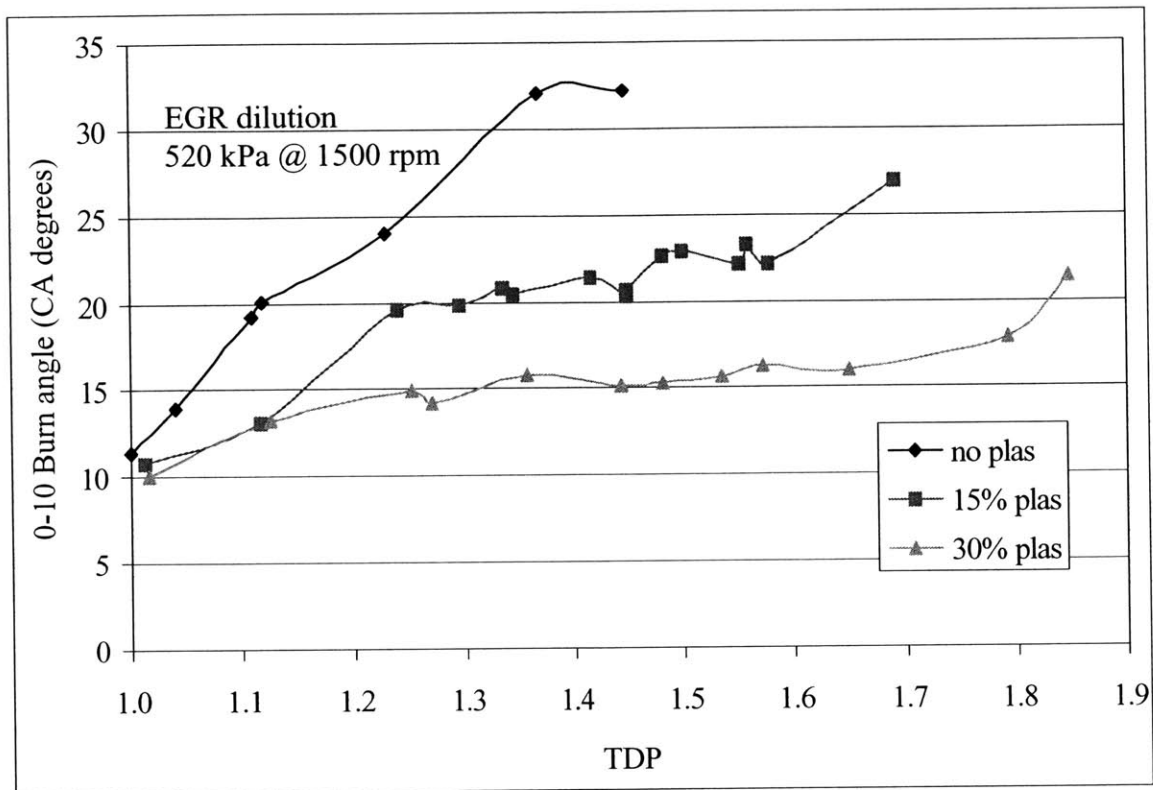


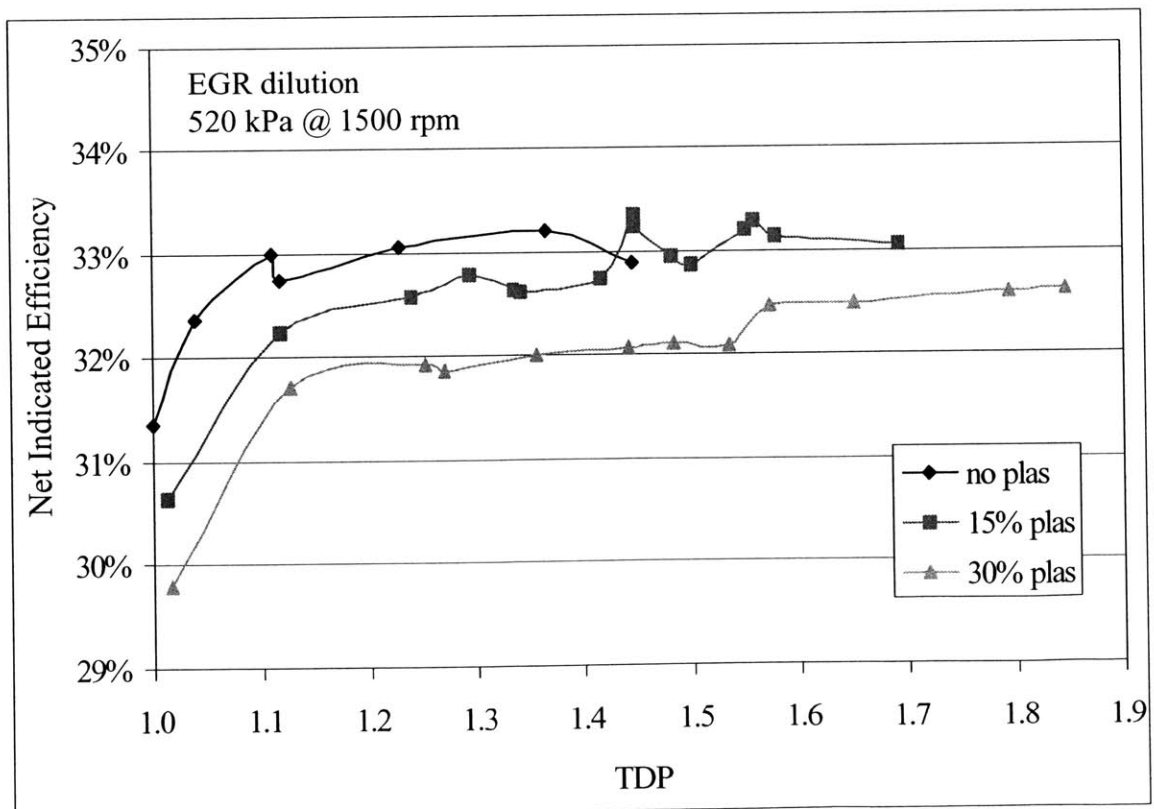
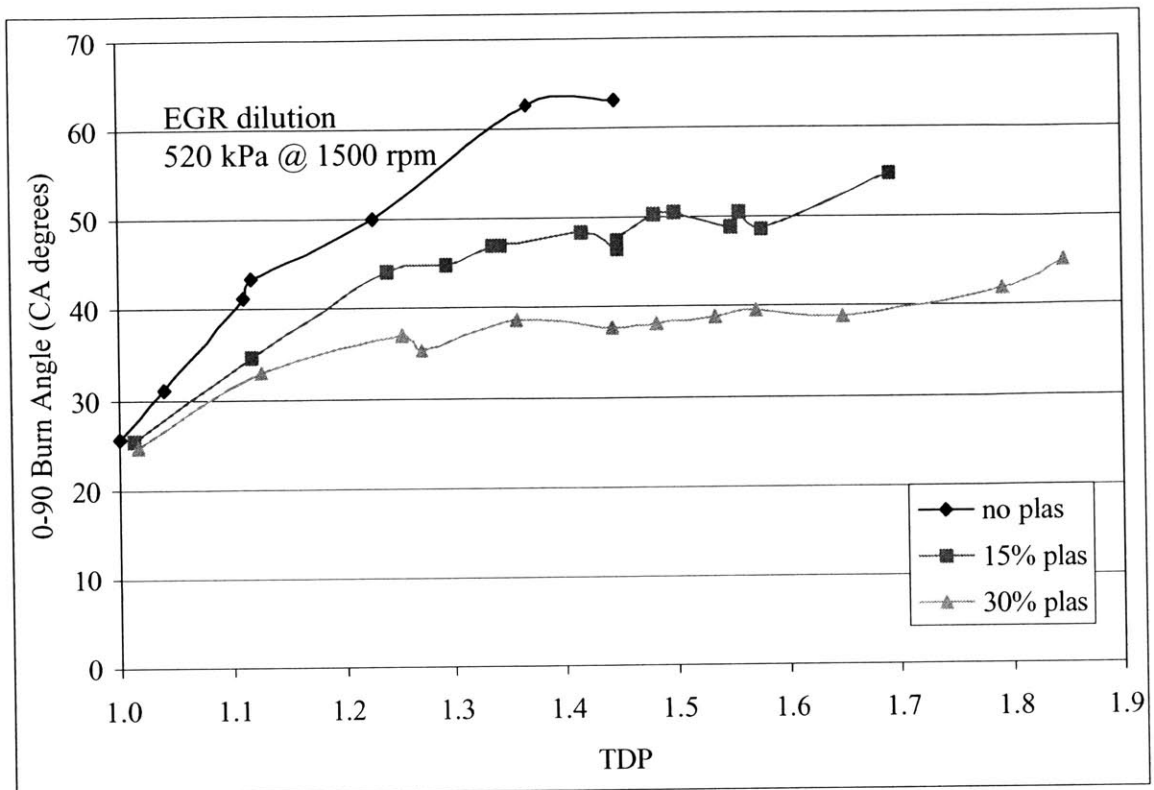
APPENDIX D: EGR data for 520 kPa NIMEP @ 1500 rpm











APPENDIX E: EGR data for 350 kPa NIMEP @ 1500 rpm

